2013-03-20

Application of Fuel Element Combustion Properties to a Semi-Empirical Flame Propagation Model for Live Wildland Utah Shrubs

Chen Shen
Brigham Young University - Provo

Application of Fuel Element Combustion Properties to a Semi-Empirical Flame Propagation Model for Live Wildland Utah Shrubs

Chen Shen

A thesis submitted to the faculty of
Brigham Young University
in partial fulfillment of the requirements for the degree of

Master of Science

Thomas H. Fletcher, Chair
David O. Lignell
W. Vincent Wilding

Department of Chemical Engineering

Brigham Young University

March 2013

ABSTRACT

Application of Fuel Element Combustion Properties to a Semi-Empirical Flame Propagation Model for Live Wildland Utah Shrubs

Chen Shen
Department of Chemical Engineering, BYU
Master of Science

Current field models for wildfire prediction are mostly based on dry or low-moisture fuel combustion research. To better study live fuel combustion behavior and develop the current semi-empirical bush combustion model, a laminar flow flat-flame burner was used to provide a convection heating source to ignite individual live fuel samples. In this research project, four Utah species were studied: Gambel oak (*Quercus gambelii*), canyon maple (*Acer grandidentatum*), big sagebrush (*Artemisia tridentata*) and Utah juniper (*Juniperus osteosperma*). Leaf geometrical parameters and time-dependent combustion behavior were recorded. Qualitative results included various combustion phenomena like bursting, brand formation and bending. Quantitative results included determination of best correlations for (a) leaf geometrical properties (individual leaf dry mass (m_{dry}), thickness (Δx), leaf width (W) and leaf length (L)) and (b) combustion characteristics (e.g., time to ignition (t_{ig}), time of flame duration (t_{fd}), time to maximum flame height (t_{fh}), time to burnout (t_{brn}), and maximum flame height ($h_{f,max}$)).

A semi-empirical bush model was expanded to describe the combustion behavior of the three Utah species (Gambel oak, canyon maple and Utah juniper). Leaf placement and bush structure were determined from the statistical model. A new flame area simulation was explored in the semi-empirical bush model in order to improve the bush burning predictions.

Keywords: shrub, combustion, ignition, wildland fire, wildfire

ACKNOWLEDGEMENTS

I wish to express my deep thanks to all the people who have helped me in completing this project. First, I would like to thank my advisor, Dr. Thomas Fletcher, for all his advice, help and guidance as well as other members of my committee: Dr. David Lignell and Dr. Vincent Wilding. I also want to extend my thanks to David Weise for his insight into this project. I would like to thank Dallan Prince for his support and suggestions in my research and all the great undergraduate students for their assistance in conducting experiment and data collecting for this project: Jay Liu, Ganesh Bhattarai, Marianne Fletcher, Kenneth Alford, Kelsey Wooley, Eddie Overy, Merete Capener, Sydney Fletcher, Victoria Lansinger, Kristen Nicholes and Kellen Mecham. I gratefully acknowledge the financial support from the National Science Foundation Grant CBET-0932842. Any opinions, findings, and conclusions or recommendations expressed in this Thesis are those of the PI and do not necessarily reflect the views of the National Science Foundation; NSF has not approved or endorsed its content. Also, thanks to Brigham Young University for allowing me to have my education. Special thanks to my parents, Min Shen and Yueming Jiang, for their support, encouragement and love.

TABLE OF CONTENTS

LIST OF TABLES

LIST OF FIGURES

NOMENCLATURE

Symbol	
FA	flame area of individual leaf combustion [cm^2]
FW_β	flame width [cm]
$F(x;\alpha,\beta)$	cumulative density function
L	length of sample [cm]
MC	moisture content of sample on a dry-basis [%]
Q_c	heat release of fuel [kW]
T	temperature [ºC]
U	wind speed [m/s]
W	width of sample [cm]
X_{dist}	bush length in semi-empirical model [cm]
Y_{dist}	bush width in semi-empirical model [cm]
Z_{dist}	bush height in semi-empirical model [cm]
d	diameter of leaf stem [cm]
$f(x;\alpha,\beta)$	probability density function
h_f	flame height [cm]
l_f	flame length [cm]

$\dot{m}_s$	mass release rate [g/s]
m	sample mass [g]
t	time during experimental run [s]
$\bar{x}$	individual leaf dry mass mean
x_{leaf}	leaf position in x direction in semi-empirical model
y_{leaf}	leaf position in y direction in semi-empirical model
z_{leaf}	leaf position in z direction in semi-empirical model

Greek

$B(\alpha,\beta)$	complete beta function
$B_x(\alpha,\beta)$	incomplete beta function
Δx	leaf thickness [mm]
ΔH_{vap}	heat of vaporization of water [kJ/kg]
$\Gamma(z)$	gamma function
α	first shape parameter of beta distribution
β	second shape parameter of beta distribution
θ_{mean}	mean flame tilt angle [degrees from vertical]
θ_{max}	maximum flame tilt angle [degrees from vertical]
ρ_{leaf}	leaf apparent density [g/cm^3]
σ	surface area to volume ratio
υ	variance of individual leaf dry mass

Subscripts

0	initial value of sample (m)
H2O	value of water in sample (m)

brn	value at burnout (flaming) (t)
dry	value of oven-dried sample (m)
fd	flame duration (t)
fh	value at maximum flame height (t)
ig	value at ignition (t)
max	value at maximum (h_f, l_f, θ)
vm	volatile matter (m)

1. INTRODUCTION

In order to improve the suppression of wildfires (unwanted and uncontrolled) and the prediction of prescribed fire (ignited intentionally to decrease the amount of live and dead fuel accumulation in forest), it is important to better understand wildland fire propagation (USDA/USDI, 2005). Weber (1991) and Sullivan (2009a, b, c) performed comprehensive reviews of wildfire modeling and classified types of fire propagation models. As a *semi-empirical model*, the Rothermel model (1972) was further developed into wildfire *field operational models* (FARSITE (Finney, 1998) and BEHAVE (Andrews, 1986)). Moreover, some computational fluid dynamic (CFD) models for wildfire modeling were developed, such as FIRETEC and WFDS (Linn, 1997; Mell et al., 2006; Clark et al., 2010). Besides CFD models and the Rothermel model (1972), many other wildland fire propagation models were developed based on experimental data from dead or dry fuel beds, which might be inappropriate for predicting live wildland fuel combustion, especially at high moisture content (Fletcher et al., 2007; Pickett, 2008). There is a need for better methods to simulate combustion of live wildland fuels, especially for shrubs.

Various kinds of live fuel combustion experimental have been conducted (Dimitrakopoulos and Papaioannou, 2001; Smith, 2005; Weise et al., 2005; Pickett, 2008; Pickett et al., 2010). At Brigham Young University (BYU), more than 2200 experiments on single live fuel samples (various species common in California and Utah) have been conducted (Engstrom

et al., 2004; Smith, 2005; Fletcher et al., 2007; Pickett, 2008). Smith (2005) performed combustion experiments on four fuels from southern California (manzanita, scrub oak, ceanothus, and chamise) and four fuels from Utah (canyon maple, Gambel oak, big sagebrush, and Utah juniper). Smith collected data on thickness and shape, and moisture content (*MC*), along with visual images and mass change during combustion. Pickett (2008) performed additional experiments on these same species along with two fir species and four sou theastern U.S. species (Fetterbush, Gallberry, Wax Myrtle, and Saw Palmetto) to improve empirical correlations and performed some computational fluid dynamic simulations of a single leaf and a two-leaf configuration.

Pickett (2008) developed a first-generation two-dimensional model of Manzanita shrub combustion, based on empirical correlations developed from single leaf experiments. This bush model was capable of predicting overall burn times and amount of fuel unburned. This model was later extended to three dimensions (Prince et al., 2010), including effects of flame coalescence and the effects of wind on flame angle and size (based on the findings of (Cole et al., 2011)). Model development is still in progress (Prince, 2012), with a need to treat more species and environmental factors.

As a result, improved combustion data on live shrub fuels from the U.S. western intermountain area must be obtained to expand the bush model. In this project, combustion experiments were conducted using a new modified flat-flame burner, an apparatus developed to simulate the wildfire front as a convective heat flux. Regression analyses were also performed to obtain improved correlations for combustion behavior predictions. This research project focused on how physical leaf parameters and moisture content affect the combustion behaviors of four Utah live shrub fuels.

2. LITERATURE REVIEW

Fire propagation is considered as a series of successive ignition events that are controlled by ignition temperature, ignition delay time, and the distance between fuel particles. Therefore, the knowledge of ignition characteristics must be known to simulate fire propagation. Moisture content (*MC*) is an important factor of live fuel combustion, and is defined on a dry-weight basis (Babrauskas, 2003) in this thesis project. The ignition characteristics will be addressed below in section 2.1. Another important parameter to describe the combustion is the flame height (h_f), which can be related to the mass release rate and volatile matter of fuel, as discussed in section 2.2. Heat transfer mechanisms during live fuel combustion will be addressed in section 2.3. Wind is a main factor in fire propagation, which is addressed in section 2.4. Bush structure simulation is discussed in section 2.5. A summary of forest fuel combustion modeling is presented in section 2.6. Previous work and achievements at Brigham Young University are reviewed in section 2.7.

2.1 Ignition Characteristics

2.1.1 Flammability

Flammability was defined as the capability to ignite and sustain the flame for a particular fuel (Anderson, 1970). Moisture content and geometry of the fuel were considered as the most

important factors of flammability (Weise et al., 2005). It was suggested by Mak (1988) that foliage flammability were mostly determined by time to ignition (t_{ig}) and ignition temperature (T_{ig}) of the fuel samples.

2.1.2 **Ignition Temperature**

Ignition of a leaf is defined as when the first visible gaseous flame is observed near the surface of a leaf (Smith, 2005). Ignition temperature (T_{ig}) is the critical temperature when a fuel starts burning by an ignition source. Values of T_{ig} vary in wood and live fuel ignition experiments. Possible major factors include the definition of ignition, experimental conditions, autoignition, specimen conditions (surface area-to-volume ratio and thickness), leaf geometry (surface area, perimeter), moisture content, and species (Babrauskas, 2001; Engstrom et al., 2004; Smith, 2005; Pickett, 2008).

2.1.3 **Time to Ignition**

Time to ignition (t_{ig}) or ignition delay is defined as the time difference between exposure to heat flux and ignition. Li and Drysdale (1992) observed an inverse relationship between t_{ig} and heat flux for wood fuels, which is consistent with the observation that fuels ignite faster with higher heat flux. Dimitrakopoulos and Papaioannou (2001) performed ignition experiments on various Mediterranean forest fuels and discovered that t_{ig} correlated better with moisture content than T_{ig}. Pickett (2008) developed linear correlations for t_{ig} and T_{ig} based on mass, MC, and geometrical properties for use in his statistical bush combustion model.

2.1.4 **Moisture Effects**

Dimitrakopoulos and Papaioannou (2001) concluded that linear regression between t_{ig} and moisture content (MC) was the best fit of the relationship between t_{ig} and MC based on their experiments. Effects of MC reported in the literature are also summarized in Table 2.1.

Table 2.1. Effects of moisture content reported in the literature.

Source	Findings and Correlations	Method
Mardini and Lavine (1995); Moghtaderi (1997)	High MC led to high t_{ig} and T_{ig}, if MC affected the T_{ig} for particular fuels.	Wood fuels
Montgomery and Cheo (1969); Pickett (2008)	t_{ig} linearly increased with increasing MC (rainy season, dry season, and oven-dry). Different live fuel samples may vary in slopes.	Several fire-retardant plants and Southern California chaparral shrubs
Xanthopoulos and Wakimoto (1993)	t_{ig} increased exponentially with increasing MC and decreasing T_{gas} (correlated as $t_{ig} = C_1 \cdot exp(-C_2 \cdot T_{gas} + C_3 \cdot MC)$ where C_1, C_2, and C_3 are species-specific coefficients to fit data and T_{gas} is apparatus gas temperature (°C)).	Live conifer branches under a hot-air convective heat flux
Weise and coworkers (2005)	Linear correlation: $t_{ig} = \alpha \cdot MC + \beta$ where α and β were species-specific coefficients to fit data. A higher slope indicated lower flammability.	Live Southern California fuels with a cone calorimeter
Smith (2005)	t_{ig} increased linearly with the amount of moisture water (m_{H2O}) in the sample.	Southern California and Utah live shrub fuels

Basically, higher MC causes more water to be evaporated from a heated leaf, which dilutes ignitable gases and possibly results in a higher T_{ig} and t_{ig} (Catchpole et al., 2002).

2.1.5 **Thickness Effects**

Leaf thickness (Δx) is an important factor in mass transfer resistance. Thickness is also the main factor of surface area-to-volume ratio (σ). Ignition will occur only when the ignitable gas concentration near the live fuel element is sufficiently high (Pickett, 2008). Babrauskas

(2003) suggested that live fuels behave as thermally-thin materials (i.e., minimal thermal gradient through the leaf). Montgomery and Cheo (1969) found that t_{ig} increases linearly with increasing Δx. Smith (2005) reported that T_{ig} and t_{ig} generally increased with increasing Δx, but only significantly for some species. Pickett (2008) furthered Smith's work and obtained a positive linear correlation of t_{ig} vs. Δx for most species.

2.2 **Flame Height**

Flame height (h_f) is defined as the vertical distance from the top edge of the flame to the bottom edge of the flame. Fletcher et al. (2007) concluded that h_f was weakly correlated to volatile mass of various shrub species based on fuel combustion experiments using a small flat-flame burner system.

In fuel bed combustion, the heat released from burning fuels can ignite nearby fuel elements to propagate flames. The heat release can linearly correlate to mass release rate ($\dot{m}_s$) for similar fuel beds, accounting for *MC*, composition, and packing ratio (Pickett, 2008). Putnam (1965) and Drysdale (1999) reported a correlation of flame height ($h_{f,max}$) with heat release of steady-state natural fuels as shown in Equation (2.1),

$$\frac{h_{f,max}}{d} \propto \left(\frac{Q_c}{d^{5/2}}\right)^{2/5} \propto \frac{{Q_c}^{2/5}}{d} \Rightarrow h_{f,max} = k \cdot {Q_c}^{2/5} \qquad \textbf{(2.1)}$$

where d is fuel diameter, Q_c is heat release rate (kW), and k is a constant specific to each species.

Dupuy et al. (2003) similarly correlated maximum flame height ($h_{f,max}$) with various powers of Q_c for unsteady state experiments on oven-dried samples of pine needles and excelsior. Sun et al. (2006) further compared live and dead chaparral species via an IR camera instead of thermocouples. They found a time delay (defined as the difference between the maximum mass release time and the maximum flame height time) linearly correlated to *MC*. For

high *MC* fuels, the 2/5 power was not effective, and the heat release rate based at the time of the maximum $h_{f,max}$ correlated better than the maximum mass release rate $\dot{m}_s$. Based on single live leaves (Engstrom et al., 2004; Smith, 2005), fuel in baskets (Sun et al., 2006), and fuel beds (Zhou et al., 2005), (Zhou et al., 2005) correlated $h_{f,max}$ with $\dot{m}_s$ as follows:

$$h_{f,max} = 0.417 \cdot \sqrt{\dot{m}_s} \quad \textbf{(2.2)}$$

where $h_{f,max}$ is in meters and $\dot{m}_s$ is in g/s.

2.3 **Heat Transfer Mode**

In wildland fire spread, the heat transfer mechanisms are still not fully understood, especially radiation and convection (Frankman et al., 2010), and current wildland fire models are therefore not sufficiently accurate (Cohen and Finney 2010). Table 2.2 summarizes the literature regarding the importance of different heat transfer modes in wildland fire propagation.

Table 2.2. Summary of reported mode of heat transfer for wildland fire propagation.

Source	Findings	Method
(Albini, 1985)	Radiation dominates fuel preheating and convection is neglected.	Modeling
(Albini, 1986)	Convection is only considered as cooling but not a possible source of preheating.	Modeling
(Pagni and Peterson, 1973)	Radiation dominates in no-wind surroundings while convection dominates in wind-aided fire spread.	Modeling
(Anderson, 1969)	Radiation is responsible for less than 40% of the heat required for flame to propagate.	Experimental analysis
(Catchpole et al., 1998)	Only intense radiation preheats the fuel and convection bring burning particles to ignite fuels.	Modeling
(Frankman et al., 2010)	Pilot ignition sources might still be needed to ignite the fuel even with intensive radiation heating.	Modeling
(Cohen and Finney 2010)	Flame contact accounts for convection heating and pilot ignition, necessary for fire propagation.	Experimental analysis
(Dupuy, 2000)	Radiation alone is not enough for flame propagation modeling.	Experimental analysis

Cohen and Finney (2010) found that radiant heating might not be sufficient for fine fuel (1-mm cross-section) ignition but may be sufficient for coarse fuel (12-mm cross-section). They suggested that 1-mm particle fuel has a significantly higher free convection coefficient, causing more convective cooling. Therefore, fuel configurations (the surface area facing the heat flux) may be more important than thickness in the study of heat transfer of live fuel combustion. Moreover, it was also suggested to include a heat transfer mechanism in the correlations for prediction of combustion characteristics for the semi-empirical bush model (Pickett, 2008; Pickett et al., 2009; Prince et al., 2010).

2.4 **Wind Effects**

Wind is an important factor for wildland fire propagation. Wind effects were studied as a major factor that influences rate of spread in fuel bed flame propagation (Welker et al., 1965; Weber, 1991; Beer, 1995; Mendes-Lopes et al., 2003). Cole et al. (2011) performed combustion experiments on individual leaf samples for five shrub species using a bench-scale wind tunnel and a small flat-flame burner. A linear relationship between wind speed and maximum flame length ($l_{f,max}$) was reported by Cole et al. (2011).

2.5 **Bush Structure**

Manzanita shrubs were approximated in the statistical model developed at BYU as a virtual box with leaves randomly placed inside (Pickett, 2008; Pickett et al., 2009; Prince et al., 2010). Stems were ignored since manzanita was a broad-leaf species. As for branch-structured bushes, it has been suggested that fractal theory might be used to simulate bush structure in the modeling (Alados et al., 1999). Spatial fuel distribution of a bush has been observed to significantly influence combustion behavior (Busing and Mailly, 2004; Parsons, 2007).

Lindenmayer-systems (L-systems) could therefore be used as the self-rewriting system to simulate the branching structure of a bush (Prusinkiewicz and Lindenmayer, 1991), which might improve the accuracy of modeling species such as Utah juniper in this research project.

2.6 **Fire Modeling Classification**

Weber (1991) classified fire models into three categories: (a) physical (involving conservation of energy and considering different modes of heat transfer); (b) empirical (involving conservation of energy without considering different modes of heat transfer); and (c) statistical (not involving physical mechanism). Sullivan classified fire models in different categories: (a) physical and quasi-physical models (Sullivan, 2009a); (b) empirical and quasi-empirical models (Sullivan, 2009b); and (c) simulation and mathematical analogue models (Sullivan, 2009c). Sullivan's classification system is summarized in Table 2.3. The bush model developed in wildfire lab at BYU (Pickett, 2008; Pickett et al., 2009; Prince et al., 2010) can be considered as a statistical model or a quasi-empirical model.

Table 2.3. Summary of Sullivan's fire modeling classification system.

Classification	Definition
Physical	Considers both physics and chemistry of fire spread
Quasi-physical	Only deals with physics
Empirical	Represents statistical method without physical understanding
Quasi-empirical	Combines physics and statistical modeling
Simulation	Integrates small-scale fire behavior model to large-scale fire spread model
Mathematical analogue	Uses mathematical concepts and methods to reproduce fire spread instead of being reproduced by physics

2.7 **Previous Work at Brigham Young University**

More than 2200 experiments on single live fuel samples (various species common in California and Utah) have been conducted at Brigham Young University, including more than 800 experiments on single Manzanita leaves (Engstrom et al., 2004; Smith, 2005; Fletcher et al., 2007; Pickett, 2008). Smith (2005) perfomed some experiments on Utah fuels, especially sagebrush, gambel oak, and canyon maple, and collected data on thickness and shape, average *MC*, visual images and mass data. Pickett (2008) furthered Smith's work and correlated most of the ignition data at BYU, and even developed $h_{f,max}$, $\dot{m}_s$ and burnout correlations.

Figure 2.1. A comparison of the experiment and the shrub combustion model (Prince, 2012).

Pickett (2008) established a first-generation two-dimensional model of Manzanita shrub combustion, based on empirical correlations concluded from single leaf experiments. The spatial domains of each leaf were specified. Fire propagates in the model by flame contact of

neighboring leaves. This model is capable of predicting overall burn times and amount of fuel unburned. Prince et al. (2010) furthered Pickett's work in three dimensions. Wind effects and flame interactions were integrated into this model (Prince et al., 2010), along with the effects of wind on flame angle and size based on the findings of (Cole et al., 2011). This semi-empirical model was also compared to bush-scale experiments with and without wind. Each leaf is treated independently and compared to the position of other leaves, avoiding the use of discretized grid. The current model simulates complete combustion characteristics and visually reproduces the flame propagation from ignition (shown in Figure 2.1). This semi-empirical model may lead to improvements in operational field-scale models. There is a need to adapt this semi-empirical model to Utah shrub species, which is part of this thesis project.

3. OBJECTIVES AND APPROACH

3.1 **Objectives**

The objectives of this study are to investigate the combustion behavior of live Utah shrubs and develop an advanced bush-scale combustion model of these shrubs. This study will mainly focus on the following Intermountain West species: Gambel oak (*Quercus gambelii*); canyon maple (*Acer grandidentatum*); big sagebrush (*Artemisia tridentata*); and Utah juniper (*Juniperus osteosperma*).

3.2 **Approach**

A flat-flame burner was used as a convective heating source to simulate a wildfire flame front. Single leaf samples or segments were exposed to convective gas and ignited. Four kinds of Utah live species were used as experimental fuels. The objective was realized by the following tasks:

1) Time-stamped images were obtained for each experimental run. Qualitative species-dependent experimental phenomena were observed.
2) Values of time to ignition, maximum flame height, time to maximum flame height, and flame duration were determined based on the time-stamped video images. Image processing was automated using a modified routine coded within MATLAB.

3) Correlations between combustion characteristics and leaf geometry measurements were developed.

4) After studying the bush structures, broad leaf placement and branching fuel structure were developed and coded into a bush structure model.

5) The above correlations and bush structure were incorporated into the semi-empirical bush combustion. Parametric simulations were performed to show capability.

4. DESCRIPTION OF EXPERIMENTS

4.1 Experimental Apparatus

The experiments were designed to simulate the live fuel combustion process in a wildfire environment. Single leaf samples or segments were exposed to convective gas and ignited. Time-stamped temperature data and images were recorded via a LabVIEW program for each experimental run. The convective gas temperature was selected to be close to the temperature in wildland fires, which is reported to be approximately 1200 K (Butler et al., 2004).

4.1.1 Flat-Flame Burner

A flat-flame burner (FFB) was used as the heat source, which can be moved directly under the leaf. Fuel gases (CH_4 and H_2) and oxidizer (air) were premixed and introduced into the FFB, providing a 1 mm thick flame at a height of 1 mm above the sintered bronze burner surface. The vertical distance between the FFB and the leaves was typically 5 cm, a point where the gas temperature was 1200 K. This premixed FFB surface was 7.5” x 10”. A cage with glass panels was placed above the FFB to avoid indraft of surrounding air, which introduced natural convection flow recirculation, leading to decreased effective flame area. This glass cage ensured 10 mol% O_2 in the post-flame gases and a laminar flow environment. The live fuel sample (leaf or twig) was placed horizontally or vertically, according to experimental purpose, on a rod

connected to a mass balance. The FFB was placed on a cart, which could be pulled and stopped exactly under the sample.

Figure 4.1. Flat-flame burner experimental set-up, including a) large flat-flame burner, b) cage with glass panel on each side, c) mass balance, d) video camera.

4.1.2 Temperature Measurements

A bare fine-wire type-K (chromel-alumel) thermocouple was used to measure the gas temperature close to the leaf sample during each experimental run. The diameter of the thermocouple was 0.003 inches and the length was 12 inches. The rate of data acquisition for the thermocouple was 18 Hz.

4.1.3 Video Images

A Sony CCD-TRV138 camcorder was originally used to record video images. A Panasonic SDR-S50P digital camcorder was used in the most recent experiments. Video images

of the each experimental run were collected at 18 Hz. The images were collected and digitized by a National Instruments PCI-1411 IMAQ device. The rate of acquisition for the video images was 18-19 Hz.

4.1.4 **LabVIEW System**

A National Instruments LabVIEW 7.1 program was used for data collection, which simplified data collection and minimized human error. Video images, temperature, and mass data (from a Mettler Toledo XS204 analytical mass balance) were collected simultaneously with a time-stamp at 18 Hz. Video images were digitized and stored as jpeg files along with the datasheets for each experimental run.

4.1.5 **Moisture Content Measurements**

Previously, a CompuTrac moisture analyzer was used to measure the moisture content (*MC*) of each sample on a dry mass basis. Values of *MC* were measured before and after the combustion experiments, and the two values were averaged together to provide an average *MC* for all the experimental runs. Since July 29 2011, a new method has been using to determine the *MC*. For every three samples, a fourth sample was prepared and measured for *MC*. This representative sample was cut from the original plant at the same part of the plant as the other three samples. The mass of each of the four samples (m_0) was measured prior to running the experiment. After all the experimental runs were completed, the representative sample was dried and then weighed to measure for the dry mass (m_{dry}). The *MC* was calculated using the equation showing below:

$$MC = \frac{m_0}{m_{dry}} - 1 \tag{4.1}$$

where m_0 and m_{dry} were single leaf total mass and dry mass, respectively.

4.1.6 **Leaf Geometric Measurements**

Leaf length (L) and width (W) were measured with a ruler to accuracy of 0.1 mm for each sample prior to each experimental run. Length was defined as the longest distance from top to bottom of a leaf sample. Width was defined as the widest distance from side to side of a leaf sample. Thickness (Δx) was determined by a Chicago Brand digital caliper with an accuracy of 0.01 mm. Thickness was measured at different positions of the sample (excluding leaf vein) and determined by taking an average of all measurements. For non-broadleaf samples, measurement of the diameter was treated as equivalent to thickness. Initial total single leaf mass (m_0) was also measured by a Mettler Toledo AB104 mass balance.

4.2 **Experimental Fuels**

Experiments were performed on four kinds of Utah species: Gambel oak, canyon maple, big sagebrush and Utah juniper. Experiments were performed on live samples with various moisture contents. Combustion experiments were performed on samples collected in no less than five days. During this time period, samples are believed as live fuels. Once the samples were collected, samples were kept moist by watering the stems until testing began if testing was on another day. Samples were selected and detached from the branches at random. These species were collected in the foothills near BYU. Characteristics of these species are summarized in Table 4.1 (adapted from Fletcher (2007)). Images for four Utah species are shown in Figure 4.2.

Table 4.1. Characteristics of intermountain west species from measured data.

Species	Ash Content* (%)	Volatile Matter Content* (%)	Moisture Content* (%)	Ultimate Analysis† (%)		Leaf Thickness (mm)	Leaf Length (cm)	Leaf Width (cm)
Gambel oak	*2.9*	*83.5*	10-138 *(50-125)*	C	*49.15*	0.15–0.35 (*0.1-0.4*)	4.0–12.0 (*3.0-11.0*)	2.0–8.0 (*1.5-9.0*)
				H	*6.23*			
				N	*2.52*			
				O	*42.10*			
Canyon maple	*3.5*	*83.9*	20-150 *(55-160)*	C	*45.93*	0.10–0.20 (*0.1-0.5*)	3.0–8.0 (*2.0-6.0*)	4.0–10.0 (*3.0-8.0*)
				H	*6.14*			
				N	*2.11*			
				O	*45.82*			
Big sagebrush	*3.9*	*85.2*	40-200 *(100-195)*	C	*48.52*	0.15–0.50 (*0.1-0.5*)	1.5–4.0 (*2.0-5.0*)	0.2–1.2 (*0.6-1.2*)
				H	*6.46*			
				N	*2.25*		2.3-8.5 (segment length)	
				O	*42.77*			
Utah juniper	*4.0*	*84.8*	30-150 *(40-100)*	C	*49.92*	0.50–2.00 (*1.0-1.5 (needle diameter)*)	1.5–8.0 (*3.5-8.0 (sprig length)*)	N/A (*0.4-1.0 (needle length)*)
				H	*6.88*			
				N	*1.33*			
				O	*41.87*			

*Wt%, Dry basis; †Wt%, Dry ash free basis. Italic numbers or numbers in parentheses are from (Fletcher et al., 2007)

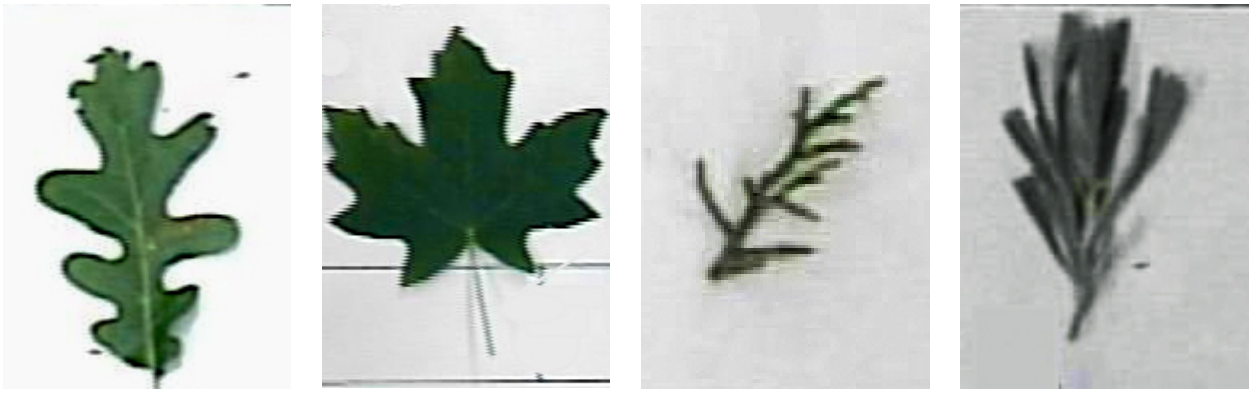

(a) Gambel oak (b) Canyon maple (c) Utah juniper (d) Big sagebrush

Figure 4.2. Images of Utah species individual samples. Dimensions are shown in Table 4.1.

4.2.1 **Gambel Oak**

Gambel oak (*Quercus gambelii* Nutt.) is widespread in the Utah mountain area. The Gambel oak samples were primarily collected from Rock Canyon, Provo, Utah. Gambel oak grows as a small tree or large shrub. Its size may vary from different locations. The Gambel oak

observed in Provo area is generally less than 5 meters tall. The samples were cut from bushes which are less than 2 meters tall. According to the experimental data collected (as shown in Table 4.1), Gambel oak leaves were basically 4 to 12 cm long and 2 to 8 cm wide. They were usually 0.15 to 0.35 mm thick and deeply lobed.

4.2.2 **Canyon Maple**

Canyon maple (*Acer grandidentatum* Nutt.), also called bigtooth maple, is common in the Utah area and was obtained in Rock Canyon, Provo. It can grow up to 15 meters tall. Samples were collected from bushes, which were from 1 to 2 meters tall. As shown in Table 4.1, the leaves are typically 6 to 12 cm long and broad. There are three major deep lobes on canyon maple leaves. The leaves collected for the experiments were generally 0.1 to 0.2 mm thick, 3 to 8 cm long and 4 to 10 cm wide.

4.2.3 **Big Sagebrush**

Big sagebrush (*Artemisia tridentate* Nutt.) was collected in Rock Canyon, Provo. It was observed that the big sagebrush plants grow to be 1 to 2 meters tall. There are typically three dents on sagebrush leaves (shown in Figure 4.3). Shiny silver hair was observed on the surface of the leaves. Moisture content of sagebrush leaves was as high as 200%. The leaves were about 6 cm long and 1.2 cm wide as shown in Table 4.1.

Figure 4.3. Single leaf sample of big sagebrush.

4.2.4 **Utah Juniper**

Utah juniper (*Juniperus osteosperma* (Torr.) Little) is widespread in Utah and was collected from Diamond Fork Canyon near Spanish Fork, Utah. Juniper varies in size from shrub to tall trees. This research focused on small juniper bushes. As shown in Table 4.1, Utah juniper leaves are needle-like with diameters of 1 to 2 mm. The leaves collected for experiment were generally cut into about 6 cm or 3 cm segments.

5. EXPERIMENTAL RESULTS AND DISCUSSION

Experiments with a flat-flame burner were performed as part of this project on over 2200 individual Utah samples (single leaf or segment), including Gambel oak, canyon maple, Utah juniper and big sagebrush. Three hundred sixty of the juniper experiments were conducted with a small wind tunnel. Both qualitative and quantitative results are discussed here.

5.1 Qualitative Results

5.1.1 Gambel Oak

Because of the shape of the Gambel oak leaves, ignition normally started at the tips of the samples when they were placed horizontally. Several sustained local ignitions from the tips would finally merge into a sustainable flame. On the other hand, for vertical leaf placement, the ignition normally started from the bottom edge closest to the FFB. Generally, these bottom edge ignition flames were intense enough to sustain and propagate towards the center of the leaf. For some runs, hissing sounds were exhibited during the burning. The hissing was explained by relatively slow moisture evaporation from the interior of the leaf sample.

Leaf bending was observed for most of the runs with the sample placed horizontally or vertically. The sample would bend towards the convective gases from the flat-flame burner. After reaching the maximum flame height, the sample would bend quickly backwards until

finally burning out. Figure 5.1 is an example of bending behavior for Gambel oak burning when the sample was placed vertically. It was observed that the sample bent towards the burner (shown as Figure 5.1 (a) to (c)) before achieving the maximum flame height (which was determined as happening at 16.875 s). The same sample then bent up to be vertical during burnout (as shown in Figure 5.1 (d), (e) and (f)). Moreover, Figure 5.2 is an example of horizontally-placed Gambel oak leaf combustion. The sample bent towards the burner against the convective heating gas flow until maximum flame height was achieved (shown as Figure 5.2 (a) to (d)). The sample bent backwards till its original horizontal placement (shown as Figure 5.2 (e) to (g)). However, the sample was eventually detached from the clip (shown as Figure 5.2 (g) and (h)), which can be regarded as formation of a detached brand.

(a) 13.328 s (b) 14.688 s (c) 16.547 s (d) 17.531 s (e) 19.656 s (f) 22.219 s

Numbers indicate the time stamp from the initial time of the experimental run and a yellow was showing the position of leaf sample.

Figure 5.1. Bending behavior of Gambel oak sample placed vertically. The yellow line shows the leaf orientation.

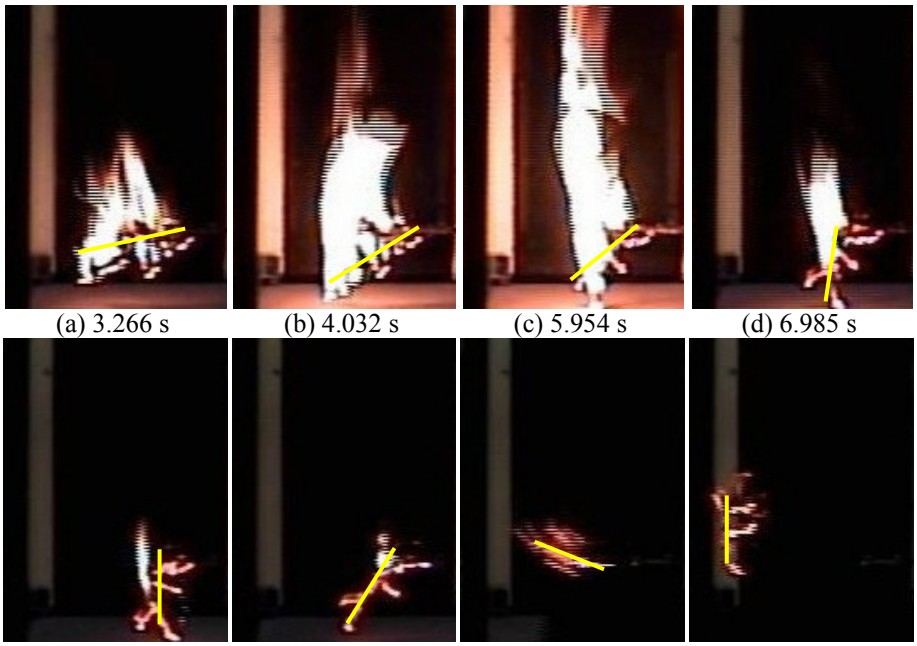

(a) 3.266 s (b) 4.032 s (c) 5.954 s (d) 6.985 s

(e) 9.063 s (f) 12.938 s (g) 16.266 s (h) 16.438 s

Numbers indicate the time stamp from the initial time of the experimental run and a yellow was showing the position of leaf sample.

Figure 5.2. Bending behavior and brand formation of Gambel oak sample placed horizontally. The yellow line shows the leaf orientation.

5.1.2 Canyon Maple

Because maple leaves were thin and exhibited small mass, they rapidly ignited and burned out. When placed vertically, the maple leaf sample mostly ignited from the bottom big saw-tooth tip or edge. When placed horizontally, the maple showed random local ignition sites on the saw-tooth tip. Once the sample ignited, it bent towards the FFB (opposite to the direction of convective gases) and the individual flames coalesced into the maximum flame simultaneously. After this, the sample bent upward and almost burned out.

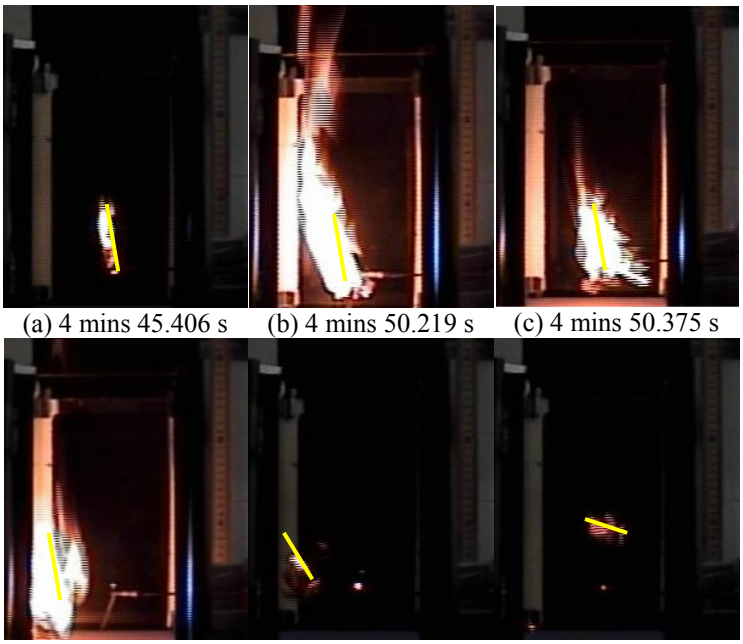

(a) 4 mins 45.406 s (b) 4 mins 50.219 s (c) 4 mins 50.375 s

(d) 4 mins 50.547 s (e) 4 mins 50.875 s (f) 4 mins 51.469 s

Numbers indicate the time stamp from the initial time of the experimental run and a yellow was showing the position of leaf sample.

Figure 5.3. Brand formation of canyon maple placed vertically. The yellow line shows the leaf orientation.

In some runs, the stem or part of leaf which was being held by the clip burned out, which resulted in the whole sample detaching from the clip. Sometimes, there was even brand formation in maple experiments, which is to say that after the pyrolysis, the portion touching the clip was not able to hold the whole leaf sample. For example, in the experimental run shown in Figure 5.3 the sample detached while still undergoing combustion (shown as Figure 5.3 (d) to (f)). It was also observed that the detached section always flew upwards because of the small mass of a single maple leaf (shown as Figure 5.3 (e) to (f)).

5.1.3 **Utah Juniper**

When juniper was burned as a segment, ignition occurred at different tips of the small needles. These small flames with local ignition eventually merged into a sustainable flame and engulfed the entire sample. Since juniper is not a broadleaf sample, no significant bending

behavior was observed. Juniper samples burned intensely, which is thought to be due to the branched structure with high surface to volume ratio. This structure allowed more oxygen and convective gases into the combustion area, which mixed with the natural fuel gases given off by the juniper sample.

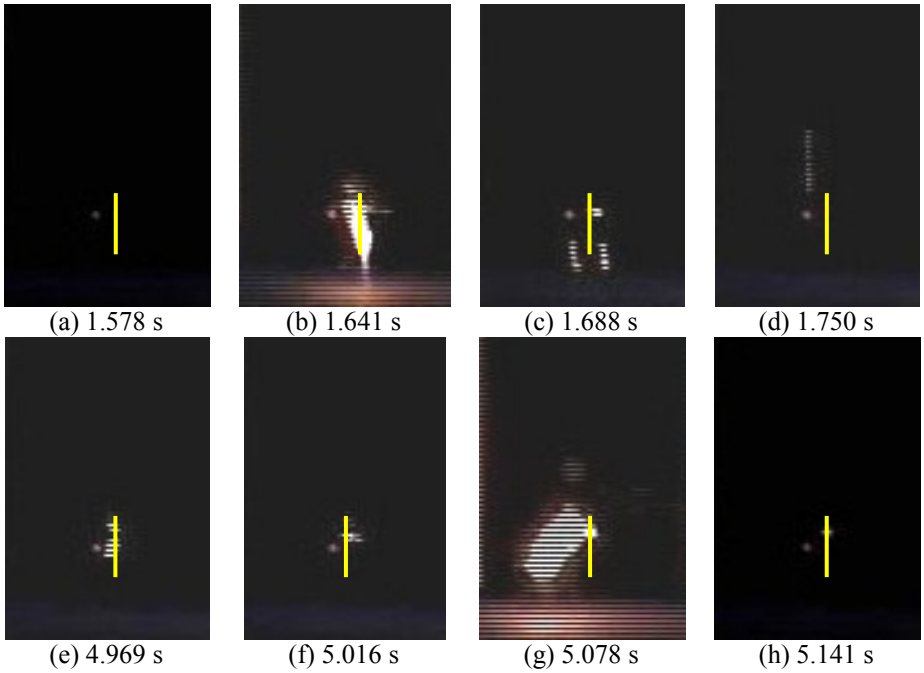

(a) 1.578 s (b) 1.641 s (c) 1.688 s (d) 1.750 s

(e) 4.969 s (f) 5.016 s (g) 5.078 s (h) 5.141 s

Numbers indicate the time stamp from the initial time of the experimental run and a yellow was showing the position of leaf sample.

Figure 5.4. Spark and bursting behavior of Utah juniper sample. The yellow line shows the leaf orientation.

Sparks were often observed before the complete ignition of the sample, as shown in Figure 5.4. The first four frames and last four frames were consecutive frames. These pictures showed the sparks appeared on frame (b) and (g) of Figure 5.4 and disappeared suddenly in next frame. Accompanying the sparks, bursting of small leaf materials was observed (shown in Figure 5.4 (d)). This behavior was always observed for the segment cut from the top section of a juniper branch. Characteristics identified for the top section of juniper included lighter surface

color and different surface structure. Figure 5.5 (a) shows a cut from the top of a juniper branch, which is different from the middle branch cut shown in Figure 5.5 (b).

(a) (b)

Figure 5.5. Comparison of Utah juniper sample cut from (a) the top and (b) the middle of a branch.

5.1.4 **Big Sagebrush**

Sagebrush samples ignited from the trident tip of the leaf for both single leaf combustion runs and segment combustion runs. Sagebrush samples were able to be ignited at high moisture content up to 200%. Segment samples ignited more easily than single leaf samples. This could be explained by larger surface area per volume of leaf exposed to the convective gases.

Brand formation occurred frequently during the combustion of sagebrush, especially for single leaf sample combustion. When brand formation happened and leaf sample might fall off on the FFB or fly away prior to complete burnout. It is shown in Figure 5.6 (e) and (f) that the sample was about to burn out and detached from clip. When this happened, complete combustion behavior could not be achieved. As for combustion of a segment of big sagebrush, when the stems burned out prior to the leaves, a section would detach from the sample (as shown in Figure 5.7 (d), (e), (j) and (h)). Leaf bending was also observed before the ignition of the sample for some experimental runs. Figure 5.7 (a) to (c) showed several leaves of a segment sample bent downwards.

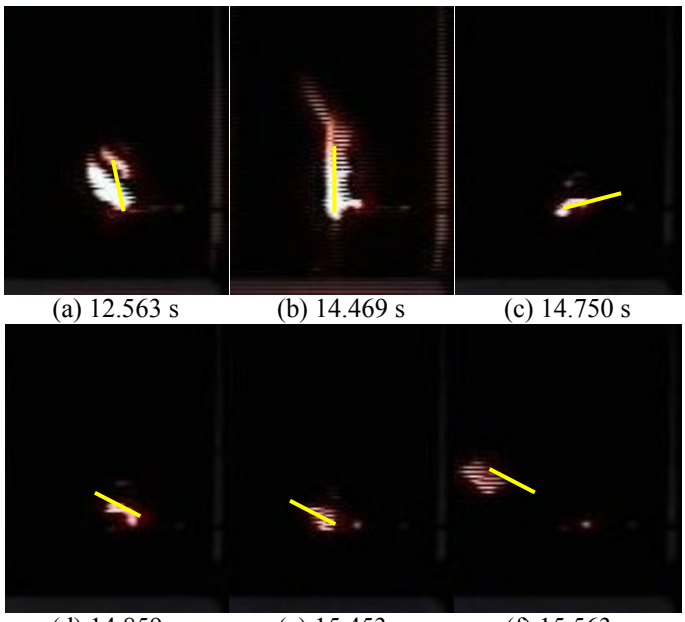

(a) 12.563 s (b) 14.469 s (c) 14.750 s

(d) 14.859 s (e) 15.453 s (f) 15.563 s

Numbers indicate the time stamp from the initial time of the experimental run and a yellow was showing the position of leaf sample.

Figure 5.6. Brand formation of big sagebrush sample placed vertically. The yellow line shows the leaf orientation.

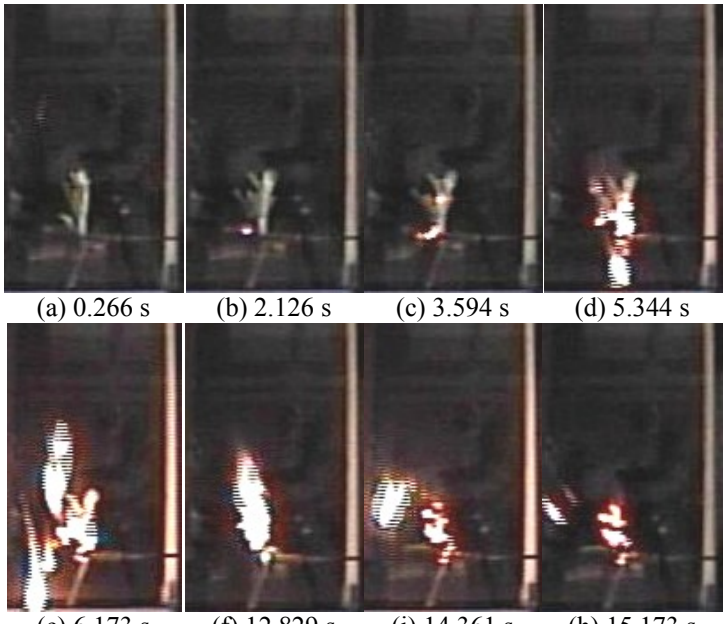

(a) 0.266 s (b) 2.126 s (c) 3.594 s (d) 5.344 s

(e) 6.173 s (f) 12.829 s (j) 14.361 s (h) 15.173 s

Numbers indicate the time stamp from the initial time of the experimental run and a yellow was showing the position of leaf sample.

Figure 5.7. Combustion behavior of big sagebrush segment placed vertically.

5.2 **Quantitative Results**

Leaf geometry variables were measured manually for each leaf or segment prior to measuring combustion characteristics. Regression analysis was conducted to provide correlations which can be used in the bush model developed in the wildfire lab at Brigham Young University.

5.2.1 **Leaf Geometric Properties**

In the semi-empirical bush model developed in the Wildfire Lab, after the bush structure and leaf placement are generated, single leaf dry mass (m_{dry}), leaf thickness (Δx), leaf width (W) and leaf length (L) are assigned to each leaf. These parameters are cross-correlated to obtain a distribution of physical leaf parameters from experimental measurements. The order of predictions for each leaf parameter is shown in the flowchart in Figure 5.8 (b), meaning that Δx can depend on m_{dry}, W can depend on both m_{dry} and Δx, *etc.*.

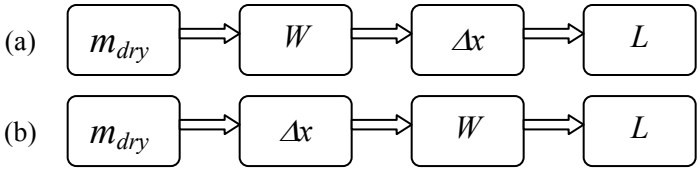

Figure 5.8. Flowchart of leaf physical parameters prediction order: (a) original approach for manzanita, (b) approach used in this project.

5.2.1.1 Single Leaf Dry Mass

Single leaf dry mass (m_{dry}) was utilized as the base indicator for all leaf parameters, and it was well represented by a beta distribution. The total single leaf mass (m_0) for each sample was measured before the experiment run, which can be calculated from:

$$m_0 = m_{dry}(MC + 1) \quad \textbf{(5.1)}$$

where the moisture content (*MC*) is defined by the user of the bush model. In the bush model, the single leaf dry mass (m_{dry}) is randomly chosen from a beta distribution which is curve-fit to the experimental data. First, the probability density function is computed from the following equations:

$$
\begin{aligned}
f(x;\alpha,\beta) &= \frac{x^{\alpha-1}(1-x)^{\beta-1}}{\int_0^1 u^{\alpha-1}(1-u)^{\beta-1}du} \\
&= \frac{\Gamma(\alpha+\beta)}{\Gamma(\alpha)\Gamma(\beta)}x^{\alpha-1}(1-x)^{\beta-1} \\
\alpha &= \bar{x}\left(\frac{\bar{x}(1-\bar{x})}{\nu}-1\right) \\
\beta &= (1-\bar{x})\left(\frac{\bar{x}(1-\bar{x})}{\nu}-1\right)
\end{aligned}
\tag{5.2}
$$

where the $\Gamma(z)$ is the gamma function; the $\bar{x}$ is the single leaf dry mass mean and the ν is the variance of single leaf dry mass (m_{dry}). The cumulative distribution function is calculating according to:

$$
F(x;\alpha,\beta) = \frac{B_x(\alpha,\beta)}{B(\alpha,\beta)} \tag{5.3}
$$

where $B(\alpha,\beta) = \frac{\Gamma(\alpha)\Gamma(\beta)}{\Gamma(\alpha+\beta)}$ and $B_x(\alpha,\beta)$ is the incomplete beta function.

The results of the beta distribution fit for single leaf dry mass (m_{dry}) of different species are summarized in Table 5.1. The goodness of the fit is shown in Figure 5.9. A single leaf was the unit sample for the broadleaf species (Gambel oak and canyon maple) and small segments were used for the non-broadleaf species (Utah juniper and big sagebrush).

Table 5.1. Shape coefficients of single leaf dry mass beta distribution

	α	β
Gambel oak	1.77	3.56
Canyon maple	2.19	4.67
Utah juniper	2.90	3.48
Big sagebrush	3.27	3.57

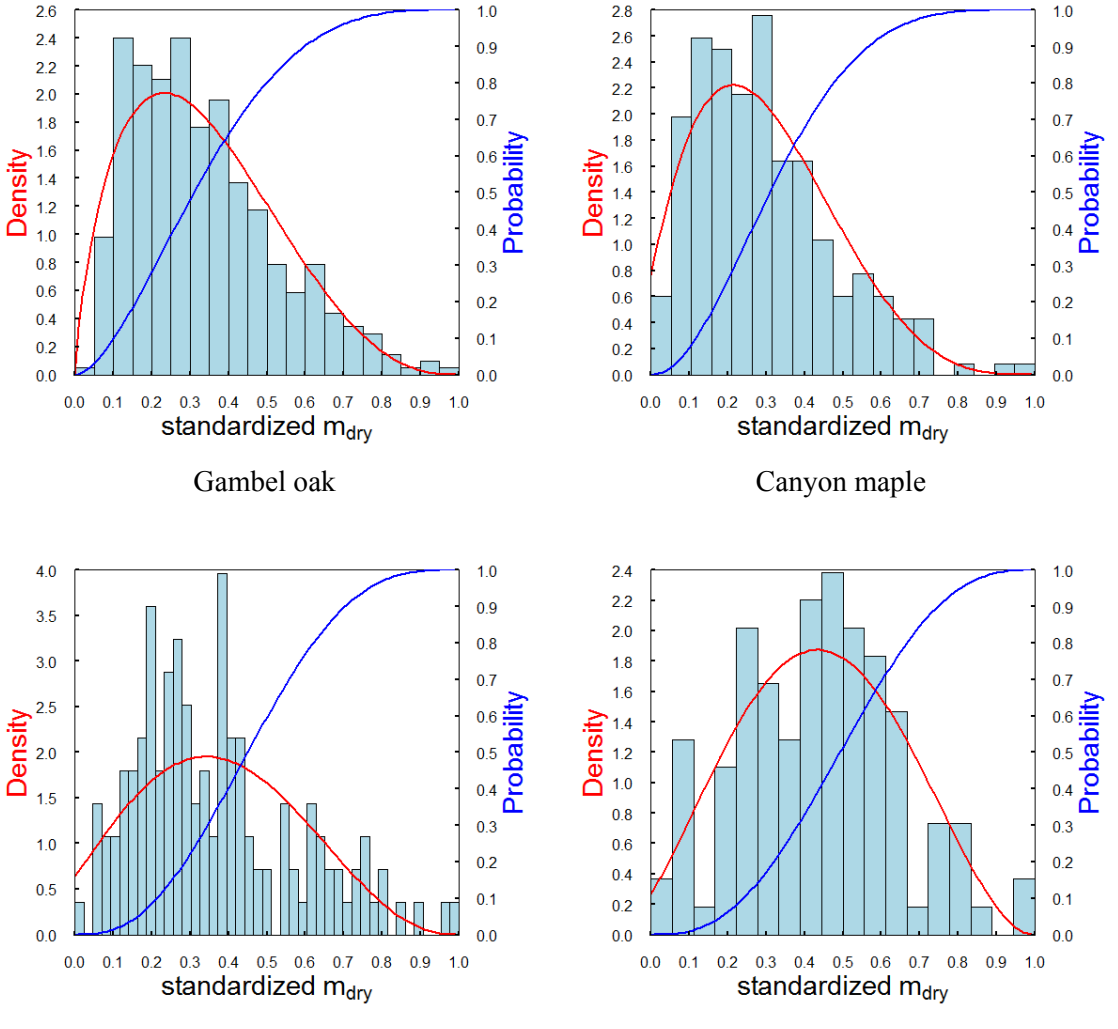

Figure 5.9. Histogram of the experimental leaf dry mass versus the fit to a beta distribution (probability density function (PDF) and the corresponding cumulative distribution function (CDF)).

5.2.1.2 Leaf Thickness

In the previous semi-empirical bush model, thickness (Δx) is predicted after W prediction but before L prediction. Therefore, this equation (shown as Equation (5.4)) will include W as a potential term for Gambel oak and canyon maple. Width was not regarded as a necessary parameter to describe the leaf geometry for Utah juniper and big sagebrush.

$$\Delta x = \beta_0 + \beta_{m_0} \cdot m_0 + \beta_W \cdot W \quad \textbf{(5.4)}$$

The goodness of fit for this original model (Equation (5.4)) was shown in Table 5.2. As shown in Figure 5.8 for this project, Δx was calculated before the prediction of W and L in the semi-empirical bush model. Further regressions with stepwise analysis to minimize the Bayesian information criterion (BIC) values were performed (shown as stepwise equations in Table 5.2) to predict the leaf thickness. The goodness of fit for the stepwise models was better than for the original models, which means even if the W was included as a term for Δx prediction for Gambel oak and canyon maple, the original model did not predict better than the stepwise. Therefore, stepwise models are recommended for Δx prediction in semi-empirical bush models.

5.2.1.3 Leaf Width

The width (W) was predicted after the prediction of m_{dry} before other leaf geometrical properties in the previous semi-empirical bush model. Equation (5.5) is the form originally used in the semi-empirical bush model developed by the wildfire lab. The coefficients fitted for this project are shown as the original equations in Table 5.2.

$$W = \beta_0 + \beta_{m_0} m_0 \quad \textbf{(5.5)}$$

Except for the Utah juniper and big sagebrush, multiple linear regressions were tested by a bidirectional stepwise routine, including the possible terms: moisture content (MC), single leaf mass (m_0), thickness (Δx) and their reasonable transformations. The models with the minimum value of BIC were achieved (shown as the stepwise equation in Table 5.2). Because the goodness of the fit for the stepwise models for prediction of W were still a little better than the original models, the stepwise models for W prediction were therefore used in the semi-empirical bush model.

5.2.1.4 Leaf Length

The length (L) correlation used in the semi-empirical bush model originally developed in the wildfire lab was

$$L = \beta_0 + \beta_{m_0} m_0 + \beta_W W \quad \textbf{(5.6)}$$

According to the experimental data in this research project, parameters were fit for four Utah species to Equation (5.6). Regression results are shown as the original equation in Table 5.2.

Multiple linear regressions with stepwise analysis by minimizing the BIC value were performed to obtain better prediction of the length (L). Possible terms included: moisture content (MC), single leaf mass (m_0), thickness (Δx), width (W), moisture mass (m_{H2O}), dry mass (m_{dry}) and their logarithm transformations, if necessary.

According to the regression results for predicting L the original models did not include fewer terms than the stepwise models. However, the stepwise model for Utah juniper only contained m_{dry} as the significant term in the model. Thus, the stepwise models were used to predict L for these four Utah species in the semi-empirical bush model.

5.2.1.5 Leaf Apparent Dry Density

The leaf apparent dry density (ρ_{leaf}) is defined as the dry mass of a single leaf over the leaf volume (as shown in Equation (5.7)). The value of ρ_{leaf} is calculated for broadleaf species (Gambel oak and canyon maple).

$$\rho_{leaf} = \frac{m_{dry}}{L \cdot W \cdot \Delta x} \tag{5.7}$$

5.2.2 **Combustion Characteristics**

Multiple linear regression was performed to achieve the models for prediction of combustion characteristics, including time to ignition (t_{ig}, in seconds), time to maximum flame height (t_{fh}, in seconds), time of flame duration (t_{fd}, in seconds), maximum flame height ($h_{f,max}$, in cm), time to maximum flame height (t_{fh}, in seconds), etc. The possible independent variables included: width (W, in cm), length (L, in cm), thickness (Δx), total single leaf mass (m_0), dry mass (m_{dry}), moisture mass (m_{H2O}) and moisture content (MC). The stepwise regression with bidirectional elimination was used to achieve the statistical best models based on Bayesian information criterion (BIC). Some nonlinear regression equations and specific equations suggested by the combustion mechanism were also fitted and compared to the statistically best models.

Table 5.2. Summary of regression analysis on leaf geometrical properties for Utah species.

Species			Predictive Equation	MSE	R^2
Gambel oak	*W*	Stepwise*:	$W = 3.51 - 7.68 \cdot \Delta x + 11.96 \cdot m_{dry} + 3.76 \cdot m_{H2O}$	0.63	0.73
		Original:	$W = 2.05 + 7.27 \cdot m_0$	0.79	0.66
	L	Stepwise*:	$L = 10.16 + 0.26 \cdot W + 1.56 \cdot Ln(m_{dry}) + 0.50 \cdot Ln(m_{H2O})$	0.76	0.77
		Original:	$L = 3.13 + 5.68 \cdot m_0 + 0.41 \cdot W + 2.17 \cdot \Delta x$	0.91	0.73
	Δx	Stepwise*:	$\Delta x = 0.27 + 0.052 \cdot MC + 0.035 \cdot Ln(m_{dry})$	0.0012	0.35
		Original:	$\Delta x = 0.23 + 0.23 \cdot m_0 - 0.015 \cdot W$	0.0012	0.35
Canyon maple	*W*	Stepwise*:	$W = 11.72 - 0.81 \cdot MC - 10.66 \cdot \Delta x + 9.51 \cdot m_{dry} + 1.67 \cdot Ln(m_{H2O})$	0.45	0.81
		Original:	$W = 4.36 + 10.06 \cdot m_0$	0.66	0.73
	L	Stepwise*:	$L = 6.82 - 1.19 \cdot MC + 0.30 \cdot W + 1.01 \cdot Ln(m_{H2O})$	0.37	0.74
		Original:	$L = 2.70 + 4.36 \cdot m_0 + 0.33 \cdot W - 4.17 \cdot \Delta x$	0.38	0.73
	Δx	Stepwise*:	$\Delta x = 0.067 + 0.046 \cdot MC + 0.21 \cdot m_{dry}$	0.0006	0.37
		Original:	$\Delta x = 0.16 + 0.23 \cdot m_0 - 0.012 \cdot W$	0.0006	0.36
Utah juniper	*L*	Stepwise*:	$L = 5.54 + 1.01 \cdot Ln(m_{dry})$	0.21	0.46
		Original:	$L = 2.57 + 4.37 \cdot m_0 - 0.17 \cdot \Delta x$	0.22	0.43
	Δx	Stepwise*:	$\Delta x = 0.88 + 0.50 \cdot MC + 0.62 \cdot m_{dry}$	0.033	0.21
		Original:	$\Delta x = 1.29 + 0.46 \cdot m_0$	0.040	0.047
Big sagebrush	*L*	Stepwise:	$L = 5.54 - 4.92 \cdot \Delta x + 8.66 \cdot m_{H2O}$	0.72	0.49
		Original:	$L = 5.23 + 5.70 \cdot m_0 - 4.60 \cdot \Delta x$	0.72	0.46
	Δx	Stepwise:	$\Delta x = 0.24 + 0.59 \cdot m_{dry}$	0.0043	0.14
		Original:	$\Delta x = 0.26 + 0.16 \cdot m_0$	0.0040	0.12

*Equation used in the bush combustion model.

5.2.2.1 Time to Ignition

Time to ignition (t_{ig}) is defined as the time difference between exposure to heat flux and ignition. The moment of exposure to heat flux is defined as when the gas temperature of the fuel is over a certain temperature. The critical temperature of 200°C was chosen the start event in this project, which is the gas temperature near the sample when the FFB is pulled under the sample. The moment of ignition is defined as the time when the first spark occurred which led to a sustainable flame.

Smith (2005) explored the effect of thickness on t_{ig}. Values of t_{ig} are plotted versus thickness for the experimental data in this project (shown in Figure 5.10). The data appeared scattered and a linear correlation was not significant. The linear regressions of t_{ig} versus Δx for Utah species for the data in this project are shown in Table 5.3. Only the slope for Gambel oak and big sagebrush was significant, though their values of R^2 were fairly small. These results also verified the conclusion drawn by (Fletcher et al., 2007) that thickness slightly influenced t_{ig}. Pickett (2008) concluded a linear correlation for t_{ig} versus Δx as well where only the slope for sagebrush was significant and the slopes for Utah species were different from the slopes shown in Table 5.3. The reason might be the differences among the definitions of initial time and differences in experimental apparatus.

Table 5.3. Linear regressions of the time to ignition versus leaf thickness for Utah species.

	intercept	slope	R^2
Gambel oak (horizontal leaf placement)	-1.23±0.62*	11.05±2.49*	0.32
Gambel oak (vertical leaf placement)	0.24±1.6	10.11±6.67*	0.037
Canyon maple (horizontal leaf placement)	0.46±0.48	2.67±3.40	0.027
Canyon maple (vertical leaf placement)	0.38±055	4.77±3.83	0.042
Utah juniper	3.55±1.97*	0.50±1.43	0.0035
Utah juniper (with wind)	2.68±1.46*	0.66±1.02	0.0085
Big sagebrush	-1.18±1.19	10.65±3.81*	0.22

± indicates the 95% confidence interval
*** indicates the term is significant (p-value < 0.05)**

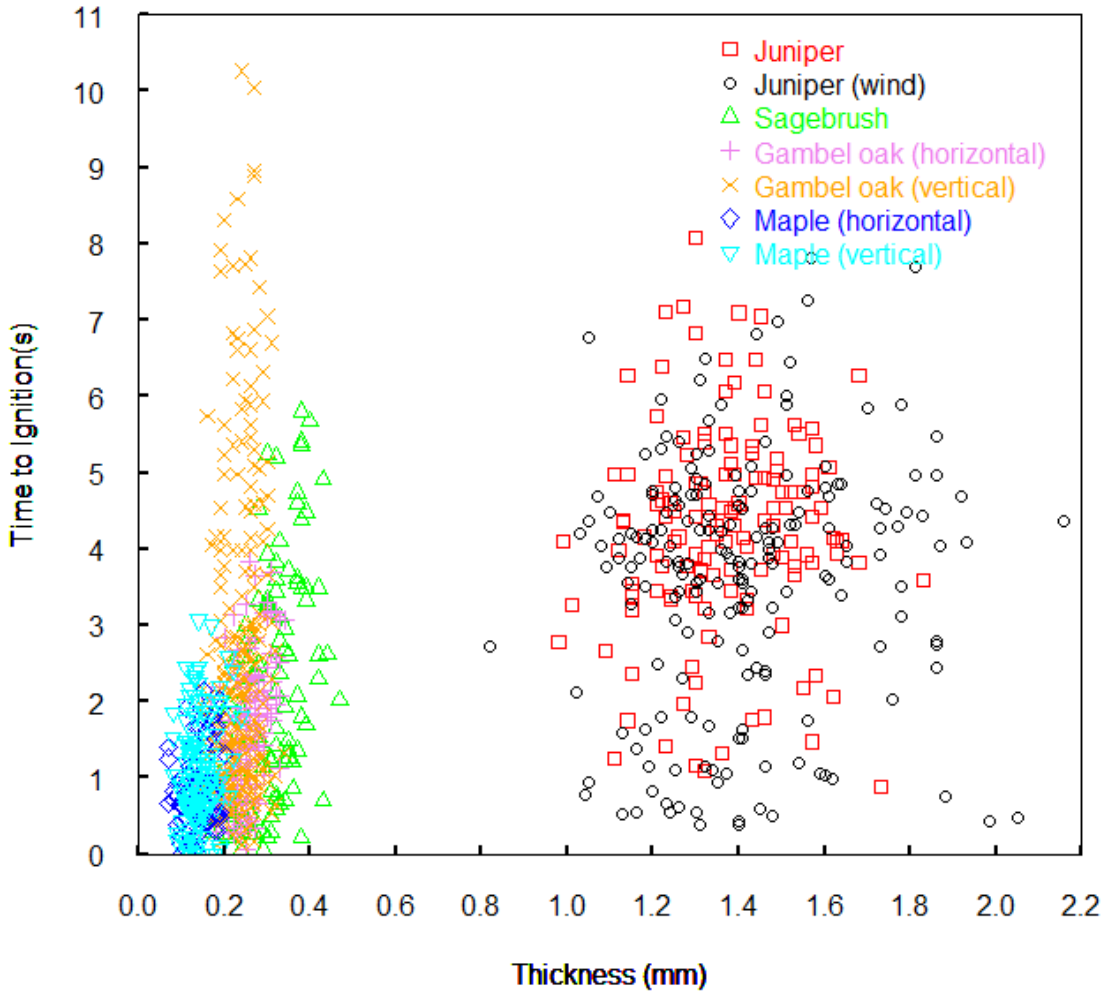

Figure 5.10. Time to ignition versus thickness for Gambel oak, canyon maple, Utah juniper and big sagebrush.

Fletcher et al. (2007) also mentioned that m_{H2O} hardly affected t_{ig}. According to the plots of t_{ig} versus m_{H2O} for experimental data in this research project (Figure 5.11) and the linear regression of t_{ig} versus m_{H2O} showed in Table 5.4, m_{H2O} did not significantly influence t_{ig}.

Table 5.4. Linear regressions of the time to ignition versus leaf moisture mass for Utah species.

	intercept	slope	R^2
Gambel oak (horizontal leaf placement)	0.89±0.21*	4.70±1.36*	0.22
Gambel oak (vertical leaf placement)	2.21±0.51*	2.98±3.37	0.013
Canyon maple (horizontal leaf placement)	0.71±0.20*	0.92±1.31	0.021
Canyon maple (vertical leaf placement)	0.81±0.24*	2.062±1.78*	0.036
Utah juniper	4.26±0.56*	-0.24±5.38	5.59E-5
Utah juniper (with wind)	3.50±0.56*	1.05±4.69	0.001
Big sagebrush	0.80±0.43*	7.74±2.16*	0.32

± indicates the 95% confidence interval
*** indicates the term is significant (p-value < 0.05)**

Other variables were considered to correlate with t_{ig}. The regression analysis for time to ignition (t_{ig}) is summarized in Table 5.5. The following equation (shown as 2nd alternate model in Table 5.5 was suggested by Smith (2005) to combine Δx and m_{H2O} as independent variables for predicting $t_{ig.}$

$$t_{ig} = \beta_0 + \beta_{\Delta x} \cdot \Delta x + \beta_{m_{H2O}} \cdot \Delta H_{vap} \cdot m_{H2O} \quad \textbf{(5.8)}$$

Another suggested model (shown as Equation (5.9) and 1st alternate model in Table 5.5) was the model originally used for manzanita combustion in the semi-empirical bush model:

$$t_{ig} = \beta_0 + \beta_{MC} \cdot MC - \beta_{\Delta x} \cdot \Delta x - \beta_{m_0} \cdot m_0 \quad \textbf{(5.9)}$$

However, the regression results indicated that the stepwise model is always statistically better than other two alternate models for all species. The 1st alternate model can be a substitute for the stepwise model for canyon maple and horizontally-placed Gambel oak leaf models due to their similar goodness of fit. It was also observed that the goodness of the fit for the Utah juniper model was not quite satisfactory because the datasets of t_{ig} for juniper were fairly scattered.

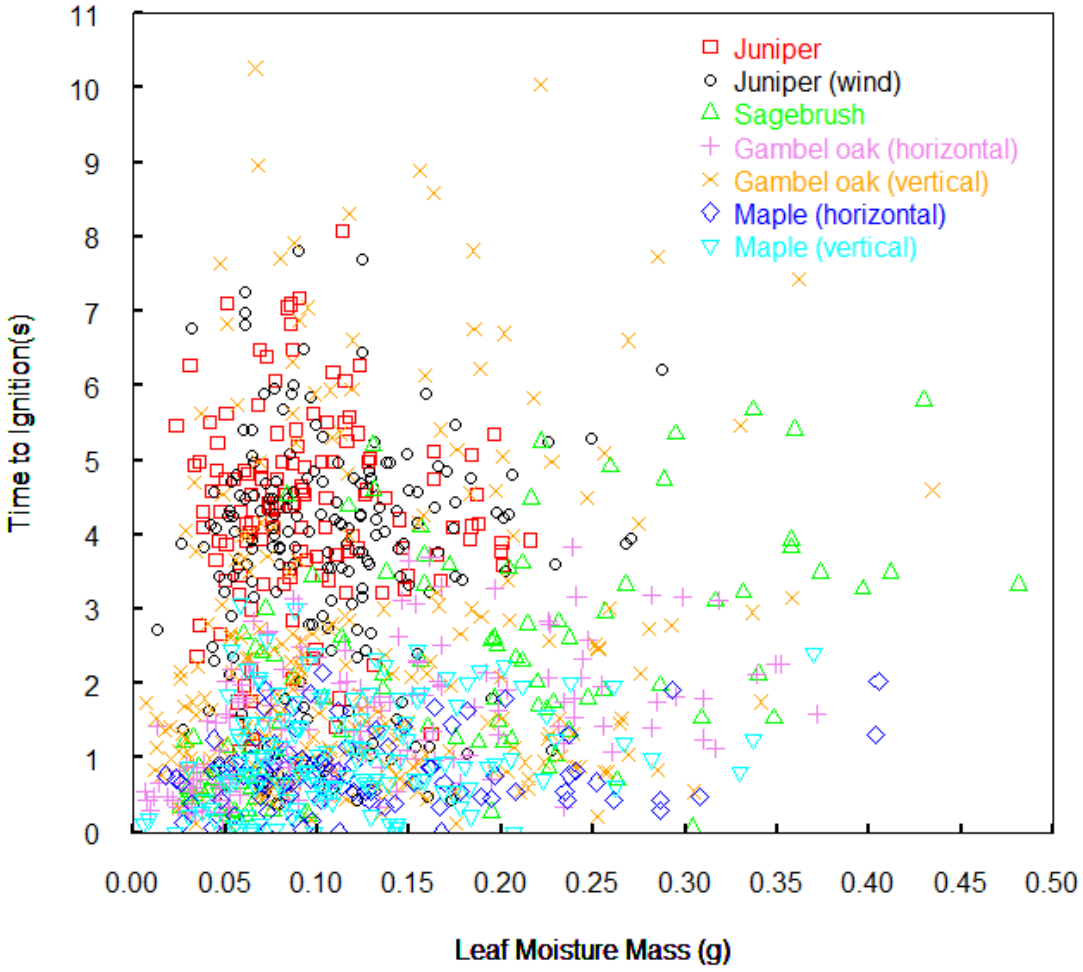

Figure 5.11. Time to ignition versus leaf moisture mass for Gambel oak, canyon maple, Utah juniper and big sagebrush.

5.2.2.2 Time of Flame Duration

The burnout was defined as the moment when the last flash of the sustainable flame was observed. The time of flame duration (t_{fd}) is the time difference between the moment of ignition and the moment of burnout. The time to burnout (t_{brn}) is the time difference between the start time (time of exposure to the heat flux) and the moment of burnout.

Table 5.5. Summary of regression analysis on time to ignition (t_{ig}) for Utah species.

Species		Predictive Equation	MSE	R^2
Gambel oak (horizontal leaf placement)	Stepwise*:	$t_{ig} = -1.15 + 1.59 \cdot MC - 0.094 \cdot W + 7.13 \cdot \Delta x$	0.32	0.58
	1st Alternate:	$t_{ig} = -1.42 + 1.68 \cdot MC + 6.98 \cdot \Delta x - 0.42 \cdot m_0$	0.32	0.57
	2nd Alternate:	$t_{ig} = -0.90 + 8.74 \cdot \Delta x + 0.82 \times 10^{-3} \cdot \Delta H_{vap} \cdot m_{H2O}$	0.50	0.34
Gambel oak (vertical leaf placement)	Stepwise:	$t_{ig} = 3.13 + 4.11 \cdot MC - 0.79 \cdot W - 0.39 \cdot L + 15.88 \cdot m_{dry}$	3.09	0.34
	1st Alternate:	$t_{ig} = -1.25 + 2.94 \cdot MC + 9.24 \cdot \Delta x - 1.50 \cdot m_0$	3.89	0.17
	2nd Alternate:	$t_{ig} = 0.32 + 9.23 \cdot \Delta x + 0.46 \times 10^{-3} \cdot \Delta H_{vap} \cdot m_{H2O}$	4.49	0.037
Canyon maple (horizontal leaf placement)	Stepwise*:	$t_{ig} = 0.92 + 0.86 \cdot Ln(MC)$	0.15	0.40
	1st Alternate:	$t_{ig} = -0.11 + 1.01 \cdot MC + 0.31 \cdot \Delta x - 0.26 \cdot m_0$	0.15	0.41
	2nd Alternate:	$t_{ig} = 0.50 + 2.04 \cdot \Delta x + 0.14 \times 10^{-3} \cdot \Delta H_{vap} \cdot m_{H2O}$	0.25	0.028
Canyon maple (vertical leaf placement)	Stepwise:	$t_{ig} = 2.11 + 0.97 \cdot Ln(MC) - 0.17 \cdot L$	0.30	0.40
	1st Alternate:	$t_{ig} = -0.07 + 1.43 \cdot MC - 0.34 \cdot \Delta x - 0.80 \cdot m_0$	0.32	0.38
	2nd Alternate:	$t_{ig} = 0.40 + 3.48 \cdot \Delta x + 0.60 \times 10^{-3} \cdot \Delta H_{vap} \cdot m_{H2O}$	0.48	0.05
Utah juniper	Stepwise*:	$t_{ig} = 4.24$	1.84	NA
	1st Alternate:	$t_{ig} = 3.42 + 0.43 \cdot MC + 0.43 \cdot \Delta x - 0.83 \cdot m_0$	1.87	0.0070
	2nd Alternate:	$t_{ig} = 3.51 + 0.61 \cdot \Delta x - 0.48 \times 10^{-3} \cdot \Delta H_{vap} \cdot m_{H2O}$	1.86	0.0045
Utah juniper (with wind blowing)	Stepwise:	$t_{ig} = 4.75 - 0.44 \cdot U - 18.06 \cdot m_{dry} + 18.03 \cdot m_{H2O}$	2.37	0.13
	1st Alternate:	$t_{ig} = 2.03 + 2.87 \cdot MC - 0.31 \cdot \Delta x - 1.68 \cdot m_0$	2.45	0.10
	2nd Alternate:	$t_{ig} = 2.67 + 0.64 \cdot \Delta x + 0.14 \times 10^{-3} \cdot \Delta H_{vap} \cdot m_{H2O}$	2.68	0.0086
Big sagebrush segment	Stepwise:	$t_{ig} = 0.49 + 1.25 \cdot MC - 0.46 \cdot L + 4.88 \cdot \Delta x + 5.78 \cdot m_{H2O}$	0.92	0.63
	1st Alternate:	$t_{ig} = -2.05 + 0.95 \cdot MC + 7.83 \cdot \Delta x + 1.31 \cdot m_0$	1.22	0.48
	2nd Alternate:	$t_{ig} = -1.24 + 7.41 \cdot \Delta x + 2.81 \times 10^{-3} \cdot \Delta H_{vap} \cdot m_{H2O}$	1.35	0.42

$\Delta H_{vap} (= 2256.9 \ \frac{kJ}{kg})$ is the heat of vaporization of water.

*Equation used in the bush combustion model.

Pickett (2008) as well as Fletcher et al. (2007) suggested correlating t_{fd} with the amount of volatile mass (m_{vm}), which is regarded as the fuel available in the leaf. Volatile mass was calculated from the following equation:

$$m_{vm} = VMC \cdot m_{dry} \quad \textbf{(5.10)}$$

Where *VMC* is the volatile matter content (%) which is a species-specific constant. The *VMC* constants were obtained from the Utah foliage analyses by Fletcher et al. (2007) (shown in the Table 4.1). Values of t_{fd} are plotted versus m_{vm} in Figure 5.12. The results for linear regression of t_{fd} versus m_{vm} are summarized in Table 5.6.

Table 5.6. Linear regressions of the time of flame duration versus leaf volatile mass for Utah species

	intercept	slope	R^2
Gambel oak (horizontal leaf placement)	2.60±0.57*	27.92±3.74*	0.57
Gambel oak (vertical leaf placement)	4.18±0.78*	30.22±4.51*	0.42
Canyon maple (horizontal leaf placement)	2.88±0.37*	15.15±2.68*	0.59
Canyon maple (vertical leaf placement)	3.28±0.52*	15.26±4.49*	0.25
Utah juniper	9.30±1.24*	61.32±13.28*	0.38
Utah juniper (with wind)	10.46±1.13*	47.76±9.54*	0.34
Big sagebrush	0.63±2.79	101.4±27.15*	0.34

± indicates the 95% confidence interval
*** indicates the term is significant (p-value < 0.05)**

It was observed that the slopes for linear regression of t_{fd} versus m_{vm} were significant for all the species. The values of R^2 shown in Table 5.6 indicated that the predictions for horizontal leaves were better than for vertical leaves, while Gambel oak and maple models predicted t_{fd} better than the juniper and big sagebrush models.

Table 5.7. Summary of regression analysis on time of flame duration (t_{fd}) for Utah species.

Species		Predictive Equation	MSE	R^2
Gambel oak (horizontal leaf placement)	1st Stepwise*:	$t_{fd} = 3.05 + 1.02 \cdot Ln(MC) + 22.82 \cdot m_{dry}$	3.11	0.61
	1st Alternate:	$t_{fd} = 1.54 - 0.07 \cdot Ln(MC) + 5.34 \cdot \Delta x + 12.13 \cdot m_0$	3.11	0.61
	2nd Stepwise:	$Ln(t_{fd}) = 3.64 + 0.20 \cdot Ln(MC) - 0.06 \cdot L + 0.70 \cdot Ln(m_{dry})$	0.06	0.67
Gambel oak (vertical leaf placement)	1st Stepwise:	$t_{fd} = -5.50 + 1.10 \cdot Ln(MC) + 1.29 \cdot W + 0.31 \cdot L + 28.12 \cdot \Delta x$	5.46	0.65
	1st Alternate:	$t_{fd} = 0.10 + 0.76 \cdot Ln(MC) + 19.81 \cdot \Delta x + 14.04 \cdot m_0$	7.02	0.55
	2nd Stepwise:	$Ln(t_{fd}) = 0.14 + 0.14 \cdot Ln(MC) + 0.14 \cdot W + 0.07 \cdot L + 3.63 \cdot \Delta x$	0.08	0.68
Canyon maple (horizontal leaf placement)	1st Stepwise*:	$t_{fd} = 1.44 + 12.44 \cdot \Delta x + 6.78 \cdot m_{dry} + 4.49 \cdot m_{H2O}$	0.57	0.71
	1st Alternate:	$t_{fd} = 1.35 - 0.23 \cdot Ln(MC) + 13.17 \cdot \Delta x + 5.55 \cdot m_0$	0.57	0.71
	2nd Stepwise:	$Ln(t_{fd}) = 1.69 + 3.25 \cdot \Delta x + 0.30 \cdot Ln(m_{dry})$	0.03	0.72
Canyon maple (vertical leaf placement)	1st Stepwise:	$t_{fd} = 5.52 + 0.71 \cdot Ln(MC) + 0.39 \cdot W - 0.38 \cdot L + 9.19 \cdot \Delta x + 1.14 \cdot Ln(m_{dry})$	1.28	0.43
	1st Alternate:	$t_{fd} = 2.67 + 0.48 \cdot Ln(MC) + 5.31 \cdot \Delta x + 6.26 \cdot m_0$	1.42	0.35
	2nd Stepwise:	$Ln(t_{fd}) = 2.34 + 0.25 \cdot Ln(MC) + 0.36 \cdot Ln(m_{dry})$	0.06	0.40
Utah juniper	1st Stepwise*:	$t_{fd} = 5.21 + 3.24 \cdot \Delta x + 53.00 \cdot m_{H2O}$	6.01	0.51
	1st Alternate:	$t_{fd} = 5.74 + 2.92 \cdot Ln(MC) + 3.15 \cdot \Delta x + 24.92 \cdot m_0$	6.06	0.51
	2nd Stepwise:	$Ln(t_{fd}) = 2.35 + 0.41 \cdot Ln(MC) + 3.44 \cdot m_{dry}$	0.03	0.49
Utah juniper (with wind blowing)	1st Stepwise:	$t_{fd} = 10.42 + 20.46 \cdot m_{dry} + 24.31 \cdot m_{H2O}$	8.63	0.37
	1st Alternate:	$t_{fd} = 7.73 - 0.34 \cdot Ln(MC) + 1.92 \cdot \Delta x + 21.83 \cdot m_0$	8.52	0.38
	2nd Stepwise:	$Ln(t_{fd}) = 2.35 + 0.05 \cdot U + 2.69 \cdot m_{H2O}$	0.04	0.37
Big sagebrush segment	1st Stepwise:	$t_{fd} = -0.56 - 1.28 \cdot L + 25.04 \cdot \Delta x + 96.53 \cdot m_{H2O}$	18.26	0.57
	1st Alternate:	$t_{fd} = -7.45 - 4.95 \cdot Ln(MC) + 41.88 \cdot \Delta x + 21.59 \cdot m_0$	24.29	0.43
	2nd Stepwise:	$Ln(t_{fd}) = 1.17 - 0.12 \cdot L + 2.33 \cdot \Delta x + 8.73 \cdot m_{dry}$	0.14	0.59

*Equation used in the bush combustion model.

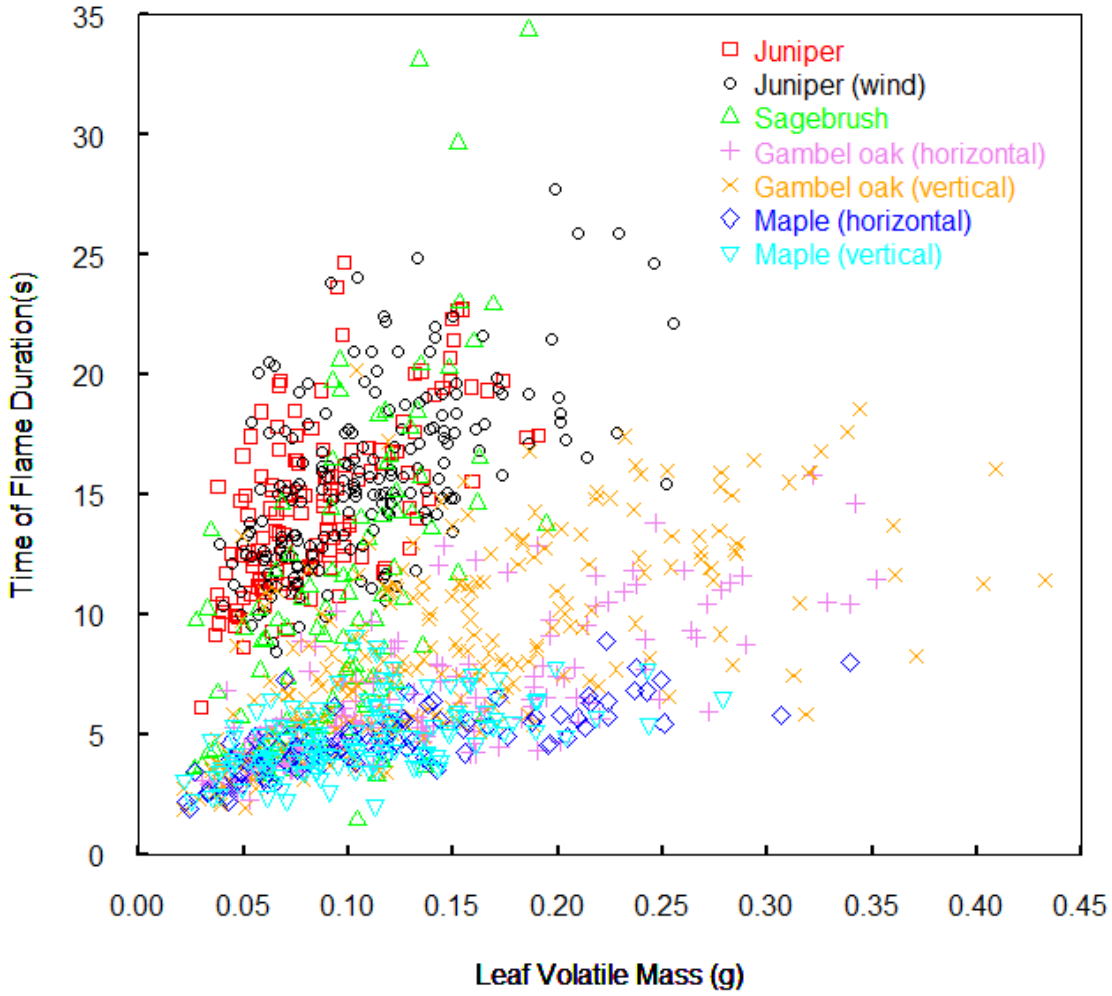

Figure 5.12. Time of flame duration versus leaf volatile mass for Gambel oak, canyon maple, Utah juniper and big sagebrush.

In order to obtain an optimized model for prediction of t_{fd}, stepwise multiple linear regressions were performed. Since *VMC* was treated as a constant for certain species in this research, and due to the ease of obtaining m_{dry}, m_{dry} was chosen as one of the possible independent variables in the regression for t_{fd}. The regression analysis of t_{fd} is summarized in Table 5.7. The 1st alternate equation was the original equation for Manzanita leaves in the semi-empirical bush model, which form is shown in Equation (5.11).

$$t_{fd} = \beta_0 + \beta_{Ln(MC)} \cdot Ln(MC) + \beta_{\Delta x} \cdot \Delta x + \beta_{m_0} \cdot m_0 \quad \textbf{(5.11)}$$

Due to the partial residual plots and the distributions of datasets for t_{fd}, stepwise regressions were conducted using the natural logarithm of t_{fd} (shown as 2nd stepwise model in Table 5.7). The values of R^2 were close to each other between those three types of regression; while the MSE of 2nd stepwise model was always much lower than that of other two models. Either of these two types of stepwise model could be used in the semi-empirical bush model. In the semi-empirical bush combustion model, the first stepwise model was use due to its ease of computation.

5.2.2.3 Maximum Flame Height

A maximum flame height ($h_{f,max}$) during combustion of each live fuel sample was determined from the video images processed by the MATLAB routine developed in wildfire lab at BYU. It was expected that $h_{f,max}$ would linearly correlate with m_{vm} (Fletcher et al., 2007; Pickett, 2008). This linear relationship was also explored and summarized in this research (shown in Figure 5.13 and Table 5.8). The results indicated that the slopes were significant for all the species. However, it also showed that only the R^2 for canyon maple with horizontal leaf placement was larger than 0.5, and that the R^2 for big sagebrush was less than 0.1.

Table 5.8. Linear regressions of the maximum flame height versus leaf volatile mass for Utah species.

	intercept	slope	R^2
Gambel oak (horizontal leaf placement)	12.07±1.63*	54.38±10.65*	0.38
Gambel oak (vertical leaf placement)	10.26±1.43*	41.45±8.27*	0.29
Canyon maple (horizontal leaf placement)	8.29±1.44*	76.46±10.41*	0.70
Canyon maple (vertical leaf placement)	7.43±2.01*	87.26±17.36*	0.42
Utah juniper	3.89±0.87*	46.37±9.27*	0.42
Utah juniper (with wind)	4.28±0.73*	29.09±6.20*	0.31
Big sagebrush	8.26±2.29*	27.28±22.28*	0.05

± indicates the 95% confidence interval
*** indicates the term is significant (p-value < 0.05)**

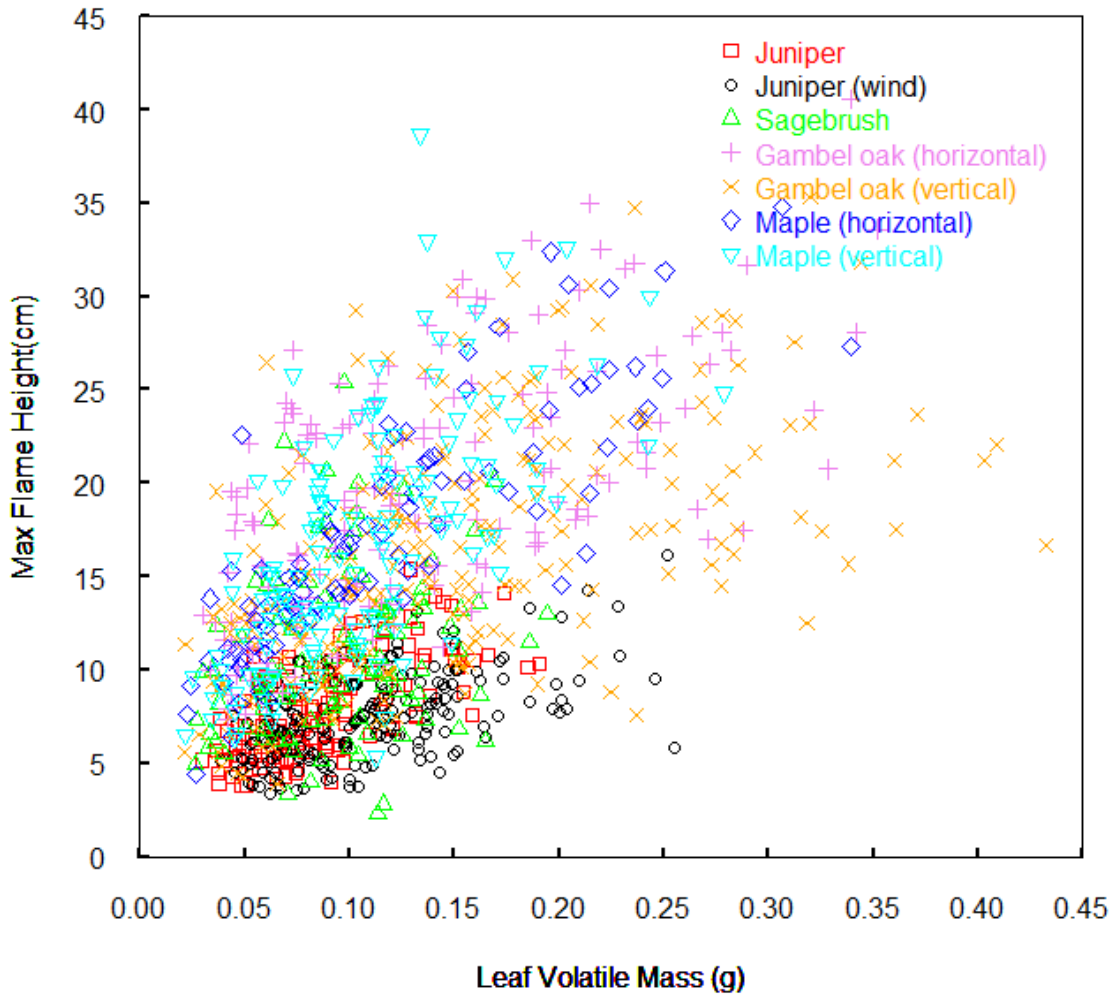

Figure 5.13. Maximum flame height versus leaf volatile mass for Gambel oak, canyon maple, Utah juniper and big sagebrush.

In order to achieve better prediction of $h_{f,max}$, regression analysis was performed and summarized in Table 5.10. The 1st alternate equation was the original equation for a manzanita leaf in the semi-empirical bush model, with the form shown in Equation (5.12).

$$h_{f,max} = \beta_0 + \beta_{m_{dry}} \cdot m_{dry} + \beta_{\Delta x} \cdot \Delta x + \beta_{m_0} \cdot m_0 \qquad \textbf{(5.12)}$$

The 2nd alternate equation included ρ_{leaf}, L and m_{H2O} for the Gambel oak and canyon maple models (shown as Equation (5.13 (a))) as well as m_{dry}, L and m_{H2O} for Utah juniper and big sagebrush models (shown as Equation (5.13 (b))). Wind speed (m/s) was also included as a term in the prediction model for Utah juniper combustion with wind.

$$\text{(a)} \quad h_{f,max} = \beta_0 + \beta_{\rho_{leaf}} \cdot \rho_{leaf} + \beta_L \cdot L + \beta_{m_{H2O}} \cdot m_{H2O}$$
$$\text{(b)} \quad h_{f,max} = \beta_0 + \beta_{m_{dry}} \cdot m_{dry} + \beta_L \cdot L + \beta_{m_{H2O}} \cdot m_{H2O} \qquad \textbf{(5.13)}$$

Stepwise multiple linear regressions were performed for $h_{f,max}$ and its logarithmic form (shown as the 1st and 2nd stepwise models in Table 5.10). The MSE of the 2nd stepwise models were always the lowest, and the goodness of the fit for these two types of stepwise models was almost always better than that of the alternate models. For Gambel oak and canyon maple, the horizontal models were better than the vertical models, which might be because the temperature of the sample surface was more uniform during the horizontal leaf experiments.

5.2.2.4 Time to Maximum Flame Height

The time to maximum flame height (t_{fh}) was defined as the amount of time from the moment of ignition to the moment of reaching the maximum flame height. It was expected that there is a linear relationship between t_{fh} and m_{vm} as well, which was plotted for the datasets in this research project (shown as Figure 5.14). The linear regression of t_{fh} versus m_{vm} was shown in Table 5.9. It was observed that although the slopes for the linear regression were usually significant for Utah species, the values of R^2 were all quite low. These results indicated that it is not sufficient to predict t_{fh} from a linear relationship with m_{vm}. More independent variables should be included into the prediction model.

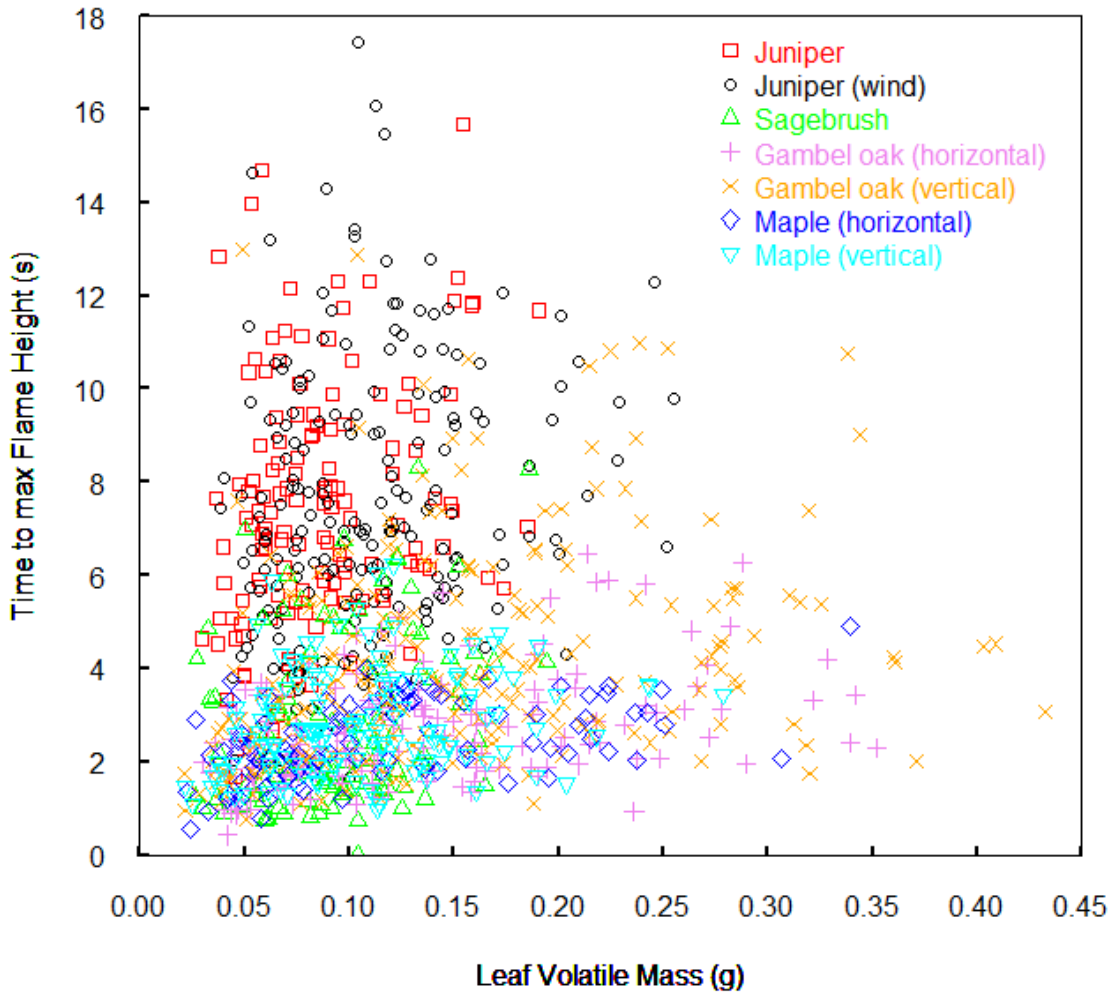

Figure 5.14. Time to maximum flame height versus leaf volatile mass for Gambel oak, canyon maple, Utah juniper and big sagebrush.

Table 5.9. Linear regressions of time to maximum flame height versus leaf volatile mass for Utah species.

	intercept	slope	R^2
Gambel oak (horizontal leaf placement)	1.81±0.34*	6.60±2.20*	0.18
Gambel oak (vertical leaf placement)	3.08±0.59*	7.31±3.39*	0.07
Canyon maple (horizontal leaf placement)	1.85±0.31*	5.41±2.28*	0.20
Canyon maple (vertical leaf placement)	2.33±0.44*	4.85±3.81	0.04
Utah juniper	5.83±1.16*	18.61±12.41*	0.06
Utah juniper (with wind)	6.17±1.08*	12.76±9.10	0.04
Big sagebrush	1.52±0.94*	13.93±9.15*	0.08

± indicates the 95% confidence interval
*** indicates the term is significant (p-value < 0.05)**

Table 5.10. Summary of regression analysis on maximum flame height ($h_{f,max}$) for Utah species.

Species		Predictive Equation	MSE	R^2
Gambel oak (Horizontal leaf placement)	1st Stepwise*:	$h_{f,max} = 2.24 - 9.15 \cdot MC + 2.04 \cdot W + 1.54 \cdot L + 24.55 \cdot \Delta x$	15.93	0.65
	2nd Stepwise:	$Ln(h_{f,max}) = 4.49 - 0.18 \cdot Ln(MC) - 2.53 \cdot \Delta x + 0.52 \cdot Ln(m_{dry})$	0.05	0.60
	1st Alternate:	$h_{f,max} = 17.50 + 138.5 \cdot m_{dry} - 26.07 \cdot \Delta x - 48.80 \cdot m_0$	18.31	0.59
	2nd Alternate:	$h_{f,max} = -14.21 + 41.15 \cdot \rho_{leaf} + 4.11 \cdot L - 35.14 \cdot m_{H2O}$	21.39	0.52
Gambel oak (Vertical leaf placement)	1st Stepwise:	$h_{f,max} = 3.09 - 6.35 \cdot MC + 1.39 \cdot W + 1.98 \cdot L - 14.43 \cdot m_{dry}$	21.76	0.49
	2nd Stepwise:	$Ln(h_{f,max}) = 1.59 - 0.13 \cdot Ln(MC) + 0.07 \cdot W + 0.10 \cdot L$	0.10	0.46
	1st Alternate:	$h_{f,max} = 14.85 + 36.21 \cdot m_{dry} - 22.89 \cdot \Delta x + 1.44 \cdot m_0$	29.51	0.30
	2nd Alternate:	$h_{f,max} = -3.10 + 7.06 \cdot \rho_{leaf} + 2.66 \cdot L - 11.07 \cdot m_{H2O}$	25.24	0.40
Canyon maple (Horizontal leaf placement)	1st Stepwise*:	$h_{f,max} = -21.55 + 2.68 \cdot W + 1.37 \cdot L + 62.14 \cdot \Delta x - 27.42 \cdot m_{H2O} + 29.72 \cdot \rho_{leaf}$	10.98	0.75
	2nd Stepwise:	$Ln(h_{f,max}) = 0.44 + 0.17 \cdot W + 0.09 \cdot L + 3.98 \cdot \Delta x - 1.97 \cdot m_{H2O} + 1.30 \cdot \rho_{leaf}$	0.04	0.75
	1st Alternate:	$h_{f,max} = 7.44 + 90.62 \cdot m_{dry} + 11.69 \cdot \Delta x - 16.74 \cdot m_0$	11.84	0.72
	2nd Alternate:	$h_{f,max} = -7.41 + 29.27 \cdot \rho_{leaf} + 2.77 \cdot L + 17.50 \cdot m_{H2O}$	16.74	0.60
Canyon maple (Vertical leaf placement)	1st Stepwise:	$h_{f,max} = 0.80 - 5.74 \cdot MC + 3.93 \cdot L$	19.44	0.54
	2nd Stepwise:	$Ln(h_{f,max}) = 1.71 - 0.36 \cdot MC + 0.25 \cdot L$	0.07	0.57
	1st Alternate:	$h_{f,max} = 9.77 + 128.9 \cdot m_{dry} - 16.59 \cdot \Delta x - 28.65 \cdot m_0$	22.50	0.47
	2nd Alternate:	$h_{f,max} = -11.88 + 18.08 \cdot \rho_{leaf} + 4.78 \cdot L - 15.37 \cdot m_{H2O}$	20.64	0.51
Utah juniper	1st Stepwise*:	$h_{f,max} = 5.47 - 4.21 \cdot MC + 1.00 \cdot L + 33.90 \cdot m_{H2O}$	3.58	0.45
	2nd Stepwise:	$Ln(h_{f,max}) = 1.76 - 0.58 \cdot MC + 0.13 \cdot L + 4.21 \cdot m_{H2O}$	0.06	0.43
	1st Alternate:	$h_{f,max} = 3.68 + 51.66 \cdot m_{dry} + 0.14 \cdot \Delta x - 6.38 \cdot m_0$	3.76	0.42
	2nd Alternate:	$h_{f,max} = 1.86 + 34.99 \cdot m_{dry} + 0.90 \cdot L - 3.27 \cdot m_{H2O}$	3.63	0.44
Utah juniper (with wind blowing)	1st Stepwise:	$h_{f,max} = 5.55 - 0.81 \cdot U + 25.72 \cdot m_{dry}$	3.49	0.37
	2nd Stepwise:	$Ln(h_{f,max}) = 1.70 - 0.10 \cdot U + 3.34 \cdot m_{dry}$	0.07	0.34
	1st Alternate:	$h_{f,max} = 6.34 + 26.68 \cdot m_{dry} - 1.49 \cdot \Delta x - 0.89 \cdot m_0$	3.69	0.33
	2nd Alternate:	$h_{f,max} = 4.6 - 0.83 \cdot U + 30.93 \cdot m_{dry} + 0.41 \cdot L - 10.09 \cdot m_{H2O}$	3.44	0.38
Big sagebrush segment	1st Stepwise:	$h_{f,max} = 2.95 - 4.71 \cdot MC + 2.03 \cdot L + 12.97 \cdot \Delta x$	10.11	0.43
	2nd Stepwise:	$Ln(h_{f,max}) = 1.62 - 0.41 \cdot MC + 0.17 \cdot L + 1.34 \cdot \Delta x$	0.07	0.43
	1st Alternate:	$h_{f,max} = 7.31 + 100.1 \cdot m_{dry} + 0.23 \cdot \Delta x - 27.92 \cdot m_0$	13.67	0.31
	2nd Alternate:	$h_{f,max} = -0.18 + 72.88 \cdot m_{dry} + 1.74 \cdot L - 39.63 \cdot m_{H2O}$	11.31	0.43

*Equation used in the bush combustion model.

Stepwise multiple linear regressions were performed for t_{fh} and its logarithm form (shown as the 1st and 2nd stepwise models in Table 5.11), comparing the original prediction model for Manzanita used in the semi-empirical bush model (shown as the 1st alternate model in Table 5.11), which equation form is shown as Equation (5.14).

$$t_{fh} = \beta_0 + \beta_{MC} \cdot MC + \beta_{\Delta x} \cdot \Delta x + \beta_{m_0} \cdot m_0 \quad \textbf{(5.14)}$$

According to the results shown in the Table 5.11, the horizontal models agree with the data better than the vertical models, especially for the Gambel oak experiments. This might be because the vertical leaf placement increased the temperature difference along the leaf sample. Since the Gamble oak leaves were larger than the canyon maple leaves, the temperature gradient in vertical leaves may be higher for the Gamble oak experiments, leading to increased uncertainty for t_{fh}. The goodness of the fit for the juniper models were also not satisfactory enough to be used as prediction models in the semi-empirical bush model. This is because during the Utah juniper combustion experiments, the samples often burst, releasing volatiles in jets, which increased the difficulty to determine flame height.

5.2.2.5 Flame Area

Flame area (*FA*) is the cross-sectional area of the sample flame viewed from the video camera in the front (shown as Figure 4.1), which was determined from the brightness of pixels for each video image by the MATLAB code routine. Flame height (h_f) was determined as the vertical distance from the bottom bright pixel of the flame image to the top bright pixel for each video image.

Table 5.11. Summary of regression analysis on time to maximum flame height (t_{fh}) for Utah species.

Species		Predictive Equation	MSE	R^2
Gambel oak (horizontal leaf placement)	1st Stepwise*:	$t_{fh} = 3.02 - 0.31 \cdot L + 14.28 \cdot m_{H2O}$	0.61	0.57
	1st Alternate:	$t_{fh} = -0.22 + 1.87 \cdot MC + 2.93 \cdot \Delta x + 2.62 \cdot m_0$	0.63	0.56
	2nd Stepwise:	$Ln(t_{fh}) = 0.18 + 0.28 \cdot Ln(MC) + 2.39 \cdot \Delta x + 1.85 \cdot m_{H2O}$	0.09	0.57
Gambel oak (vertical leaf placement)	1st Stepwise:	$t_{fh} = 0.20 + 12.23 \cdot \Delta x + 8.94 \cdot m_{H2O}$	4.35	0.20
	1st Alternate:	$t_{fh} = -0.81 + 1.89 \cdot MC + 11.15 \cdot \Delta x + 3.28 \cdot m_0$	4.30	0.21
	2nd Stepwise:	$Ln(t_{fh}) = 0.28 + 3.03 \cdot \Delta x + 2.34 \cdot m_{H2O}$	0.23	0.24
Canyon maple (horizontal leaf placement)	1st Stepwise*:	$t_{fh} = 10.79 + 1.07 \cdot Ln(MC) - 0.54 \cdot W + 2.05 \cdot Ln(m_{dry})$	0.38	0.48
	1st Alternate:	$t_{fh} = 0.89 + 0.03 \cdot MC + 8.31 \cdot \Delta x + 1.58 \cdot m_0$	0.52	0.30
	2nd Stepwise:	$Ln(t_{fh}) = 4.73 + 0.49 \cdot Ln(MC) - 0.25 \cdot W + 0.96 \cdot Ln(m_{dry})$	0.07	0.51
Canyon maple (vertical leaf placement)	1st Stepwise:	$t_{fh} = 4.38 + 1.05 \cdot Ln(MC) + 0.65 \cdot Ln(m_{dry})$	0.96	0.23
	1st Alternate:	$t_{fh} = 1.08 + 0.98 \cdot MC + 1.89 \cdot \Delta x + 2.31 \cdot m_0$	1.01	0.19
	2nd Stepwise:	$Ln(t_{fh}) = 1.59 + 0.41 \cdot Ln(MC) + 0.26 \cdot Ln(m_{dry})$	0.11	0.28
Utah juniper	1st Stepwise*:	$t_{fh} = 6.23 + 2.75 \cdot Ln(MC) + 14.78 \cdot m_{dry}$	6.41	0.10
	1st Alternate:	$t_{fh} = 2.07 + 2.14 \cdot MC + 1.50 \cdot \Delta x + 7.02 \cdot m_0$	6.40	0.11
	2nd Stepwise:	$Ln(t_{fh}) = 1.75 + 0.40 \cdot Ln(MC) + 2.29 \cdot m_{dry}$	0.13	0.11
Utah juniper (with wind blowing)	1st Stepwise:	$t_{fh} = 6.17 + 10.82 \cdot m_{dry}$	8.13	0.04
	1st Alternate:	$t_{fh} = 5.81 + 2.06 \cdot MC - 1.01 \cdot \Delta x + 6.09 \cdot m_0$	8.01	0.06
	2nd Stepwise:	$Ln(t_{fh}) = 1.77 + 0.29 \cdot Ln(MC) + 1.83 \cdot m_{dry}$	0.16	0.09
Big sagebrush segment	1st Stepwise:	$t_{fh} = 3.41 + 1.19 \cdot MC - 0.85 \cdot L + 22.46 \cdot m_{dry}$	2.46	0.32
	1st Alternate:	$t_{fh} = -0.18 - 0.21 \cdot MC + 9.31 \cdot \Delta x + 1.74 \cdot m_0$	2.93	0.15
	2nd Stepwise:	$Ln(t_{fh}) = 1.02 + 0.43 \cdot MC - 0.30 \cdot L + 8.28 \cdot m_{dry}$	0.29	0.35

*Equation used in the bush combustion model.

It was expected that FA would correlate with h_f for each leaf sample. Linear regressions were performed for each experimental run, using the following equation:

$$FA = \beta \cdot h_f \quad \textbf{(5.15)}$$

The average of R^2 and its 95% confidence interval are summarized in Table 5.12. The intercept was set to zero, assuming that there is no FA if h_f is zero.

Table 5.12. R-squared of predicting *FA* by h_f

	R^2
Gambel oak	0.95±0.0025
Bigtooth maple	0.94±0.0026
Utah juniper	0.93±0.0038
Big sagebrush	0.94±0.0039

The ± represents 95% confidence interval for R-squared.

The values of R^2 in Table 5.12 suggest that the prediction of FA is linearly correlated with h_f, which means that the width of the flame from a frontal view can be regarded as constant during the sample combustion. This flame width is just the slope fit in Equation (5.15) and named as FW_β.

The values of FW_β for different species were expected to be a function of physical leaf parameters. Stepwise multiple linear regression analysis was performed on FW_β for all experimental runs and summarized in Table 5.13. Two types of alternate equations were tested and compared to the lowest BIC model obtained by stepwise regression. The first type alternate equation included L and MC as independent variables. For vertically-placed broad-leaf experiments, the L was replaced by W because values of FW_β were generated based on front view pictures of flame. Except for the stepwise model of Gambel oak with horizontal leaf placement and Utah juniper, MC was a significant term for all other stepwise models. Due to this, MC was

Table 5.13. Summary of regression analysis on FW_β for Utah species.

Species		Predictive Equation	MSE	R^2
Gambel oak (Horizontal leaf placement)	Stepwise*:	$FW_\beta = 1.42 + 0.14 \cdot L + 5.30 \cdot m_{dry} - 3.70 \cdot m_{H2O}$	0.13	0.65
	1st Alternate:	$FW_\beta = 1.45 + 0.27 \cdot L - 0.62 \cdot MC$	0.15	0.61
Gambel oak (Vertical leaf placement)	Stepwise:	$FW_\beta = 1.57 - 0.65 \cdot MC + 0.10 \cdot W + 0.21 \cdot L$	0.24	0.56
	2nd Alternate:	$FW_\beta = 2.13 + 0.28 \cdot W - 0.46 \cdot MC$	0.30	0.44
Canyon maple (Horizontal leaf placement)	Stepwise*:	$FW_\beta = 0.95 - 0.48 \cdot MC + 0.36 \cdot W$	0.23	0.61
	1st Alternate:	$FW_\beta = 1.51 + 0.35 \cdot L - 0.46 \cdot MC$	0.36	0.40
Canyon maple (Vertical leaf placement)	Stepwise:	$FW_\beta = 0.52 - 0.78 \cdot MC + 0.38 \cdot W + 5.40 \cdot \Delta x$	0.39	0.50
	2nd Alternate:	$FW_\beta = 1.03 + 0.38 \cdot W - 0.57 \cdot MC$	0.41	0.47
Utah juniper	Stepwise*:	$FW_\beta = 1.26 + 5.35 \cdot m_{dry}$	0.06	0.43
	1st Alternate:	$FW_\beta = 0.70 + 0.34 \cdot L + 0.07 \cdot MC$	0.08	0.28
Utah juniper (with wind blowing)	Stepwise:	$FW_\beta = 1.89 - 0.76 \cdot MC + 0.07 \cdot U + 3.25 \cdot m_{H2O}$	0.09	0.27
	1st Alternate:	$FW_\beta = 1.70 + 0.12 \cdot L - 0.46 \cdot MC$	0.11	0.11
Big sagebrush segment	Stepwise:	$FW_\beta = 1.38 - 0.58 \cdot MC + 0.15 \cdot L + 1.48 \cdot \Delta x$	0.13	0.42
	1st Alternate:	$FW_\beta = 1.85 + 0.14 \cdot L - 0.55 \cdot MC$	0.13	0.46

*Equation used in the bush combustion model.

selected as a term in the alternate equation. The alternate equation form is shown as Equation (5.16).

$$\text{(a)} \quad FW_\beta = \beta_0 + \beta_L \cdot L + \beta_{MC} \cdot MC$$
$$\text{(b)} \quad FW_\beta = \beta_0 + \beta_W \cdot W + \beta_{MC} \cdot MC \qquad \textbf{(5.16)}$$

The MSE of the alternate models were all slightly larger than the MSE of stepwise models. Except for the R^2 of alternate models for sagebrush, the R^2 of the alternate models for other species are smaller than from the stepwise models. According to these evaluations of the goodness of fit, the alternate models for Gambel oak with horizontal leaf placement, canyon maple with vertical leaf placement and sagebrush were good enough to be used in the shrub combustion model.

5.2.3 **Effects of Wind**

Individual sample combustion experiments with wind were also performed for Utah juniper. The wind speed (U) was set to be 0.59, 1.85, 2.17, and 2.48 $m \cdot s^{-1}$. Only slight differences in the means of t_{ig}, t_{fd}, and t_{fh} between the no wind combustion experiments and the wind experiments were observed, as shown in Figure 5.15. Analysis of variance (ANOVA) was performed on t_{ig}, t_{fd}, t_{fh} and h_f, respectively, to compare the difference between means of various wind speed (U) group. The p-values of ANOVA are summarized in Table 5.14. There was significant evidence that there are at least two different means among the various U groups in t_{ig}, t_{fd} and t_{fh}. However, there was no significant evidence to draw a conclusion that the means of h_f were different among various U groups, including the no wind condition (U = 0 $m \cdot s^{-1}$). Box-plots h_f for the various U groups are shown as Figure 5.16.

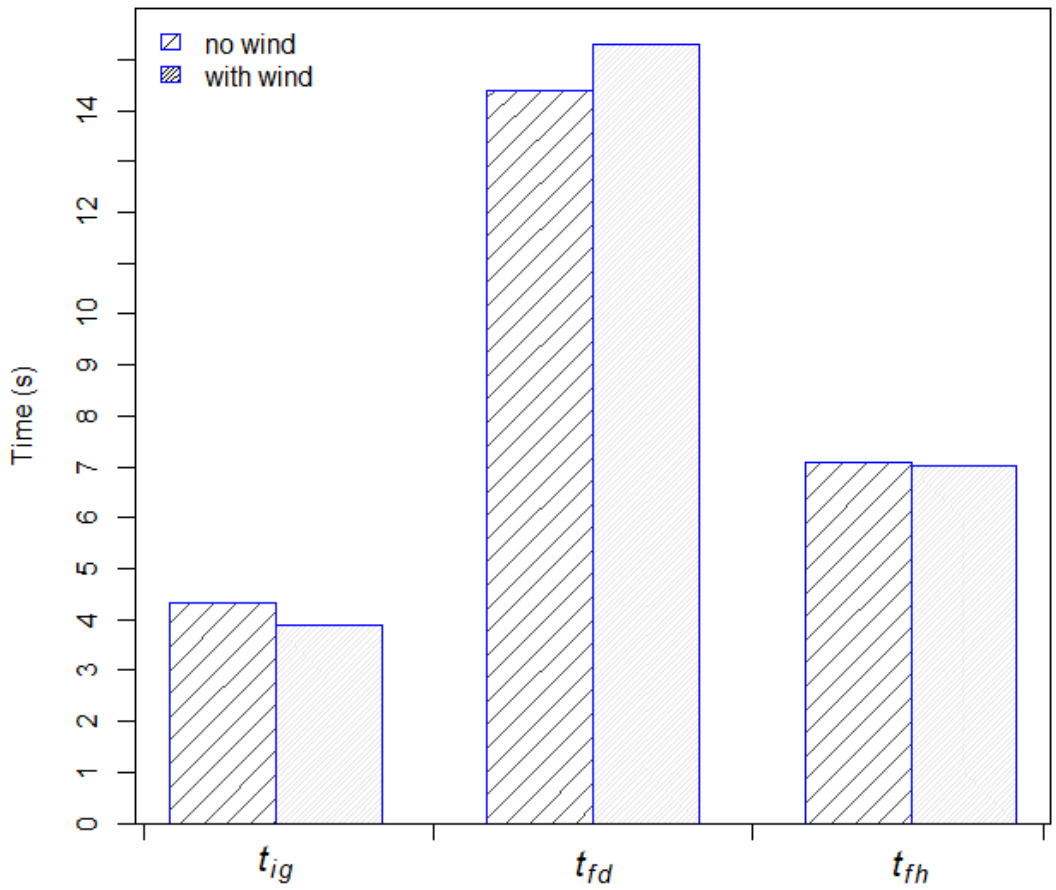

"with wind" means data were averaged from data with wind speeds of 0.59, 1.85, 2.17 and 2.48 m/s.

Figure 5.15. The effects of wind on time to ignition, time of flame duration and time to maximum flame height for the Utah juniper experiments.

Table 5.14. The p-values of analysis of variance for time to ignition, time of flame duration and time to maximum flame height and maximum flame height for Utah juniper experiment.

Combustion variables	p-values
t_{ig}	1.54e-06
t_{fd}	0.43e-03
t_{fh}	0.35e-02
h_f	0.81e-02

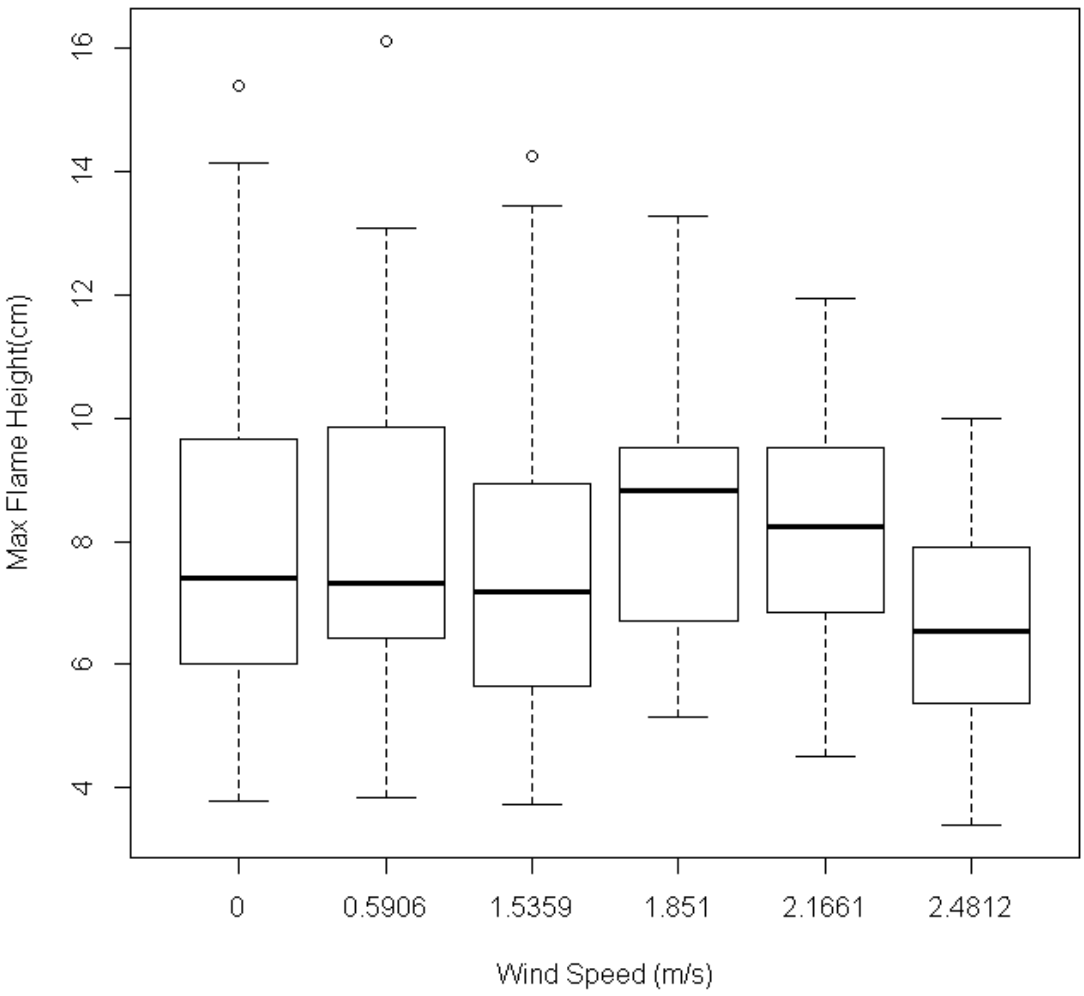

Figure 5.16. Box-plots of maximum flame height grouped as various wind speed.

Since U influenced t_{ig}, t_{fd}, t_{fh} and h_f slightly as well, U was included in the stepwise regression models. Regression results for the combustion characteristics of the Utah juniper wind experiments are shown in Table 5.5, Table 5.7, Table 5.10, Table 5.11 and Table 5.13. It was observed that U was kept as a significant term in the stepwise models except for the regression to

t_{fd} without the logarithm transform. It was observed that when U had a negative correlation with t_{ig}, t_{fh} and h_f, a positive correlation was observed with t_{fd}.

Maximum flame length ($l_{f,max}$) was also measured by a MATLAB code developed to capture the largest flame length on the video images. Regression analysis was performed for $l_{f,max}$ to obtain an optimized prediction equation (regression results are shown in Table 5.15).

In the minimized BIC value stepwise model, U was not left in the model, which validated the result of the ANOVA test performed on $l_{f,max}$ grouped with various U. The p-value was 0.6460 and this meant U did not influence the means of $l_{f,max}$. The first alternate model was suggested by (Cole et al., 2011). A non-linear form of U was another possible option to be introduced to predict $l_{f,max}$ as shown in 2nd alternate model.

Flame tilt angle was determined as max flame tile angle (θ_{max}) and mean flame tilt angle (θ_{mean}). The maximum value of flame tilt angle was determined among twenty frames around the frame showing maximum flame length. The value of θ_{mean} was the average of these twenty flame tilt angles. Regressions for θ_{max} and θ_{mean} are also shown in Table 5.15. (Cole et al., 2011) obtained the best-fit model for θ_{max} by only including U, which form was fitted on the datasets in this project (shown as first alternate model in Table 5.15). The minimized BIC value stepwise models for flame angles were slightly better than the alternate models.

The regressed values for goodness of fit for $l_{f,\max}$, θ_{max} and θ_{mean} were not satisfactory. This might be the reason that wind experiments were performed on the big flat-flame burner rather than on the small burner used by Cole. It is possible that during the combustion process, the upward convective gases might affect the horizontal wind velocity, and since the larger burner had more heat release, the measured effects of wind were different than in the small burner. A better designed experiment might improve the study of the effects of wind.

Table 5.15. Summary of regression analysis on $l_{f,\max}$, θ_{max} and θ_{mean} for Utah juniper.

Combustion variables		Predictive Equation	MSE	R^2
Max flame length ($l_{f,max}$)	Stepwise:	$l_{f,max} = 7.42 - 1.06 \cdot \Delta x + 18.95 \cdot m_{dry} - 11.12 \cdot m_{H2O}$	1.77	0.20
	1st Alternate:	$l_{f,max} = 6.27 - 0.21 \cdot U - 15.61 \cdot m_0 + 38.32 \cdot m_{dry}$	1.80	0.19
	2nd Alternate:	$l_{f,max} = 7.65 - 3.60 \cdot exp(-19.94 \cdot U) - 5.34 \cdot m_0 + 25.21 \cdot m_{dry} - 1.423 \cdot \Delta x - 0.10 \cdot L$	2.35	NA
Max flame tilt angle (θ_{max})	Stepwise:	$\theta_{max} = 25.69$	93.95	NA
	1st Alternate:	$\theta_{max} = 26.87 - 0.69 \cdot U$	94.24	0.0023
Mean flame tilt angle (θ_{mean})	Stepwise:	$\theta_{max} = 19.04 - 35.71 \cdot m_{H2O}$	88.20	0.04
	1st Alternate:	$\theta_{max} = 18.89 - 2.20 \cdot U$	89.18	0.02

6. MODELING

Most current wildfire field models have been based on dry or low moisture fuel combustion. Moreover, these models also focus on fire spread over a fuel bed rather than through a 3-dimensional shrub. Therefore, it was necessary to develop a 3-dimensional model describing the bush burning based on combustion characteristics of individual live fuel samples. A semi-empirical bush model was developed in the wildfire lab at Brigham Young University and expanded to adapt to Utah species in this research project. In this semi-empirical bush model, the number of leaves and *MC* were defined by user. After the physical leaf parameters were assigned to each leaf, the bush shape could be chosen for specific Utah species. Leaves were then placed in the bush shape space (for Gambel oak and Canyon Maple). A fractal-based L-systems approach was also developed for the Utah juniper structure. Bush structure studies are addressed in section 6.1. Although it is a semi-empirical bush model, the effects of heat transfer mechanisms are included through the use of correlations of combustion characteristics. To start, a first leaf or several leaves in the corner of a bush were ignited. The flaming zone for individual leaf combustion was modified to simulate flame volume more precisely, which is addressed in section 6.2. Once nearby leaves are covered by a flame, leaves began preheating until ignition occurred. The flame propagates until all accessible and available fuel burned out for the whole bush.

6.1 **Bush Structure**

Bush structures were studied for Gambel oak, canyon maple and Utah juniper. Two different methods were used to generate 3-dimensional geometrical locations of flammable fuel for an individual bush. The first method was first designed by Prince (2010) and modified to describe bushes of Gambel oak and canyon maple. A fractal-based L-systems approach was used to describe a Utah juniper bush because of its strand-like nature. Observations and measurements of the bushes from the field study were compared to the bushes generated in the model as well.

6.1.1 **Gambel Oak and Canyon Maple**

For broad-leaf bushes, only leaves are treated as flammable fuel in the semi-empirical bush model. After leaf number and *MC* were defined by the user of the bush model, single leaf geometrical properties (m_{dry}, m_0, L, W and Δx) are assigned to each leaf based on the statistical prediction procedure addressed in Section 5.2.1. Leaves are randomly placed into a defined 3-dimesional space. The shape of this space (i.e. bush shape) is specific to the species (summarized in Table 6.1).

It was also observed that bush shapes were different for various places where bushes grew. For example, the Gambel oak on hills or in canyon areas are typically small bushes clustered together, which can be treated as a rectangular box for leaf placement (shown as Figure 6.1). However, some of the Gambel oak bushes in a broad plain area grew together into a hemi-sphere or hemi-ellipsoid shape (shown as Figure 6.2). Canyon maple might also vary in size and shape for different surroundings and only small-size canyon maple was treated in this research project.

Table 6.1. Bush shape and leaf placement in the semi-empirical bush model for Gambel oak and canyon maple.

Bush Shape	Description	Species
Small-hollow-space Box	A cube was divided into 27 (=3×3×3) equal compartments, among which 2 middle inner compartments were left empty. Leaf position was randomly assigned in remaining 25 compartments.	Canyon maple
Large-hollow-space Box	A cube was divided into 64 (=4×4×4) equal compartments, among which 8 middle inner compartments were left empty. Leaf position was randomly assigned in remaining 56 compartments.	Gambel oak
Hemi-ellipsoid	x_{Leaf}, y_{Leaf} and z_{Leaf} are randomly assigned as leaf position, satisfying the following three equations: $$0.176 < \frac{\left(x_{Leaf} - \frac{X_{dist}}{2}\right)^2}{X_{dist}^2} + \frac{\left(y_{Leaf} - \frac{Y_{dist}}{2}\right)^2}{Y_{dist}^2} + \frac{\left(z_{Leaf} - \frac{Z_{dist}}{2}\right)^2}{Z_{dist}^2} < 1$$ $$z_{Leaf} > \frac{Z_{dist}}{2}$$ X_{dist}, Y_{dist} and Z_{dist} are bush length, width and height defined by bush model user.	Gambel oak

Figure 6.1. Gambel oak on Y Mountain (photo taken on July 1, 2011).

Figure 6.2. Gambel oak in Rock Canyon (photo taken on June 17, 2011).

Figure 6.3. Canyon maple in Rock Canyon (photo taken on July 6, 2011).

The canyon maple was simulated as a small-hollow-space box in the semi-empirical bush model. Figure 6.3 is an example of canyon maple grown in Rock Canyon. It was observed that the canyon maple bushes were hollow inside (i.e., there was an absence of leaves in the interior volume). According to the measurements from the field study, the ratio of inside hollow space volume to the whole bush volume was close to 2:27. The description of this method is shown in Table 6.1 and a sketch is shown as Figure 6.4 (a). The two inner opaque boxes were left empty and leaves were randomly assigned in the remaining transparent boxes. The result for simulation of canyon maple bush leaf placement is shown as Figure 6.4 (b). As for Gambel oak, the ratio of inside hollow space volume to the whole bush volume was close to 8:64, which is larger than that of canyon maple (shown as Figure 6.5 (a)). The inner eight opaque boxes were therefore left empty for Gambel oak, as shown in Figure 6.5 (b). The green rectangles represent the leaves. The middle part of the bushes was hollow. Leaves were also placed without existing on the same plane (touching each other or one leaf inside another).

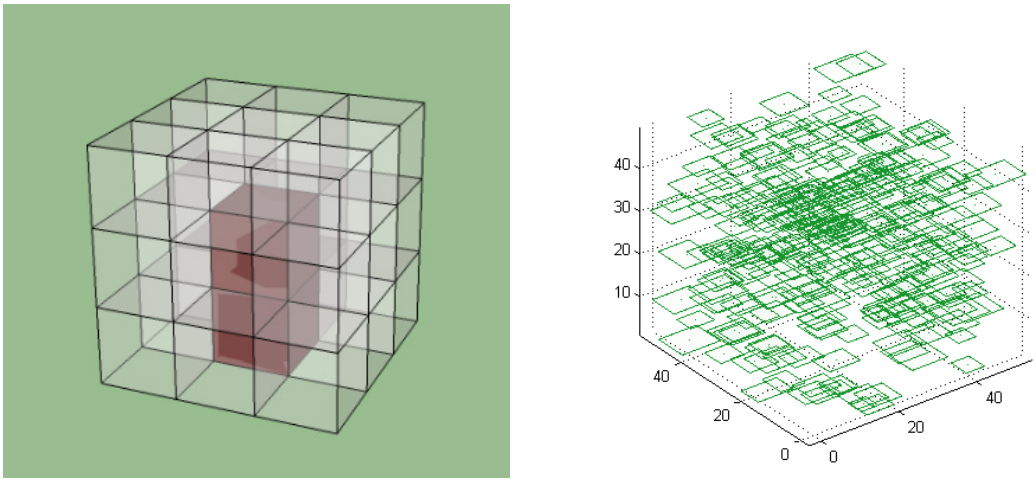

(a) (b)

Figure 6.4. Comparison of (a) sketch of small-hollow-space box to (b) simulation of canyon maple bush leaf placement in semi-empirical bush model.

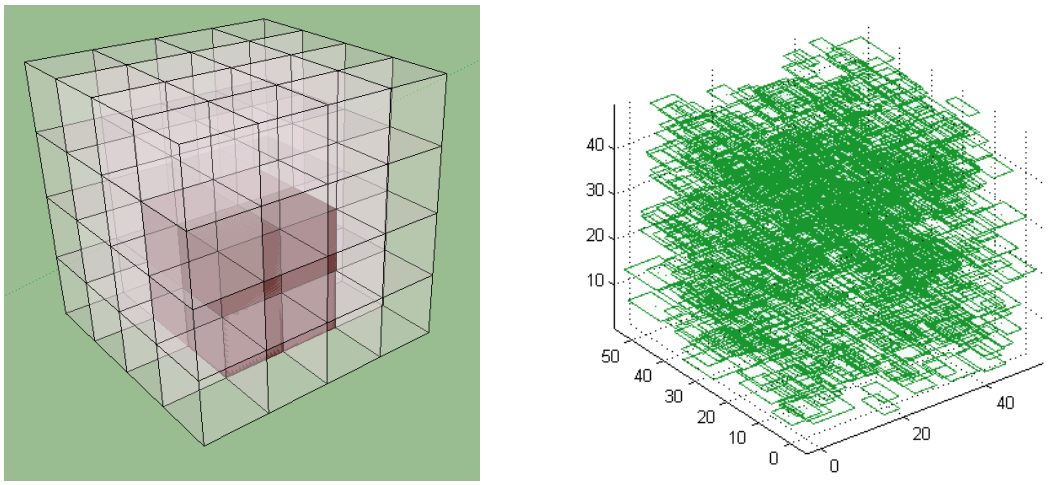

(a) (b)

Figure 6.5. Comparison of (a) sketch of large-hollow-space box to (b) simulation of Gambel oak bush leaf placement in semi-empirical bush model.

The leaf number was defined by the user for the semi-empirical bush model. In order to obtain the knowledge of leaf number for a live bush in the field, leaf number estimates were performed in the field. After counting the leaf number for a typical branch unit, the leaf number for a bush in a prescribed volume was determined by counting the number of units in that volume.

6.1.2 **Utah Juniper**

The fuel segment of Utah juniper is like a strand or needle, whose structure is different from that of a broad-leaf fuel. A fractal-based L-systems approach was adapted for modeling this branching structure, which is often used for describing plant structure (Fletcher and Fletcher, 2013).

Individual fuel elements of Utah juniper were studied and several strings were obtained as the basic fractals. Stochastic grammar was also used in this "rewriting" system to allow different strings to occur at a certain given probability. Branches were combined into a bush with user-

given bush height. The distance between starting points of primary branches on the trunk was decreased from the bottom to the top, with a scaling factor determined by the semi-empirical bush model user. According to the measurements from the field study, a scaling factor was used to make the length of primary branches decrease from the bottom to the top. Due to the curved shape of a Utah juniper tree, primary branches were divided into two parts. Secondary branches and fuel units were placed onto the outside part of the primary branch, which direction was generally vertical. Primary and secondary branch growth followed the self-similar fractals. The fuel elements were evenly placed onto the primary and secondary branches. Figure 6.6 shows a photo of a juniper shrub compared with a simulated juniper bush.

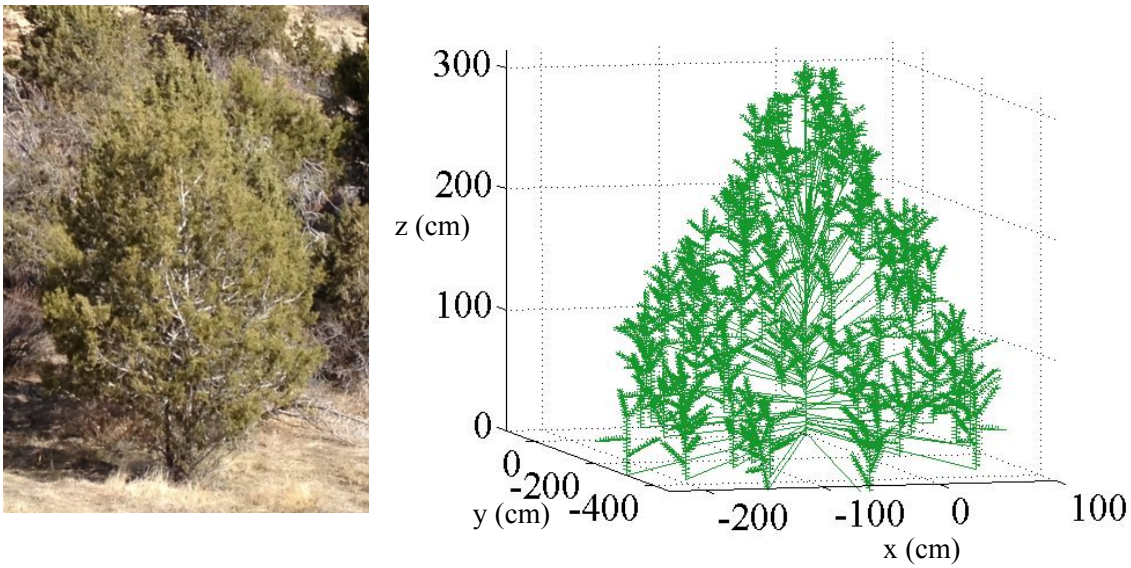

(a) (b)

Figure 6.6. Comparison of (a) a Utah juniper bush with (b) the simulation in the semi-empirical bush model.

6.2 **Single-Leaf Combustion**

6.2.1 **Flame Volume Simulation**

Simulation of the volume of the flaming zone during single leaf combustion in the semi-empirical bush model was modified in order to predict the flame volume more precisely for Utah species. The flame height h_f of the ignited horizontal leaf was linearly increased from zero to $h_{f,max}$ (at t_{fh}) and then decreased to zero (at t_{brn}) (as shown in Figure 6.7). A certain percentage (R_d) of the h_f was assigned below the leaf, which is named as bottom flame height ($h_{f,bottom}$). The remaining h_f is the top flame height ($h_{f,top}$), which is above the leaf. Both 15% and 25% were used as R_d in this research for bush combustion modeling and their effects on the modeling results are discussed in Section 6.3.7.

In the previous coding for production of the flame volume, the widths of the flame were equal to the leaf length (L) or width (W) plus an additional 11% of h_f at each side (shown in Figure 6.8).

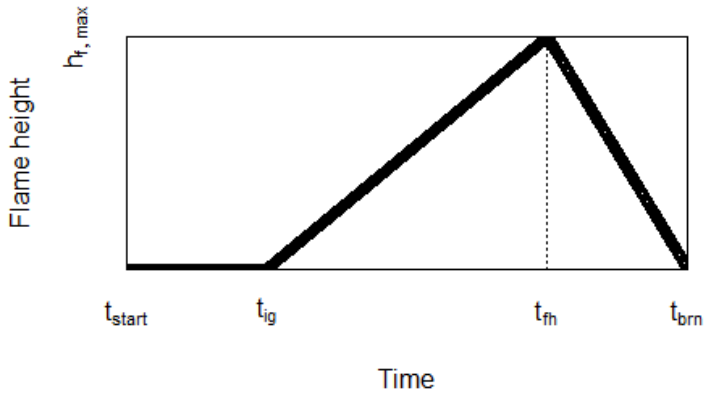

Figure 6.7. Flame zone history for individual leaf combustion (distances not to scale).

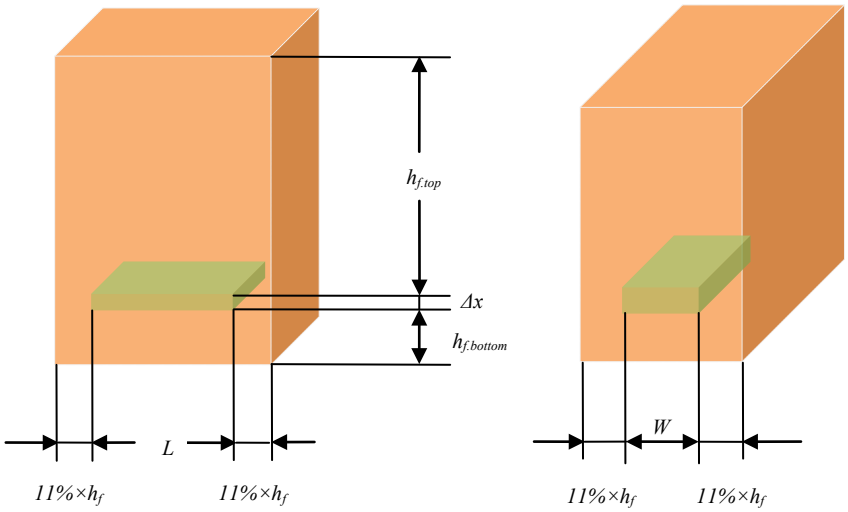

Figure 6.8. 3-D representation of leaf flame volume via the previous method. (The orange shaded rectangle represents the flame and the green shaded rectangle represents the leaf. Distances are not to scale.)

This coding method was based on the combustion behavior of Manzanita leaves, whose size is smaller than the Gambel oak and canyon maple. By using this previous coding method to simulate flame volume, unrealistically large values of h_f were sometimes obtained from the semi-empirical bush model for Gambel oak and canyon maple. This previous flame width was dependent on h_f, and the h_f of Gambel oak and canyon maple were larger than h_f of Manzanita for individual leaf fuel combustion. This might increase the actual flame area, and nearby leaves might be involved in the flame earlier than observed naturally. It is recommended that flame widths should be studied further during individual leaf combustion for Utah species.

In order to achieve better simulation of the flame volume, the coding of the flaming zone was modified by introducing the FW_β to replace the flame width in the previous coding method. The definition of FW_β and its multiple linear regressions were addressed in section 5.2.2.5. It was assumed that flame widths of the front and the side were equal. FW_β was a constant during

individual leaf combustion and a function of leaf geometrical properties. After leaf geometrical properties had been assigned to each leaf, FW_β was computed for each leaf in the semi-empirical bush model. A sketch for this flame volume simulation method is shown in Figure 6.9.

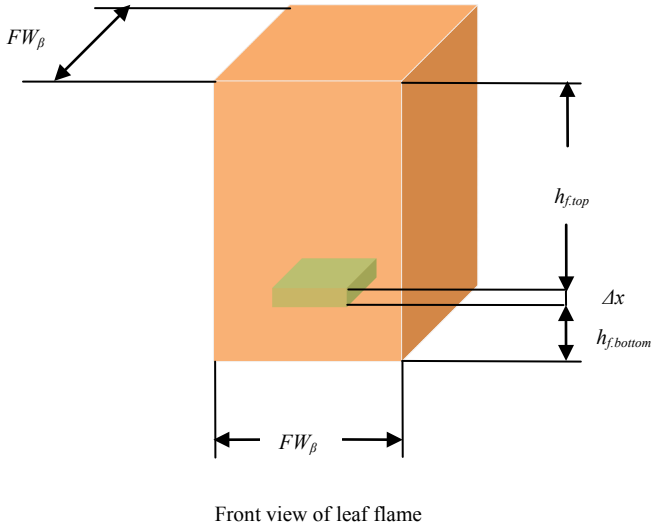

Figure 6.9. 3-D representation of leaf flame volume via current modified method. (The orange shaded rectangle represents the flame and the green shaded rectangle represents the leaf. Distances are not to scale.)

This new method was able to generate more reasonable widths of the flame zone. It was observed that flame width could be regarded as constant during individual leaf combustion based on the linear regression discussed in section 5.2.2.5. FW_β was also predicted by leaf geometrical properties instead of h_f. In the semi-empirical bush model, it was reasonable to occasionally have a flame width less than L or W because the flame zone was approximated as a rectangle. However, the previous method was not able to provide this feature. The detailed description of the semi-empirical bush model is given elsewhere (Pickett, 2008; Prince et al., 2010; Prince, 2012). This new method effectively improved the flame volume simulation. Figure 6.10 shows

the computed combustion behaviors of two identical bushes when using the previous method and the modified method. Both pictures are the frame at 12 seconds after several leaves in the left corner were ignited. The bush flame height obtained by the previous method was unreasonably large, which was also observed for all the Gambel oak and canyon maple bushes combustion simulations.

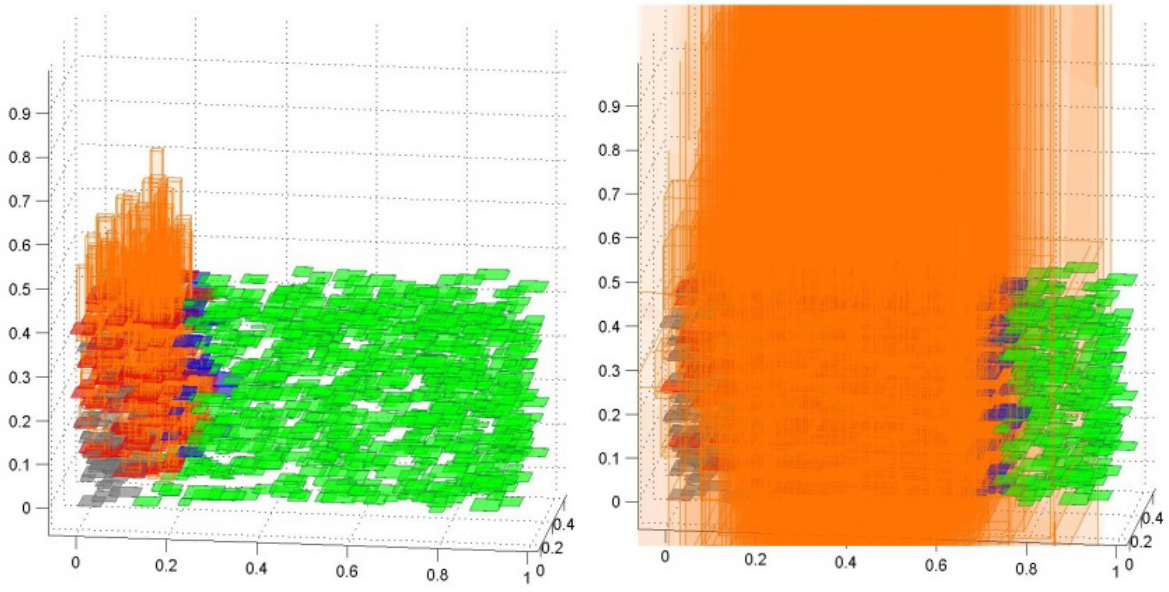

(a) current flame volume simulation

(b) previous flame volume simulation

Figure 6.10. Comparison of bush combustion of Gambel oak at 12 seconds after ignition using different flame volume simulation methods.

6.2.2 **Effect of Wind**

The effect of wind was also included in the shrub combustion simulation. For Gambel oak and canyon maple combustion, the flame tilt angle (θ) was defined as the angle of the flame from the vertical axis. A correlation for θ was suggested by Albini (1981) to correlate with h_f and U (shown as Equation (6.1)).

$$\theta = tan^{-1}[1.22(\frac{U^2}{g \cdot h_f})^{0.5}] \quad \textbf{(6.1)}$$

where g is the gravitational constant. Flame length (l_f) was calculated from

$$l_f = cos^{-1}\theta \cdot h_f \quad \textbf{(6.2)}$$

Flame length was used to construct the flame volume rather than flame height in this semi-empirical model. Prince et al. (2010); (2012) described a simulation of flame with wind in the semi-empirical model in detail.

6.3 **Modeling Results for Gambel Oak and Canyon Maple**

The semi-empirical bush model was modified to deal with the combustion of high *MC* bushes including Gambel oak and canyon maple. Prediction equations from the different species were integrated into the semi-empirical bush model. After leaf placement and geometrical properties were determined, a unique 3-D bush was created specific to species. The bush combustion was based on the combustion behavior of individual leaves. Heat transfer mechanisms were not treated separately, since they are indirectly embedded into the prediction correlations of combustion characteristics (addressed in section 5.2.2). The flame coalescence behavior from multiple leaves was also determined to increase the flame zone (Pickett, 2008; Pickett et al., 2009; Prince et al., 2010).

Modeling results are discussed in the following sections. Different configuration inputs were set up to study the effect of the following factors: bush shape, bush size, leaf properties, *MC*, bulk density, local density and wind speed. The percentage of the bottom part of the individual leaf flame (R_d) was assigned to be 15% for modeling results shown in Section 6.3.1-6.3.6. In Section 6.3.7, the effects of R_d were studied by increasing its value to 25%.

The maximum bush flame height ($h_{f,bush}$) was defined as the maximum value of the flame height above the bush during flame propagation, which could be zero if there was no flame above the bush. The bush burnout time ($t_{brn,bush}$) was defined as the time difference between the moment that flame stopped propagation and the moment first ignition happened. The extent of burnout (Xs) was defined as the percentage of the total number of leaves that were completely burned. Bulk density (ρ_{bulk}) was defined as the number of leaves divided by the total volume of the bush. Local density (ρ_{local}) was referred to the number of leaves in the bush volume without counting the inside hollow space.

6.3.1 **Bush Size**

Bush size was expected to influence the percent of bush burned (Xs). The configuration inputs of the first three runs were measurements from real bushes in the fields where we usually collected our experiment samples. The bush size and leaf number of bushes were scaled down by 1/8 as run 4, 5, 6 or 1/27 as run 7, 8, 9 while other inputs were keeping the same (shown as Table 6.2). It was observed that the Xs did not change significantly, even for large-hollow-space rectangular box Gambel oak bushes which burned most intensely among three bush shapes.

6.3.2 **Bush Shape**

Bush shape is specific to species and influenced by surroundings. The hemi-ellipsoid shape Gambel oak bush shown as run 1 in Table 6.2 was 2.7% burned. However, the hollow rectangular box Gambel oak was 28.1% burned. Although configuration inputs of those two runs were the measurements of real Gambel oak bushes in the field, the hemi-ellipsoid bush was found to be sparser than the rectangular box bush, according to the bulk density.

Table 6.2. Semi-empirical modeling results of Utah bushes combustion (Part I).

Run #	Species	Bush shape	Width (cm)	Length (cm)	Height (cm)	Leaf number	ρ_{local} (leaves/m^3)	ρ_{bulk} (leaves/m^3)	*MC* (%)	*WS* (m/s)	$h_{f,bush}$ (cm)	*Xs*	$t_{brn,bush}$ (seconds)
1	Gambel oak	I	473	500	212	36,000	1,375	1,371	100	0	0	2.7%	51
2	Gambel oak	II	128	288	133	16,056	3,743	3,274	100	0	40	28.1%	110
3	Canyon maple	III	146	285	132	3,748	737	682	100	0	0	1.4%	20
4	Gambel oak	I	237	250	106	4,500	1,375	1,371	100	0	0	3.5%	36
5	Gambel oak	II	64	144	67	2,007	3,743	3,275	100	0	40	21.8%	62
6	Canyon maple	III	73	143	66	469	737	682	100	0	0	2.4%	11
7	Gambel oak	I	157	167	71	1,333	1,375	1,371	100	0	0	1.1%	13
8	Gambel oak	II	43	96	44	595	3,743	3,274	100	0	38	20.5%	38
9	Canyon maple	III	49	95	44	139	737	682	100	0	0	2.2%	6
10	Gambel oak	II	128	288	133	5,899	1,375	1,203	100	0	28	6.7%	56
11	Canyon maple	II	128	288	133	16,056	3,742	3,275	100	0	39	28.4%	59
12	Gambel oak	III	146	285	132	3,748	737	682	100	0	0	1.5%	14
13	Gambel oak	I	473	500	212	36,000	1,375	1,371	70	0	0	2.9%	38
14	Gambel oak	II	128	288	133	16,056	3,743	3,275	70	0	64	33.6%	107
15	Canyon maple	III	146	285	132	3,748	737	682	70	0	0	1.9%	18

Bush shape (I) means hemi-ellipsoid.
Bush shape (II) means large-hollow-space rectangular box.
Bush shape (III) means small-hollow-space rectangular box.

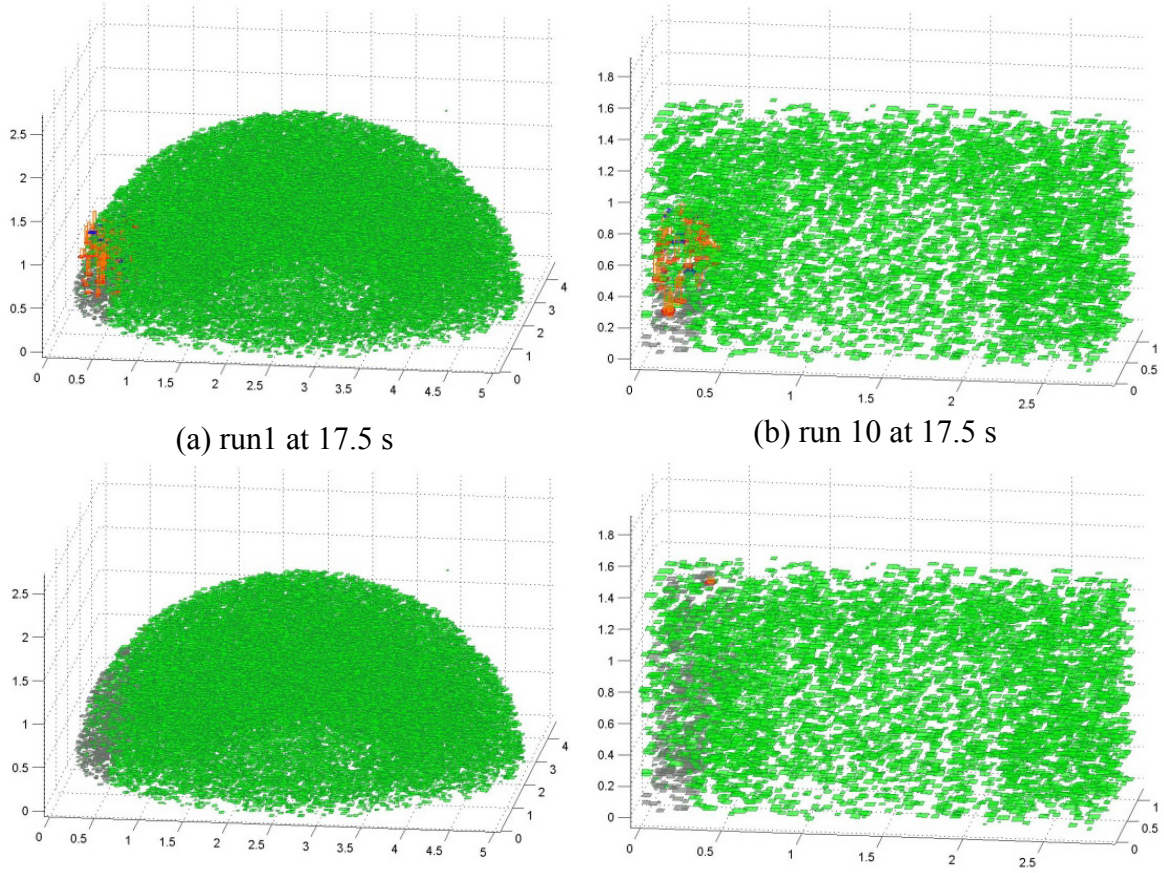

(a) run1 at 17.5 s

(b) run 10 at 17.5 s

(c) run1 at burnout

(d) run 10 at burnout

Figure 6.11. Bush combustion modeling results of run 1 and run10 at 17.5 seconds after ignition and burnout.

Besides influencing the bulk density, the bush shape still affected the flame propagation. In order to study the effect of bush shape, run 10 was designed to match the ρ_{local} of run 1 by adjusting the leaf number (shown in Table 6.2). Figure 6.11 (a) and (b) showed that when both hemi-ellipsoid (run 1) and rectangular box (run 10) Gambel oak bushes burned for 17.5 seconds, there were less leaf neighbors (particularly on the top) which could be preheated in the hemi-ellipsoid shape than in the rectangular box shape. Both run 1 and run 10 burned the fuels above the ignition location (shown in Figure 6.11 (c) and (d)) without much horizontal spread. The *Xs* of run 10 (6.7%) was higher than that of run 1 (2.7%). This indicated that the rectangular box

shape might provide more accessible fuel to be ignited on the top part of the bush than the hemi-ellipsoid shape.

6.3.3 **Bush Species**

Run 11 and run 12 were designed to study the effect of bush species by switching the species of run 2 and run 3 but keeping the geometry the same as the original species. When comparing run 2 to run 11 and run 3 to run 12, it was observed that values of *Xs* were fairly close (shown in Table 6.2). However, the value of $t_{brn,bush}$ of run 11 was much smaller that of run 2 (59 s compared to 110 s, or 46% smaller), which was consistent with the understanding that it took longer to burn out an individual Gambel oak leaf than a canyon maple leaf. Since the *Xs* for run 2 and run 11 were larger than 28%, which indicated vigorous flame propagation, the effects of leaf combustion properties seemed to be a significant factor affecting the bush combustion more than the geometry in this case. Similarly, $t_{brn,bush}$ of run 12 was 27% smaller than that of run 3. This semi-empirical model was able to embed the bush species characteristics separately from the geometrical aspects, and it was therefore concluded that canyon maple burned much faster than Gambel oak.

6.3.4 **Moisture Content**

Runs 13, 14 and 15 were set up by decreasing the *MC* from 100% to 70% based on runs 1, 2 and 3. It was observed that when decreasing the *MC*, the *Xs* increased while $t_{brn,bush}$ decreased. Although the $t_{brn,bush}$ of run 14 was 107 seconds and only slightly less than that of run 2 (110 seconds), *Xs* of run 14 (33.6%) was 5.5% more than that of run 2 (28.1%). The value of $h_{f,bush}$ of run 14 also increased as expected. Lowering *MC* generally increases *Xs* and decreases $t_{brn,bush}$, especially for intense bush combustion.

Table 6.3. Semi-empirical modeling results of Utah bushes combustion (Part II).

Run #	Species	Bush shape	Width (cm)	Length (cm)	Height (cm)	Leaf number	ρ_{local} (leaves/m^3)	ρ_{bulk} (leaves/m^3)	*MC* (%)	*WS* (m/s)	$h_{f,bush}$ (cm)	*Xs*	$t_{brn,bush}$ (seconds)
1	Gambel oak	I	473	500	212	36,000	1,375	1,371	100	0	0	2.7%	51
2	Gambel oak	II	128	288	133	16,056	3,743	3,275	100	0	40	28.1%	110
3	Canyon maple	III	146	285	132	3,748	737	682	100	0	0	1.4%	20
16	Gambel oak	I	473	500	212	72,000	2,750	2,743	100	0	3	7.6%	119
17	Gambel oak	II	128	288	133	32,112	7,485	6,550	100	0	80	98.3%	264
18	Canyon maple	III	146	285	132	7,496	1,474	1,365	100	0	0	1.6%	15
19	Gambel oak	I	473	500	212	18,000	688	686	100	0	0	1.1%	31
20	Gambel oak	II	128	288	133	8,028	1,871	1,637	100	0	34	12.7%	63
21	Canyon maple	III	146	285	132	1,874	368	341	100	0	0	1.4%	7
22	Gambel oak	I	473	500	212	36,000	1,375	1,371	100	1	0	3.5%	82
23	Gambel oak	II	128	288	133	16,056	3,743	3,275	100	1	44	34.6%	116
24	Canyon maple	III	146	285	132	3,748	737	682	100	1	0	1.3%	11
25	Gambel oak	I	473	500	212	36,000	1,375	1,371	100	3	0	1.0%	24
26	Gambel oak	II	128	288	133	16,056	3,743	3,275	100	3	38	37.4%	136
27	Canyon maple	III	146	285	132	3,748	737	682	100	3	0	1.6%	17

Bush shape (I) means hemi-ellipsoid.
Bush shape (II) means large-hollow-space rectangular box.
Bush shape (III) means small-hollow-space rectangular box.

6.3.5 **Local Density and Bulk density**

Because the difference between local density (ρ_{local}) and bulk density (ρ_{bulk}) is related to the bush volume in calculations, the values of ρ_{local} and ρ_{bulk} are proportional to the leaf number if bush volume is not changing. In order to study the effects of ρ_{local} and ρ_{bulk}, leaf numbers of runs 1, 2 and 3 were doubled in runs 16, 17, 18 and halved in runs 19, 20, 21. Results from these calculations are shown in Table 6.3. It was observed that values of *Xs* were increased when ρ_{local} and ρ_{bulk} increased while *Xs* decreased when ρ_{local} and ρ_{bulk} decreased. It was noted that when density was doubled for run 2, *Xs* increased from 28% to 98% (run 17). This result indicates that when more fuels are accessible near the ignition or preheating source, this semi-empirical model predicts enhanced flame propagation. With increased density, $t_{brn,bush}$ also seemed to increase.

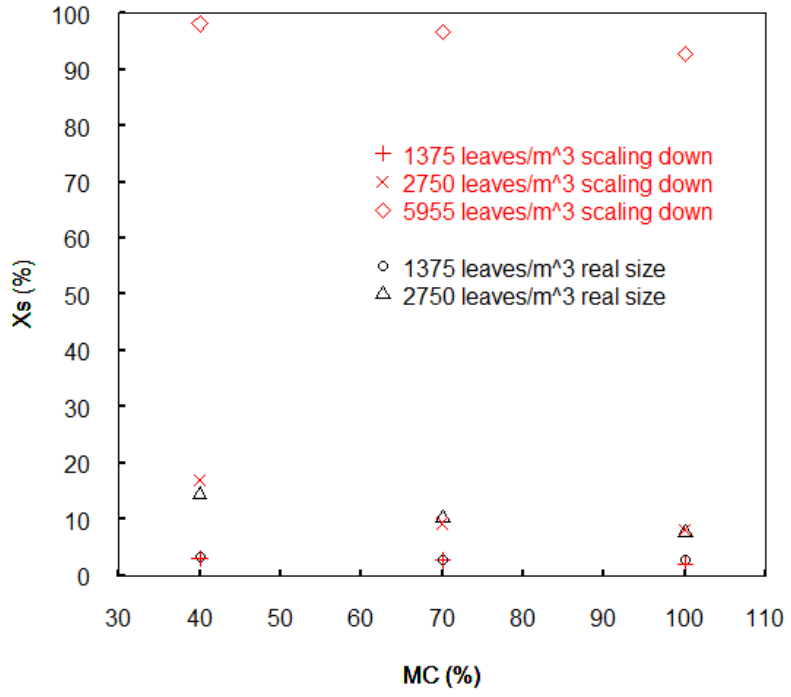

Figure 6.12. Percentage of burnt versus moisture content at different levels of local density for hemi-ellipsoid Gambel oak bush.

Since density and *MC* are the two most influential factors on *Xs*, different levels of density and *MC* were set up to run the bush models for the three types of bush shape. Figure 6.12 shows the modeling results for the hemi-ellipsoid Gambel oak bush. The real size means the bush geometry measured in the field (shown as black points in Figure 6.12). The geometry of the bush was also scaled down to 290 cm × 307 cm × 130 cm (shown as red points in Figure 6.12), which enable the bush model to handle a high ρ_{local} (at 5955 leaves/m^3). Since the scaled-down predictions matched the predicted values of *Xs* as a function of *MC* for the two lower densities, it is reasonable to expect that the predicted *Xs* at the large scale for the higher density (5955 leaves/m^3) would match the scaled-down prediction as well. With constant ρ_{local}, *Xs* increased as *MC* decreased. Conversely, *Xs* also increased as ρ_{local} increased if *MC* was held constant, which confirmed the previous results. It was also found that the bush would almost burn out when ρ_{local} was equal to 5955 leaves/m^3 while *Xs* was less than 20% for ρ_{local} at 2750 leaves/m^3.

Figure 6.13 shows predicted *Xs* versus *MC* at different values of ρ_{local} for a Gambel oak bush in the shape of a large-hollow-space rectangular box. The change of *Xs* followed the same trend in Figure 6.12. It was observe that the value of *Xs* at ρ_{local} = 5988 leaves/m^3 in Figure 6.13 was close to the value of *Xs* at ρ_{local} = 5955 leaves/m^3 in Figure 6.12. It was also noticed that *Xs* dramatically increased from 34% to 82% when *MC* decreased from 70% to 40% at ρ_{local} = 5988 leaves/m^3.

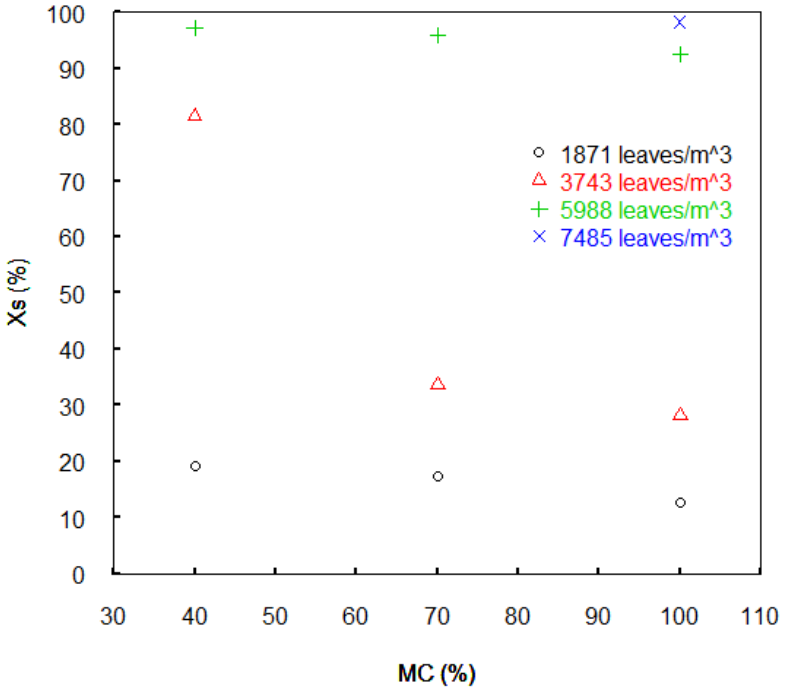

Figure 6.13. Percentage burned versus moisture content at different levels of local density for large-hollow-space rectangular box Gambel oak bush.

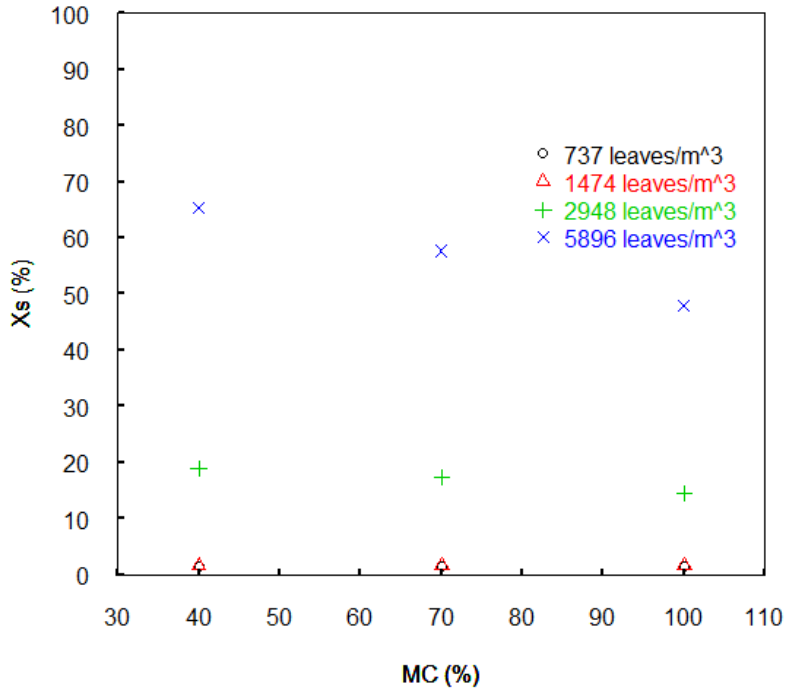

Figure 6.14. Percentage burned versus moisture content at different levels of local density for small-hollow-space rectangular box maple bush.

Predicted values of *Xs* at different values of *MC* and ρ_{local} for a maple bush are shown in Figure 6.14. The trend of changes in *Xs* was similar to that in Figure 6.12 and Figure 6.13. However, the value of *Xs* at *MC* = 40% and ρ_{local} = 5896 leaves/m^3 was 65.4%, which could be explained by individual maple leaf properties.

In conclusion, both density and *MC* affected *Xs* significantly in the bush model. Different species also resulted in a different range of *Xs*. It appears that the flame might not propagate in bushes vigorously unless a high enough density and low enough *MC* were present.

6.3.6 **Effect of Wind**

It was expected that wind would enhance the flame propagation and decrease the value of $t_{brn,bush}$. In order to study the effect of wind, wind speeds of 1 m/s and 3 m/s were added into the configuration of runs 1, 2 and 3 to set up runs 22, 23, 24 and runs 25, 26, 27 (shown in Table 6.3). It was observed that if *Xs* was originally low, wind might not enhance the propagation (e.g. runs 24 and 25). The reason could be that wind blowing made the flame difficult to merge and preheat more leaf neighbors. However, if there was a certain extent of flame propagation, wind would be able to increase *Xs* (e.g. runs 23 and 26). Moreover, *Xs* generally increased when wind speed increased. Runs 2, 23 and 26 at 28.5 seconds after ignition and at burnout are shown in Figure 6.15. When wind speed was larger, the flame extended further away from the ignition source. This effect of wind increases the possibility of flame propagation between bushes in wildfire.

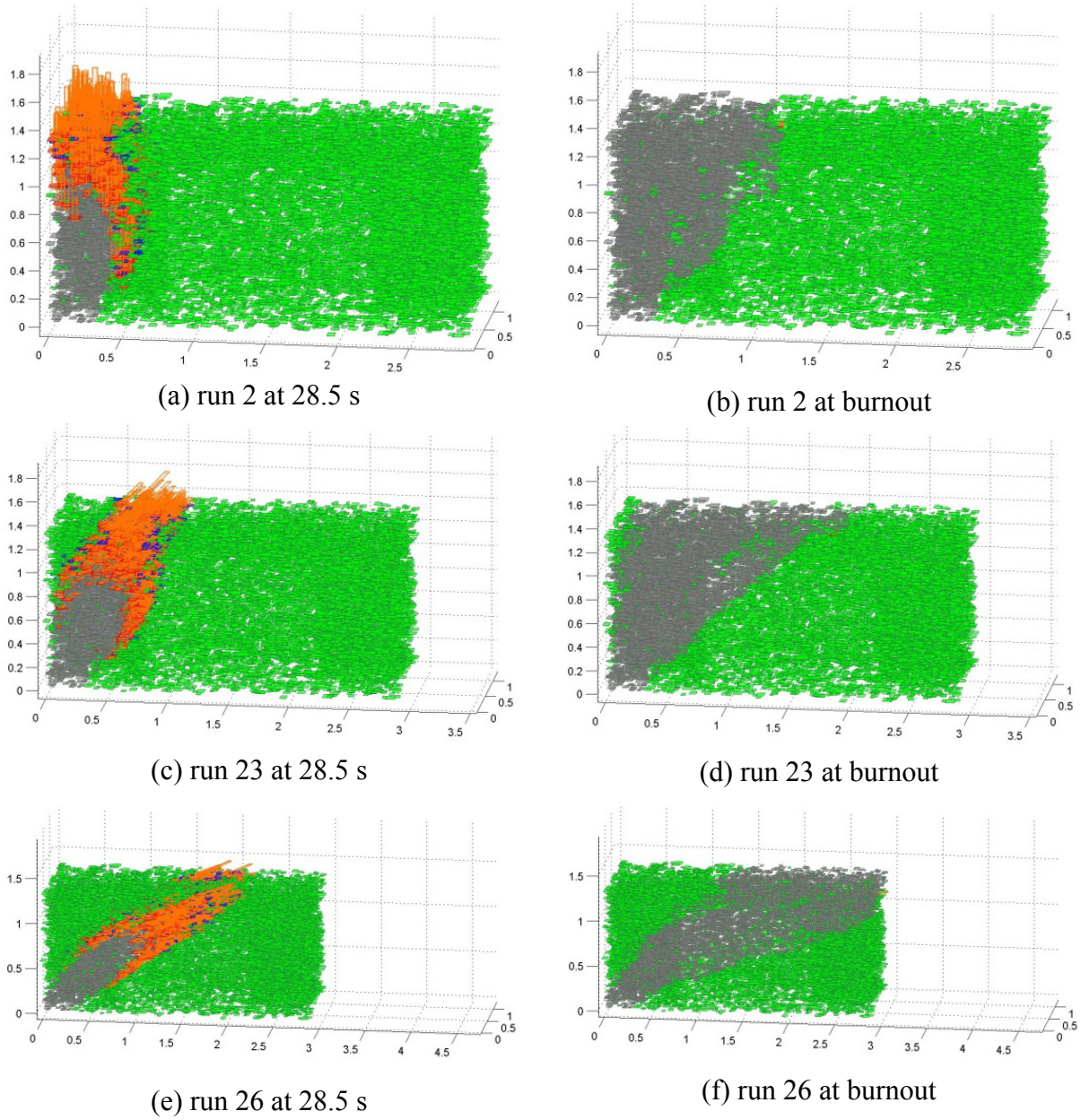

(a) run 2 at 28.5 s

(b) run 2 at burnout

(c) run 23 at 28.5 s

(d) run 23 at burnout

(e) run 26 at 28.5 s

(f) run 26 at burnout

Figure 6.15. Bush combustion modeling results of run 2, 23 and 26 at 28.5 seconds after ignition and burnout.

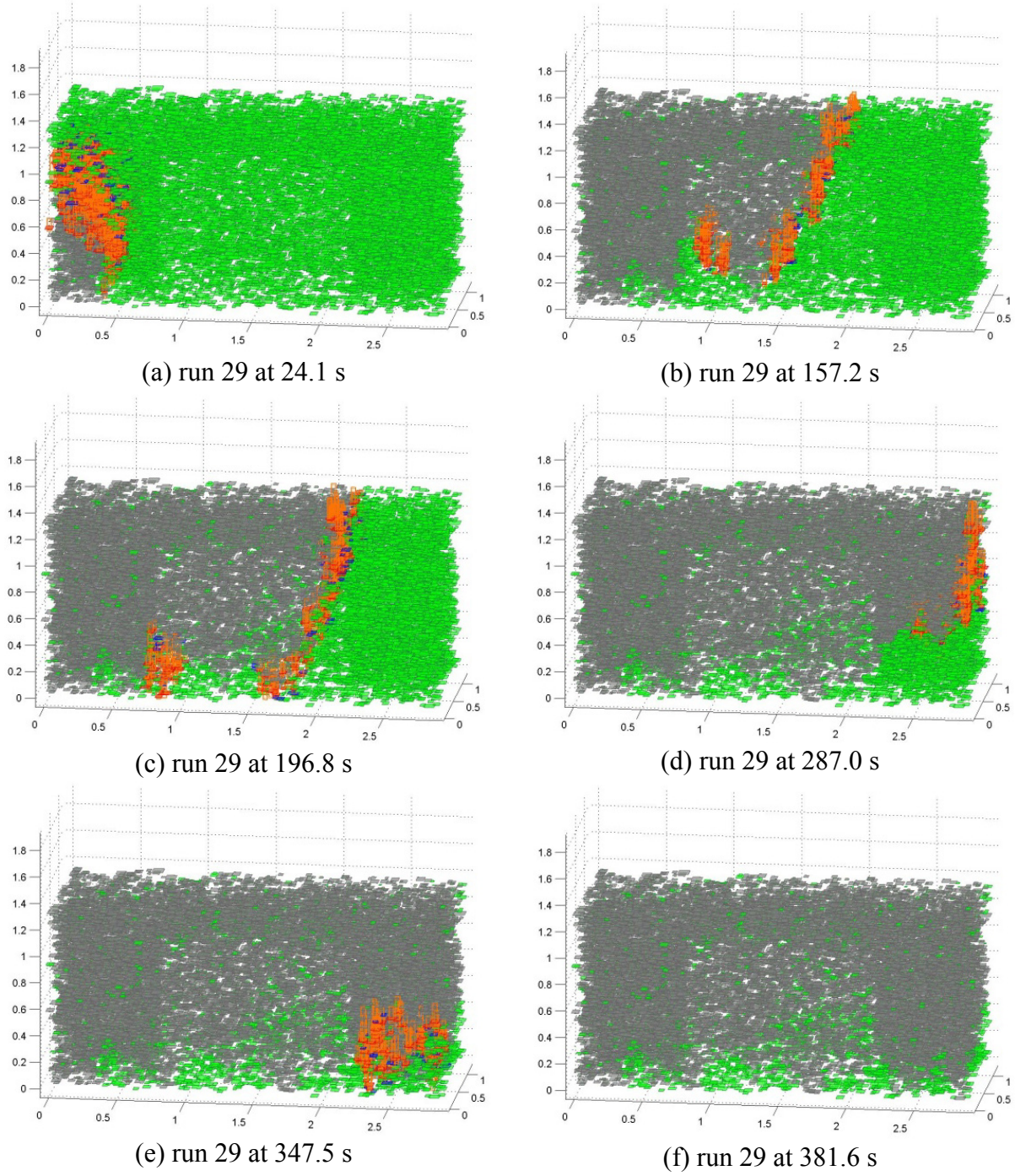

(a) run 29 at 24.1 s (b) run 29 at 157.2 s

(c) run 29 at 196.8 s (d) run 29 at 287.0 s

(e) run 29 at 347.5 s (f) run 29 at 381.6 s

Figure 6.16. Bush combustion modeling results of run 29.

6.3.7 **Percentage of Bottom Part of Individual Leaf Flame (*Rd*)**

The value of *Rd* was assigned to be 15% in the previous bush combustion simulations. To study the effect of *Rd*, runs 1, 2 and 3 were run again with 25% assigned to *Rd* (shown as run 28,

29 and 30 in Table 6.4). It was observed that the Xs of run 2 increased from 28% to 87% (run 29). However, flames were still not able to propagate significantly in the other two bush configurations (shown as run 28 and 30). It was also found in run 29 that flame occasionally propagated backwards in the bottom part of the bush, which was believed to be caused by the increased value of *Rd* (shown in Figure 6.16). This behavior in run 29 enabled the flame to propagate through the whole bush rather than just part of the bush in run 2 (shown in Figure 6.15 (b)). The wind speed (WS) was raised from 1 m/s and 3 m/s, with modeling results shown as runs 31 and 32 in Table 6.4. It was observed that Xs decreased as WS increased, which was different from the trend with *Rd* at 15% (shown as run 23 and 26). The reason could be that the wind improved the flame propagation when Xs was low (shown as run 23 and 26); but the flame tilted by wind might result in less flame propagation in the upper part of the bush (especially run 32 shown as Figure 6.17) compared to a thoroughly burned bush (run 29).

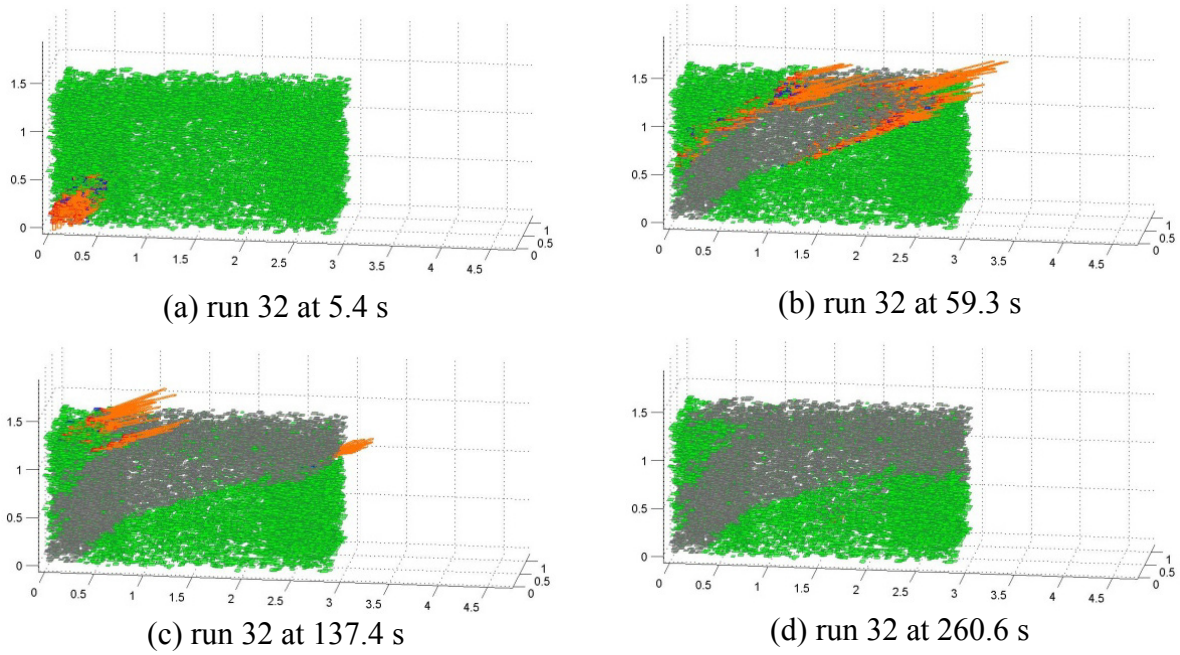

(a) run 32 at 5.4 s

(b) run 32 at 59.3 s

(c) run 32 at 137.4 s

(d) run 32 at 260.6 s

Figure 6.17. Bush combustion modeling results of run 32.

Table 6.4. Semi-empirical modeling results of Utah bushes combustion (Part III).

Run #	Species	Bush shape	Width (cm)	Length (cm)	Height (cm)	Leaf number	ρ_{local} (# of leaves/m^3)	ρ_{bulk} (# of leaves/m^3)	*MC* (%)	*WS* (m/s)	$h_{f,bush}$ (m)	*Xs*	$t_{brn,bush}$ (seconds)
1	Gambel oak	I	473	500	212	36,000	1,375	1,371	100	0	0	2.7%	51
2	Gambel oak	II	128	288	133	16,056	3,743	3,275	100	0	40	28.1%	110
3	Canyon maple	III	146	285	132	3,748	737	682	100	0	0	1.4%	20
23	Gambel oak	II	128	288	133	16,056	3,743	3,275	100	1	44	34.6%	116
26	Gambel oak	II	128	288	133	16,056	3,743	3,275	100	3	38	37.4%	136
28	Gambel oak	I	473	500	212	36,000	1,375	1,371	100	0	0	2.7%	55
29	Gambel oak	II	128	288	133	16,056	3,743	3,275	100	0	46	86.5%	382
30	Canyon maple	III	146	285	132	3,748	737	682	100	0	0	1.3%	14
31	Gambel oak	II	128	288	133	16,056	3,743	3,275	100	1	49	82.6%	788
32	Gambel oak	II	128	288	133	16,056	3,743	3,275	100	3	45	60.4%	262

Bush shape (I) means hemi-ellipsoid.
Bush shape (II) means large-hollow-space rectangular box.
Bush shape (III) means small-hollow-space rectangular box.

6.4 **Modeling Results for Utah Juniper**

The semi-empirical bush model was also able to treat the combustion of Utah juniper bushes based on the prediction equations shown in Section 5.2 and bush structure discussed in Section 6.1.2. A correlation (shown as Equation (6.3)) was developed to predict total Utah juniper bush dry weight (W_{dry}), which was also embedded in the bush model.

$$W_{dry} = 30.05 \cdot D_{crown} - 1763.33 \tag{6.3}$$

where D_{crown} is the crown diameter of Utah juniper bush in cm and W_{dry} is in grams. The regression to this equation was based on the measurements of Utah juniper bushes at Diamond Fork Canyon near Spanish Fork, Utah. Percentage of individual leaf flame bottom part (*Rd*) was assigned as 15% for the modeling results shown in this section. Values of ρ_{local} and ρ_{bulk} (number of leaves per m^3) were calculated according to the following equations.

$$\rho_{local} = \frac{Number\ of\ leaves}{Volume\ of\ cone} = \frac{Number\ of\ leaves}{\frac{\pi}{12} \cdot {D_{crown}}^2 \cdot H_{bush}}$$
$$\rho_{bulk} = \frac{Number\ of\ leaves}{Volume\ of\ cylindar} = \frac{Number\ of\ leaves}{\frac{\pi}{4} \cdot {D_{crown}}^2 \cdot H_{bush}} \tag{6.4}$$

Different configurations were set up for running bush combustion model according to the real geometrical measurements. The effect of bush size, moisture content, density were studied mainly by comparison of *Xs* and $t_{brn,bush}$.

Table 6.5. Semi-empirical modeling results of Utah bushes combustion (Part VI).

Run #	Species	Bush shape	Crown Diameter (cm)	Height (cm)	segment number	ρ_{local} (# of leaves/m^3)	ρ_{bulk} (# of leaves/m^3)	*MC* (%)	*WS* (m/s)	$h_{f,bush}$ (m)	*Xs*	$t_{brn,bush}$ (seconds)
33	Utah juniper	V	170	244	27,268	14,771	4,924	90	0	59	44.2%	534
34	Utah juniper	V	119.5	176	15,805	24,020	8,007	90	0	74	41.1%	413
35	Utah juniper	V	133	348	18,467	11,459	3,820	90	0	0	8.6%	148
36	Utah juniper	V	177	189	28,445	18,350	6,117	90	0	58	41.4%	658
37	Utah juniper	V	170	244	27,268	14,771	4,924	70	0	59	45.8%	579
38	Utah juniper	V	170	244	27,268	14,771	4,924	110	0	59	42.0%	605
39	Utah juniper	V	170	244	27,268	14,771	4,924	90	1	59	44.2%	534
40	Utah juniper	V	170	244	15,805	24,020	8,007	90	3	74	41.1%	413

Bush shape (V) means L-system fractal structure.

Values of D_{crown} and H_{bush} for run 33 thru 36 were all measurements of real Utah juniper bushes in the field. The value of MC was assigned as 90% for run 33 thru 36. Both D_{crown} and H_{bush} of run 34 were smaller than those of run 33, which meant run 34 was a smaller bush than run 33. The number of fuel segments for run 34 was also smaller than that of run 33 but ρ_{local} and ρ_{bulk} of run 34 were higher. As shown in Table 6.5, values of Xs for both runs 33 and run 34 were more than 40%. Flame in run 33 and 34 were able to propagate from the left bottom corner (where ignite) to the top of the bush (shown in Figure 6.18).

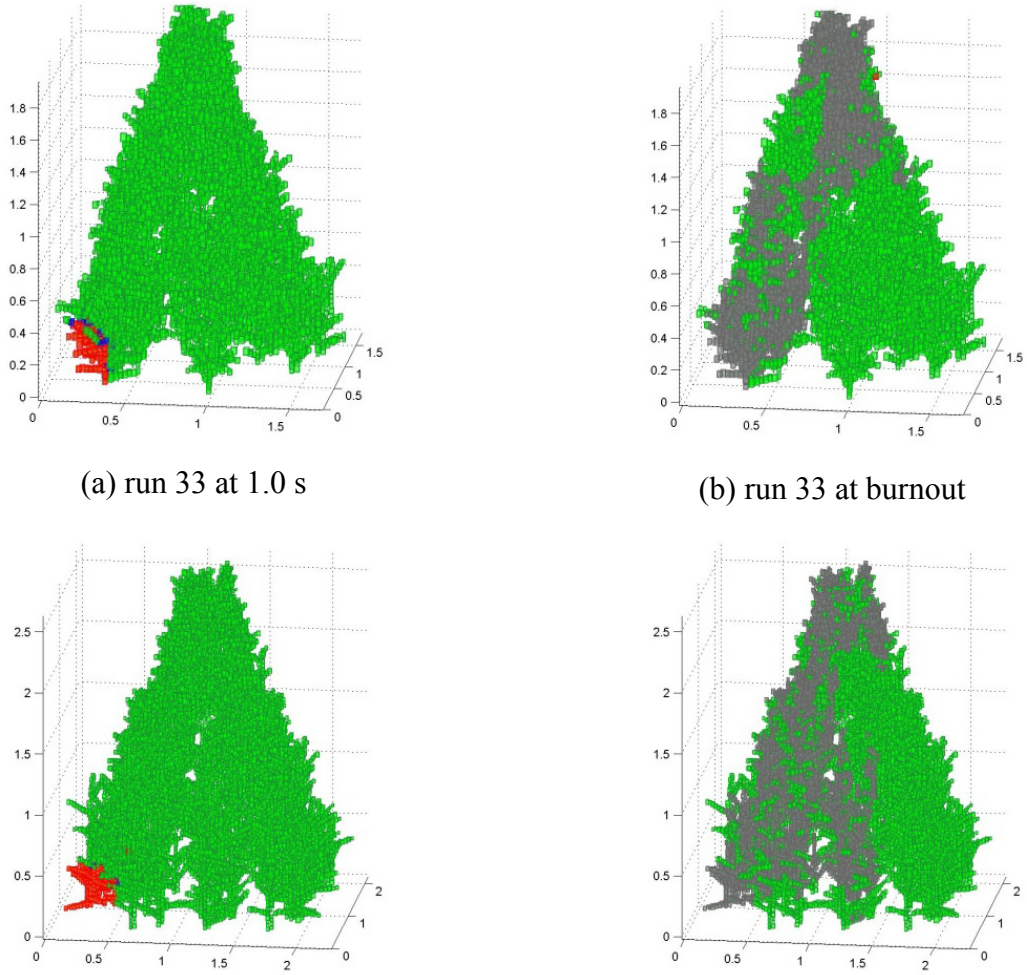

(a) run 33 at 1.0 s

(b) run 33 at burnout

(c) run 34 at 1.0 s

(d) run 34 at burnout

Figure 6.18. Bush combustion modeling results of run 33 and run 34.

The value of H_{bush} for run 35 was larger than that of run 33 and D_{crown} of run 35 was smaller than that of run 33. The reverse of this condition was set for run 36 as shown in Table 6.5. It was observed that *Xs* was smaller when the juniper bush was thinner according to run 35 (shown in Figure 6.19). It was also possible that density (ρ_{local} or ρ_{bulk}) of run 35 was not high enough for flame propagation.

(a) run 35 at 1.0 s (b) run 35 at burnout

Figure 6.19. Bush combustion modeling results of run 35.

To study the effect of *MC* on juniper bush combustion, *MC* of run 33 was switched into 70% for run 37 and 110% for run 38 as shown in Table 6.5. When *MC* decreased, the *Xs* increased as expected. Wind speeds at 1 m/s and 3 m/s were assigned to run 33 as run 39 and 40 (shown in Table 6.5). It was observed that flame propagation was worse when wind was introduced. This could be the reason that there was less chance for flame to ignite the fuel above when wind tilted the flame.

6.5 **Discussion**

Bush structure was studied and fuel placement was simulated for different species in the semi-empirical model. A rectangular box with a different portion size of the hollow inside space was determined for Gambel oak and canyon maple bushes. A hemi-ellipsoid Gambel oak bush shape was also constructed as an option in the semi-empirical model. A fractal-based L-systems approach was adapted for fuel placement in a Utah juniper bush.

Flame volume simulations were modified to integrate a new approach to flame width (FW_{β}). This modification was able to solve the problem of unreasonable huge flame heights (h_f) during flame propagation, especially for large broadleaf species like Gambel oak.

Different parametric runs were performed to study the effects of bush size, fuel placement shape, different leaf properties, fuel density, and wind. Slight changes in bush size did not have significant effects on *Xs*. Fuel placement shape influenced the bush burning path and accessible fuels. Different leaf properties affected the percent burned (*Xs*) and particular the burning time ($t_{brn,bush}$). Reducing moisture content (*MC*), increasing ρ_{local} , ρ_{bulk} or *U* would all increase *Xs* and enhance flame propagation for the cases where *Xs* was significant. Wind could even stretch the flame further away from the ignition source, which was important to the flame propagation between bushes in wildfire.

7. CONCLUSIONS AND RECOMMENDATIONS

Combustion experiments were performed on individual samples of four Utah species. A flat-flame burner on wheels was used as the convective heating source to represent a moving fire front. Experimental data and images were recorded and processed for analysis. Qualitative and quantitative combustion characteristics were determined for four species. Statistical models were explored to predict leaf geometrical properties and combustion characteristics for these four species. Conclusions and recommendations are given here.

7.1 Summary and Conclusions

7.1.1 Qualitative Results

It was observed that ignition typically started at the tips of the horizontally placed samples. When samples were placed vertically, ignition mostly occurred from the bottom edge of the samples. This observation indicated that when temperature was uniform on leaf sample, ignition would be initiated at the tip of the leaf, where local surface area was relative larger. Bending behavior was observed during combustion experiments of Utah species except for Utah juniper. It was observed that leaf samples typically bent towards convective gas until the time to maximum flame height (t_{fh}) was reached. After the maximum flame height was reached, the leaf sample would bend backwards and burn out. Brand formation was observed for broad-leaf and

big sagebrush. Some samples detached from the clip after burnout and some samples detached from the clip when samples were still flaming, especially for canyon maple. Brand formation was mainly observed for combustion of light leaf samples. Sparks and bursting behavior were observed during Utah juniper experiments, which occurred particularly for juniper segments cut from the top of the branch. Sparks or flashes were accompanied by leaf material being injected, but this behavior usually occurred before ignition.

7.1.2 **Quantitative Results**

Quantitative results included statistical analysis of both leaf geometrical properties and combustion characteristics. A beta distribution was used to describe individual leaf dry mass (m_{dry}), and m_{dry} was chosen as the base indicator variable. Multiple linear regressions were performed to correlate leaf thickness (Δx), leaf width (W), leaf length (L) (in this order). These leaf properties were correlated in order, so that W was correlated to Δx, etc. (as shown in Table 5.2). Minimized BIC value models were achieved by stepwise regression analysis, which were recommended to be used in the semi-empirical bush model. Multiple linear regression correlations for combustion characteristics (time to ignition (t_{ig}), time of flame duration (t_{fd}), time to maximum flame height (t_{fh}), time to burnout (t_{brn}), maximum flame height ($h_{f,max}$) etc.) were also developed by stepwise regression analysis. The goodness of the fit for those regressions was compared to results using previous equations developed for Manzanita combustion and other alternate models. Observed values of t_{ig} were quite scattered, which caused unsatisfactory regression results for this variable. A linear correlation between flame area (FA) and flame height (h_f) was developed, and the slope was introduced as the flame width (named as FW_β).

An existing semi-empirical bush combustion model was modified to treat Gambel oak, canyon maple and Utah juniper. Bush structure and leaf placement were determined for different

species. A rectangular box shape with a hollow middle was used to simulate both Gambel oak and canyon maple shrubs. The portion of hollow space was determined based on measurements in the field. A hemi-ellipsoid shape with a hollow center was also used to simulate a Gambel oak shrub. Branching structure was modeled for a Utah juniper bush via a fractal-based L-systems approach (Fletcher and Fletcher, 2013). A correlation between bush crown diameter (D_{crown}) and total bush dry weight (W_{dry}) was developed and embedded in the semi-empirical bush model for Utah juniper. The algorithm for describing the flame volume for large leaf samples was modified to use FW_{β} as the width of the flame cross section area. This improvement enabled the bush model to generate a reasonable flame height, especially for large broadleaf species. Prediction equations of leaf geometrical properties and combustion characteristics were integrated into the bush model for Utah species. Parametric runs of different configurations were set up to run the semi-empirical bush combustion model for each species. The rectangular box shape seemed to provide more accessible fuel above the initial flame for fire propagation than the hemi-ellipsoid shape. For different bush species, not only density affected predicted fire propagation, but also leaf properties had an impact on burning time and maximum flame height above the bush. Decreased moisture content and increased bulk density caused the extent of burnout for the bush to increase. When wind was introduced and wind speed increased, the extent of burnout did not necessarily increase though the distance that the flame propagated from the ignition source increased.

For simulated bushes matching geometrical measurements in the field, flame propagation and extent of conversion in this semi-empirical bush model were not as intense as expected, especially for the hemi-ellipsoid Gambel oak bush and rectangular box maple bush. Since density and moisture content influenced the extent of burnout significantly, more precise

estimation of the leaf number of a bush and the moisture content appear to be necessary for improved predictions. A better flame coalescence algorithm in the bush combustion model seems necessary as well.

7.2 **Recommendations**

During the course of this research project new questions were raised, resulting in the following recommendations.

- Study and develop a method to describe the bush structure of big sagebrush. It is likely that an L-systems self-rewriting method can be used to describe sagebrush structure.
- Conduct individual leaf sample combustion experiments over the flat-flame burner with a radiant panel to study the role of radiation versus convection in live fuel combustion.
- Perform multiple leaf combustion experiments for Utah species to study flame merging behavior, which will facilitate the flame coalescence treatment in the semi-empirical bush model.
- Conduct individual combustion experiments for Gambel oak, canyon maple and big sagebrush with a bench scale wind tunnel. Improve the wind tunnel apparatus to increase the accessible wind speed.
- Validate the whole bush combustion modeling of Utah species in the semi-empirical bush model by performing whole bush large-scale combustion experiments.
- Use the IR camera to determine the ignition temperature for Utah species and explore the main factors influencing flaming ignition (e.g., mass release rate).

REFERENCES

Alados, C., J. Escos, J. Emlen and D. Freeman, "Characterization of Branch Complexity by Fractal Analyses," *International Journal of Plant Sciences,* **160**(S6), S147-S155 (1999).

Albini, F. A., "A Model for the Wind-Blown Flame from a Line Fire," *Combustion and Flame,* **43**, 155-174 (1981).

Albini, F. A., "A Model for Fire Spread in Wildland Fuels by Radiation," *Combustion Science and Technology,* **42**, 229-258 (1985).

Albini, F. A., "Wildland Fire Spread by Radiation -- a Model Including Fuel Cooling by Natural Convection," *Combustion Science and Technology,* **45**, 101-113 (1986).

Anderson, H. E., "Heat Transfer and Fire Spread," INTERMOUNTAIN FOREST AND RANGE EXPERIMENT STATION OGDEN UTAH (1969).

Anderson, H. E., "Forest Fuel Ignitability," *Fire Technology,* **6**(4), 312-319 (1970).

Andrews, P. L., "Behave: Fire Behavior Prediction and Fuel Modeling System- Burn Subsystem, Part 1," General Technical Report INT-194, USDA Forest Service (1986).

Babrauskas, V., "Ignition of Wood: A Review of the State of the Art," *Interflam*, 71-88 (2001).

Babrauskas, V., Ignition Handbook, Issaquah, WA, Fire Science Publishers (2003).

Balbi, J.-H., J.-L. Rossi, T. Marcelli and P.-A. Santoni, "A 3d Physical Real-Time Model of Surface Fires across Fuel Beds," *Combustion Science and Technology,* **179**(12), 2511 - 2537 (2007).

Beer, T., "Fire Propagation in Vertical Stick Arrays - the Effects of Wind

" *International Journal of Wildland Fire,* **5**(1), 43-49 (1995).

Busing, R. T. and D. Mailly, "Advances in Spatial, Individual-Based Modelling of Forest Dynamics," *Journal of Vegetation Science,* **15**(6), 831-842 (2004).

Butler, B. W., J. Cohen, D. J. Latham, R. D. Schuette, P. Sopko, K. S. Shannon, D. Jimenez and L. S. Bradshaw, "Measurements of Radiant Emissive Power and Temperatures in Crown Fires," *Canadian Journal of Forest Research,* **34**, 1577-1587 (2004).

Catchpole, W. R., E. A. Catchpole, B. W. Butler, R. C. Rothermel, G. A. Morris and D. J. Latham, "Rate of Spread in Free-Burning Fires in Woody Fuels in a Wind Tunnel," *Combustion Science and Technology,* **131**, 1-37 (1998).

Catchpole, W. R., E. A. Catchpole, A. G. Tate, B. W. Butler and R. C. Rothermel, A Model for the Steady Spread of Fire through a Homogeneous Fuel Bed, Rotterdam, Millpress (2002).

Clark, M. M., T. H. Fletcher and R. R. Linn, "A Sub-Grid, Mixture–Fraction-Based Thermodynamic Equilibrium Model for Gas Phase Combustion in Firetec: Development and Results," *International Journal of Wildland Fire,* **19**(2), 202-212 (2010).

Cohen , J. D. and M. A. Finney "An Examination of Fuel Particle Heating During Fire Spread," VI Internaltional Conference on Forest Fire Research (2010).

Cole, W. J., M. K. H. Dennis, T. H. Fletcher and D. R. Weise, "The Effects of Wind on the Flame Characteristics of Individual Leaves," *International Journal of Wildland Fire,* **20**(5), 657-667 (2011).

Dimitrakopoulos, A. P. and K. K. Papaioannou, "Flammability Assessment of Mediterranean Forest Fuels," *Fire Technology,* **37**(2), 143-152 (2001).

Drysdale, D., An Introduction to Fire Dynamics, Chichester, England, John Wiley & Sons (1999).

Dupuy, J. L., "Testing Two Radiative Physical Models for Fire Spread through Porous Forest Fuel Beds," *Combustion Science and Technology,* **155**, 149-180 (2000).

Dupuy, J. L., J. Marechal and D. Morvan, "Fires from a Cylindrical Forest Fuel Burner: Combustion Dynamics and Flame Properties," *Combustion and Flame,* **135**(1-2), 65-76 (2003).

Engstrom, J. D., J. K. Butler, S. G. Smith, L. L. Baxter, T. H. Fletcher and D. R. Weise, "Ignition Behavior of Live California Chaparral Leaves," *Combustion Science and Technology,* **176**, 1577-1591 (2004).

Finney, M. A., "Farsite: Fire Area Simulator-Model Development and Evaluation," Research Paper RMRS-RP-4, USDA Forest Service (1998).

Fletcher, M. E. and T. H. Fletcher, "Application of L-Systems to Geometrical Construction of Chamise and Juniper Shrubs," *Ecological Modeling*, in press (2013).

Fletcher, T. H., B. M. Pickett, S. G. Smith, G. S. Spittle, M. M. Woodhouse, E. Haake and D. R. Weise, "Effects of Moisture on Ignition Behavior of Moist California Chaparral and Utah Leaves," *Combustion Science and Technology,* **179**, 1183-1203 (2007).

Frankman, D., B. W. Webb, B. W. Butler and D. J. Latham, "Fine Fuel Heating by Radiant Flux," *Combustion Science and Technology,* **182**(2), 215-230 (2010).

Li, Y. and D. Drysdale, "Measurement of the Ignition Temperature of Wood," Fire Science and Technology - First Asian Conference, Beijing (1992).

Linn, R. R., "A Transport Model for Prediction of Wildfire Behavior," Ph. D., Department of Mechanical Engineering, New Mexico State University (1997).

Mak, E. H. T., "Notes: Measuring Foliar Flammability with the Limiting Oxygen Index Method," *Forest Science,* **34**(2), 523-529 (1988).

Mardini, J. A. and A. S. Lavine, "Effects of Species and Green Wood Moisture Variation on Its Time to Ignition During Fires," University of California - Los Angeles (1995).

Mell, W. E., S. L. Manzello and A. Maranghides, "Numerical Modeling of Fire Spread through Trees and Shrubs," V International Conference on Forest Fire Research, Coimbra, Protugal (2006).

Mendes-Lopes, J. M. C., J. M. P. Ventura and J. M. P. Amaral, "Flame Characteristics, Temperature–Time Curves, and Rate of Spread in Fires Propagating in a Bed of *Pinus Pinaster* Needles," *International Journal of Wildland Fire,* **12**(1), 67-84 (2003).

Moghtaderi, B., V. Novozhilov, D. F. Fletcher and J. H. Kent, "A New Correlation for Bench-Scale Piloted Ignition Data of Wood," *Fire Safety Journal,* **29**, 41-59 (1997).

Montgomery, K. R. and P. C. Cheo, "Moisture and Salt Effects on Fire Retardance in Plants," *American Journal of Botany,* **56**(9), 1028-1032 (1969).

Pagni, P. J. and G. Peterson, "Flame Spread through Porous Fuels," 14th Symposium (International) on Combustion (1973).

Parsons, R. A., "Spatial Variability in Forest Fuels: Simulation Modeling and Effects on Fire Behavior," Dissertation, Forestry, University of Montana (2007).

Pickett, B. M., "Effects of Moisture on Combustion of Live Wildland Forest Fuels," Ph.D., Chemical Engineering, Brigham Young University (2008).

Pickett, B. M., T. H. Fletcher, B. W. Butler and D. R. Weise, "Single-Leaf, Two-Leaf, and Multi-Leaf Models for Live Wildland Fire Combustion," (2009).

Pickett, B. M., C. Isackson, R. Wunder, T. H. Fletcher, B. W. Butler and D. R. Weise, "Experimental Measurements During Combustion of Moist Individual Foliage Samples," *International Journal of Wildland Fire,* **19**, 1-10 (2010).

Prince, D., B. Andersen, W. Cole, M. Dennis and T. H. Fletcher, "Modeling a Burning Shrub with and without Wind Using a Semi-Empirical Model," International Association of Wildland Fire 3rd Fire Behavior and Fuels Conference, Spokane, Washington, Brigham Young University (2010).

Prince, D. R., "Fire Spread in Sparse Vegetation," PhD Dissertation in progress, Chemical Engineering Department, Brigham Young University (2012).

Prusinkiewicz, P. and A. Lindenmayer, "The Algorithmic Beauty of Plants (the Virtual Laboratory)," (1991).

Putnam, A. A., "A Model Study of Wind-Blown Free-Burning Fires," 10th Symposium (International) on Combustion, Pittsburg, PA (1965).

Rothermel, R. C., "A Mathematical Model for Predicting Fire Spread in Wildland Fuels," Research Paper INT-115, USDA Forest Service (1972).

Smith, S. G., "Effects of Moisture on Combustion Characteristics of Live California Chaparral and Utah Foliage," M.S., Chemical Engineering, Brigham Young University (2005).

Sullivan, A. L., "Wildland Surface Fire Spread Modelling, 1990–2007. 1: Physical and Quasi-Physical Models," *International Journal of Wildland Fire,* **18**(4), 349-368 (2009a).

Sullivan, A. L., "Wildland Surface Fire Spread Modelling, 1990–2007. 2: Empirical and Quasi-Empirical Models," *International Journal of Wildland Fire,* **18**(4), 369-386 (2009b).

Sullivan, A. L., "Wildland Surface Fire Spread Modelling, 1990–2007. 3: Simulation and Mathematical Analogue Models," *International Journal of Wildland Fire,* **18**(4), 387-403 (2009c).

Sun, L., X. Zhou, S. Mahalingam and D. R. Weise, "Comparison of Burning Characteristics of Live and Dead Chaparral Fuels," *Combustion and Flame,* **144**(1-2), 349-359 (2006).

USDA/USDI, "Federal Fire and Aviation Operations Action Plan," F. a. A. M. USDA Forest Service/Department of the Interior (2005).

Weber, R. O., "Modelling Fire Spread through Fuel Beds," *Progress in Energy and Combustion Science,* **17**(1), 67-82 (1991).

Weise, D. R., R. H. White, F. C. Beall and M. Etlinger, "Use of the Cone Calorimeter to Detect Seasonal Differences in Selected Combustion Characteristics of Ornamental Vegetation," *International Journal of Wildland Fire,* **14**(3), 321-338 (2005).

Welker, J. R., O. A. Pipkin and C. M. Sliepcevich, "The Effect of Wind on Flames," *Fire Technology,* **1**, 122-129 (1965).

Xanthopoulos, G. and R. H. Wakimoto, "A Time to Ignition - Temperature - Moisture Relationship for Branches of Three Western Conifers," *Canadian Journal of Forest Research,* **23**, 253-258 (1993).

Zhou, X., S. Mahalingam and D. Weise, "Modeling of Marginal Burning State of Fire Spread in Live Chaparral Shrub Fuel Bed," *Combustion and Flame,* **143**(3), 183-198 (2005).

APPENDIX

A. Raw Data

More than 2200 experimental runs were performed on four Utah species over the big flat-flame burner. The leaf properties and combustion characteristics were recorded on a spreadsheet, which can be found in the disc as the file named 'raw_data.xlsx'.

B. Experimental Video Images

Examples of experimental video images can be found in the disc under the folder named as 'B. Experimental Video Images'. The table below lists image folder names and their corresponding figure names shown in this thesis.

Table A-1. Experimental video images appended in the disc.

Date	Run #	Species	Folder Name	Corresponding Figure
July 13, 2011	11	Gambel oak	1	Figure 5.1
Aug 25, 2011	1	Gambel oak	2	Figure 5.2
July 1, 2011	7	Canyon maple	3	Figure 5.3
Oct 14, 2011	1	Utah juniper	4	Figure 5.4
July 6, 2011	5	Big sagebrush	5	Figure 5.6
June 27, 2011	15	Big sagebrush	6	Figure 5.7

C. Computer Codes

Semi-empirical bush combustion model were coded in MATLAB, which is appended in the disc under the folder named as 'C. Computer codes'

D. Modeling Results Images

Examples of modeling results images can be found in the disc under the folder named as 'D. Modeling Results Images'. The table below lists image folder names and their corresponding figure names shown in this thesis.

Table A-2. Modeling results images appended in the disc.

Run #	Species	Folder Name	Corresponding Figure
1	Gambel oak	run 1	Figure 6.11 (a), (c)
2	Gambel oak	run 2	Figure 6.15 (a), (b)
10	Gambel oak	run 10	Figure 6.11 (b), (d)
23	Gambel oak	run 23	Figure 6.15 (c), (d)
26	Gambel oak	run 26	Figure 6.15 (e), (f)
28	Gambel oak	run 28	Figure 6.16
32	Gambel oak	run 32	Figure 6.17
33	Utah juniper	run 33	Figure 6.18 (a), (b)
34	Utah juniper	run 34	Figure 6.18 (c), (d)
35	Utah juniper	run 35	Figure 6.19